APPLICATION OF INERTER IN PASSENGER VEHICLE SUSPENSION SYSTEMS

SOONG MING FOONG

FACULTY OF ENGINEERING
UNIVERSITY OF MALAYA
2015

APPLICATION OF INERTER IN PASSENGER
VEHICLE SUSPENSION SYSTEMS

SOONG MING FOONG

THESIS SUBMITTED IN FULFILMENT OF THE
REQUIREMENT FOR THE DEGREE OF
DOCTOR OF PHILOSOPHY

FACULTY OF ENGINEERING
UNIVERSITY OF MALAYA
KUALA LUMPUR

2015

ORIGINAL LITERARY WORK DECLARATION

UNIVERSITY OF MALAYA
ORIGINAL LITERARY WORK DECLARATION

Name of the candidate: SOONG MING FOONG
Registration/Matriculation Number: KHA100067
Name of Degree: DOCTOR OF PHILOSOPHY
Title of Project Paper/Research Report/Dissertation/Thesis ("this Work"):
APPLICATION OF INERTER IN PASSENGER VEHICLE SUSPENSION SYSTEMS

Field of Study: VEHICLE SUSPENSION

I do solemnly and sincerely declare that:

(1) I am the sole author/writer of this Work;
(2) This Work is original;
(3) Any use of any work in which copyright exists was done by way of fair dealing and for permitted purposes and any excerpt or extract from, or reference to or reproduction of any copyright work has been disclosed expressly and sufficiently and the title of the Work and its authorship have been acknowledged in this Work;
(4) I do not have any actual knowledge nor do I ought reasonably to know that the making of this work constitutes an infringement of any copyright work;
(5) I hereby assign all and every rights in the copyright to this Work to the University of Malaya ("UM"), who henceforth shall be owner of the copyright in this Work and that any reproduction or use in any form or by any means whatsoever is prohibited without the written consent of UM having been first had and obtained;
(6) I am fully aware that if in the course of making this Work I have infringed any copyright whether intentionally or otherwise, I may be subject to legal action or any other action as may be determined by UM.

Candidate's Signature   Date

Subscribed and solemnly declared before,

Witness's Signature   Date

Name:
Designation:

ABSTRACT

Inerter is a suspension element with the property that the force generated at its two terminals is directly proportional to the relative acceleration between the terminals, similar to the way a spring reacts to relative displacement and a damper to relative velocity. Studies have shown the inerter's effectiveness in providing superior performance in various suspension applications, including passive vehicle suspensions. However, presently two issues limiting its application in passenger vehicle suspensions are the non-prominent ride improvement for some studied suspension layouts such as the parallel layout using parameter values in the passenger vehicle's range, and the practical considerations of its physical implementation. This research aims to achieve greater application of inerter in passenger vehicle suspensions by studying several changes or modifications in employing the inerter and its concept. Firstly, the interaction of parallel inerter with controllable vehicle suspension systems was studied to determine the working principle of inerter in vehicle suspensions and also to determine its effectiveness when paired with controllable suspensions. Also, the practicality of a parallel inerter implementation was studied by investigating the feasibility of an inerter incorporating damping. Then, switching algorithms were implemented to the inerter to evaluate potential further ride performance improvement brought by these modifications. Finally, a working mechanism originated from inerter was adopted in vehicle suspension to evaluate its effect on suspension characteristic. In general, the outcomes of these analyses demonstrated the applicability of inerter in passenger vehicle suspensions: in the first part, it was shown that the parallel inerter worked by cancellation with spring force to reduce total suspension force which brought ride improvement, and it was similarly effective even when paired with controllable suspension systems, giving consistent 2 % to 4 % improvement. Additionally, the

practicality of parallel inerter implementation was demonstrated by the incorporation of eddy current damping in an inerter. In the second part, the use of semi-active switching algorithm on an inerter showed greater ride improvement of up to 12 % than that brought by passive inerter, while the non-linearity which was also modeled as switching law for the inerter managed better sprung mass transient response. Lastly, the analysis of vehicle suspension adopting inerter-derived mechanism demonstrated the capability of varying suspension characteristics, hence a potential of realizing semi-active suspension system for improved performance. Overall, this research shows that greater application of inerter in passenger vehicle suspensions can be achieved through the modifications to, and the derivations from, its initial concept, for example by interacting it with controllable suspension systems as in the research.

ABSTRAK

Inerter merupakan satu elemen suspensi dengan sifat bahawa daya yang dijanakan pada kedua-dua terminalnya adalah berkadar terus dengan pecutan relatif antara terminal, sebagaimana pegas bertindak terhadap sisihan relatif ataupun peredam terhadap halaju relatif. Kajian telahpun menunjukkan keberkesanan inerter dalam pelbagai penggunaan suspensi, termasuklah suspensi kenderaan pasif. Namun, terdapat dua isu yang membatasi penggunaannya dalam suspensi kenderaan penumpang, iaitu peningkatan keselesaan penunggangan yang tidak ketara bagi sesetengah aturan suspensi seperti aturan selari, dan tahap praktikal perlaksanaan fisikalnya. Penyelidikan ini bertujuan untuk mencapai penggunaan inerter yang lebih besar dalam suspensi kenderaan penumpang dengan mengkaji pengubahsuaian dalam penggunaan inerter serta konsepnya. Pertama sekali, interaksi antara inerter selari dengan sistem suspensi kenderaan boleh-kawal telah dikaji demi menentukan prinsip kerja inerter dalam suspensi kenderaan dan keberkesanannya apabila digunakan bersama suspensi boleh-kawal. Selain itu, tahap praktikal inerter selari juga dikaji dengan menyelidik kemungkinan penggunaan inerter yang digabungkan dengan redaman. Seterusnya, algoritma penukaran turut dilaksanakan ke atas inerter untuk menilai kemampuan peningkatan lanjutan dalam prestasi penunggangan hasil daripada pengubahsuaian ini. Akhirnya, mekanisme yang didapati daripada inerter juga digunakan dalam suspensi kenderaan demi menilai kesan penggunaan mekanisme ini terhadap ciri suspensi. Secara umumnya, hasil daripada analisis-analisis di atas telah menunjukkan kebolehgunaan inerter dalam suspensi kenderaan penumpang. Pertama sekali, kajian ini menunjukkan bahawa inerter selari berfungsi dengan membatalkan daya daripada pegas dan dengan ini mengurangkan daya suspensi lalu menambahbaik keselesaan penunggangan kenderaan, dan keberkesanannya turut wujud apabila digunakan bersama dengan sistem

suspensi boleh-kawal dengan peningkatan yang kekal, iaitu 2 % hingga 4 %. Lebih-lebih lagi, tahap praktikal penggunaan inerter selari turut dibuktikan dengan memperkenalkan redaman arus pusar ke dalam inerter. Dalam bahagian kedua penyelidikan, penggunaan algoritma penukaran bagi suspensi separa-aktif ke atas inerter membawa peningkatan penunggangan yang lebih ketara iaitu sehingga 12 % berbanding dengan penggunaan inerter pasif. Sementara itu, keadaan tidak-linear bagi inerter yang juga boleh diwakili dengan algoritma penukaran memberi reaksi kenderaan yang lebih baik. Akhir sekali, analisis perlaksanaan mekanisme daripada inerter ke atas suspensi kenderaan menunjukkan keberkesanan dalam mengawal perubahan ciri suspensi dan memberikan kemampuan untuk merealisasikan sistem suspensi separa-aktif demi peningkatan prestasi. Secara keseluruhan, penyelidikan ini menunjukkan bahawa penggunaan inerter yang lebih besar dalam suspensi kenderaan penumpang dapat dicapai melalui pengubahsuaian daripada konsep asal, contohnya dengan membenarkan interaksi antara inerter dengan sistem suspensi boleh-kawal sebagaimana yang dipertengahkan dalam penyelidikan ini.

ACKNOWLEDGEMENTS

First and foremost, I wish to express my gratitude to my institution, University of Malaya, for providing the facilities and support which have led to the completion of the research project. It is worth mentioning here that this project is supported by Postgraduate Research Fund (PPP Grant, Project number PV051-2011A) from the Institute of Research Management and Monitoring, University of Malaya.

I sincerely thank my project supervisors, Dr Rahizar Ramli from Mechanical Engineering Department, University of Malaya and Dr Wan Nor Liza Wan Mahadi from Electrical Engineering Department, University of Malaya for their guidance and supervision throughout my entire duration of study. In particular, my supervisor Dr Rahizar Ramli has provided advice on the directions and the details of the research project as well as guidance in the field of vehicle modeling and analysis. Meanwhile, my co-supervisor Dr Wan Nor Liza Wan Mahadi has guided me in the area of electromagnetic or eddy current damping, and has been helpful in giving feedbacks to the thesis and other relevant reports.

In addition, I would like to further extend my gratitude to my fellows Ms Sim Hoi Yin, Mr Kong Keen Kuan and Mr Khoo Shin Yee from Mechanical Engineering Department for their invaluable help in the project. I deeply appreciate their advice and other miscellaneous help especially in the experimental work related to the project.

Finally, I thank my family members for their endless support during the period of my study, especially during difficult times.

TABLE OF CONTENTS

LIST OF FIGURES

LIST OF TABLES

LIST OF SYMBOLS AND ABBREVIATIONS

Symbols

a	Limit of relative displacement
b	Inertance
B	Magnetic flux density
b_{eq}	Equivalent inertance
b_{off}	Off-state inertance
b_{on}	On-state inertance
c	Damping rate or coefficient
c_{max}	Maximum damping rate or coefficient
c_{min}	Minimum damping rate or coefficient
$c_{rotational}$	Rotational damping coefficient
$c_{translational}$	Linear or translational damping coefficient
d_i	Flywheel's inner diameter
d_o	Flywheel's outer diameter
d_p	Pinion diameter in rack-and-pinion mechanism
e_b	Inertance error
F_{damper}	Damping force
$F_{inerter}$	Inerter force
f_{sp}	Spatial frequency
F_{spring}	Spring force
F_x	Longitudinal tire force
F_y	Lateral tire force
G	Road profile roughness coefficient
I_x	Sprung mass moment of inertia about x-axis

I_y	Sprung mass moment of inertia about y-axis
I_z	Sprung mass moment of inertia about z-axis
k	Suspension stiffness
k_{gr}	Gear ratio
k_{gr_hard}	Gear ratio of hard suspension setting
k_{gr_soft}	Gear ratio of soft suspension setting
k_t	Tire stiffness
l_f	Distance from center of gravity to front axle
l_r	Distance from center of gravity to rear axle
M	Total vehicle mass
m	Mass of inerter's flywheel
m_{gr}	Gear mass
M_s	Total sprung mass
m_s	Quarter vehicle sprung mass
m_u	Quarter vehicle unsprung mass
p	Pitch of ball-screw mechanism
R^2	Coefficient of determination
s	Spectral density
T_f	Front half-track
T_r	Rear half-track
U	Control signal or control force
z_g	Vertical road displacement
z_{gr}	Gear mass displacement
z_s	Sprung mass displacement
z_u	Unsprung mass displacement
θ	Pitch displacement

ρ	Flywheel's material density
φ	Roll displacement
ψ	Yaw displacement

Abbreviations

DOF	Degree of freedom
RMS	Root-mean-squared

LIST OF APPENDICES

CHAPTER 1 INTRODUCTION

A vehicle suspension is a system of spring and damper in a vehicle that fundamentally serves the functions of isolating the chassis from roughness in the road for ride comfort, and keeping the tires in contact with the road with minimal load variations for good road holding ability and, indirectly, good handling of vehicle (Gillespie, 1992). Clearly, ride and tire road holding ability (and thus handling) are the main performance criteria to have in mind when designing vehicle suspensions. It follows logically that these are also the important criteria, among others, which dictate the overall quality of a vehicle.

The quest for performance improvement in terms of ride and handling has resulted in the introduction of controllable suspension systems that are capable of varying the suspension forces through the use of variable dampers or actuators, as well as the introduction of a new element in suspension system, that is the inerter which is an additional two-terminal suspension element apart from spring and damper with the property that the equal and opposite force applied at the two terminals is proportional to the relative acceleration between the terminals (Smith, 2002), similar to the way a spring reacts to relative displacement and a damper to relative velocity. While controllable suspension systems have been extensively studied since the past decades, the inerter, on the other hand, has only been introduced and researched recently. Previous researches have shown that the passive inerter is effective as a method of isolating vibration from the ground in several suspension applications, such as building suspensions (Wang et al., 2010), train suspensions (Wang et al., 2006) and passive vehicle suspensions (Smith & Wang, 2004). In the case of passive vehicle suspensions, improvement to performance measures of ride and road holding ability has been shown possible with optimum suspension parameters. In fact, there has been successful

implementation of the inerter device in race vehicles for better handling performance, as mentioned in a past study (Chen et al., 2009). However, even though inerter has already been proven in these earlier studies to be effective in benefiting ride and handling of a vehicle suspension, it is observed that there are still some limitations that restrict its application in typical passenger vehicles. Firstly, observing from the analysis of previous study (Smith & Wang, 2004), one can see that at suspension stiffness values typical of passenger vehicles (lower stiffness as opposed to those for race vehicles), the improvement in ride performance measure is not prominent for certain suspension layouts such as the parallel layout. Additionally, while various suspension layouts employing inerter are possible in theoretical analysis, their physical implementation certainly requires practical considerations because of the limited design space around passenger vehicle suspensions, which is seldom brought to attention in past researches. These limitations lead to the problem that the current form of implementation of inerter (that is, using it as passive element, in passive suspensions, and as separate device from other elements) lacks applicability in passenger vehicle suspensions, and they represent the gap between present development of inerter and its eventual adoption in passenger vehicle suspension systems.

Following the matter above, this research aims to narrow the gap by achieving greater application of inerter in passenger vehicle suspensions through new ways of employment which involve the interaction with controllable suspension systems. The attainment of greater applicability is important as manufacturers can then benefit from adopting the inerter to produce vehicles with superior quality, particularly in the ride aspect for passenger vehicles. Specifically, the research work deals with the evaluation of several departures from the current form of implementation, including the pairing of inerter with controllable suspension systems as well as the incorporation of damping to

an inerter for a combined suspension device, the implementation of switching algorithm to an inerter for a switchable element, and the adoption of inerter-derived concept in vehicle suspensions. These will be elaborated in the following sections.

1.1 Research Objectives

As first indicated from the preceding section, the problem statement is that the existing form of implementation of inerter lacks applicability in passenger vehicle suspensions, which prevents its widespread adoption. So, the aim of research is to achieve better applicability of inerter in this area. Breaking down from the main aim, as the research involves the evaluation on several modifications in employing the inerter, the individual objectives of study (corresponding to the implementations mentioned in the preceding section) are listed below:

- To analyze the effectiveness of interacting a passive inerter with various passenger vehicle suspension systems, including passive and controllable suspension systems, in terms of ride performance benefit;

- To determine the feasibility and practicality of a realization of parallel inerter layout in vehicle suspensions by incorporating damping in an inerter;

- To investigate potential further performance advantage in vehicle ride brought by the implementation of switching algorithms to the inerter element in vehicle suspensions;

- To evaluate the potential of adopting an inerter-derived gear mechanism in vehicle suspensions for realization of a variable suspension with improved performance.

1.2 Scope of Research

In general, the scope of this research covers two areas of study, namely the inerter and the controllable suspension systems, as the underlying idea of the implementations mentioned previously involves the interaction of both concepts. As described earlier, the research work involves evaluating several modifications in employing the inerter to determine whether there is greater application in passenger vehicle suspensions or not. For these evaluations, the applicability of inerter was separately assessed based on three aspects, namely practicality, performance and further concept adoption or utilization. Consistently, the research work can be structured into three parts. In the first part, the pairing of parallel inerter with controllable vehicle suspension systems was studied to determine the working principle of inerter in vehicle suspensions as well as its effectiveness and versatility when paired with various controllable suspensions. Also, the practicality of such a parallel inerter implementation was evaluated by investigating the feasibility of an inerter incorporating eddy current damping (in terms of achievable inertance and damping rate). For the second part of the work, switching algorithms were implemented to the inerter to determine the potential further ride performance improvement. Specifically, a switchable inerter and a passive but non-linear inerter, of which the behaviors were modeled by switching algorithms, were considered in the study. Finally, the research work also considered the adoptability of inerter-derived concept in vehicle suspensions by assessing a modified suspension layout with a gear mechanism taken from inerter and studying its potential of achieving a variable or switchable suspension. To summarize, the overview of this research is illustrated in Figure 1.1.

A Study on the **Application** of **Inerter** in Passenger **Vehicle Suspension** Systems

Purpose: Better applicability* in passenger vehicle suspensions

Method: Interactions between inerter & controllable suspension systems

(I) Passive Inerter with Controllable Suspensions

(II) Incorporating Switching Algorithm on Inerter

(III) Adopting Concept Derived from Inerter

Analysis of controllable suspensions with inerter [1,2]

Incorporating damping in parallel with inerter [1]

Force-cancellation-based switchable inerter [2]

Study on a switching, non-linear inerter [2]

Applying gear mechanism in vehicle suspensions [2,3]

*Evaluation on aspects:
[1]Practicality
[2]Performance
[3]Concept utilization

Figure 1.1: Illustration of the overview of research

1.3 Outline of Thesis

This thesis reports the study on interactions between inerter and controllable suspension systems in an effort to obtain greater application in passenger vehicle suspensions. Specifically, the thesis is composed of six chapters, and the descriptions for these chapters are presented here.

In the beginning part of the thesis, Chapters 1 and 2 introduce the current research. Firstly, Chapter 1 (the current chapter) provides a general introduction to vehicle suspension and the inerter, and highlights the present limitations of this suspension element in passenger vehicle suspension application which becomes the motivation of the research. In addition, the objectives and scope of research are identified for an overview of the research. Then, in Chapter 2, the key areas of research, for instance inerter and controllable suspension systems, are reviewed. Particularly,

previous studies on inerter, its realizations and its benefits in various applications are comprehensively reviewed to provide a glance on the present development and the trend of this field of research.

Following these, Chapters 3, 4 and 5 form the main part of the thesis as they describe the work carried out in the current research. Chapter 3 presents the work related to the practical implementation of passive inerter in passenger vehicle suspension systems, including the analysis of performance improvements due to inerter when used in various controllable suspension systems and the feasibility study of a realization of the parallel inerter layout by incorporating damping to an inerter. Then, venturing further from the passive inerter, Chapter 4 involves the incorporation of switching algorithms to an inerter. Specifically, the performance analyses for suspension involving switchable inerter based on force cancellation strategy and a non-linear inerter, of which its behavior is represented by displacement-based switching algorithm, are discussed in the chapter. Meanwhile, Chapter 5 demonstrates a further utilization of the concept of inerter through the adoption of an inerter-derived mechanism in a typical vehicle suspension. This chapter describes the study of a modified suspension layout consisting of a gear mechanism adopted from inerter device and presents the potential of realizing a semi-active suspension with improved performance due to the mechanism's capability of varying suspension characteristic.

Finally, in the last part of the thesis, Chapter 6 concludes the current research by summarizing the outcomes from the work done in the previous chapters, stating the contributions of knowledge from the research, and providing recommendations for future research.

CHAPTER 2 LITERATURE REVIEW

This chapter serves as a review of several research areas or topics that are related to the current research. Judging from the scope of research described in Chapter 1, three key topics can be identified, namely the inerter, the control strategies of controllable suspension systems and the electromagnetic or, more specifically, eddy current damping. These are relevant to various studies associated with the current research. Of the three topics, inerter is the core element of this research. Chapter 2 is structured as follows: in Section 2.1, a comprehensive review of the past studies on inerter is presented; this is followed by an introduction on the controllable suspension systems and several well-established control strategies in Section 2.2. Then, as eddy current damping is also considered in part of the present research work, Section 2.3 provides a brief review of recent studies showing the development of electromagnetic and eddy current dampers as well as their application in vehicle suspension system. Finally, Section 2.4 presents the general concept of multi-objectivy optimization, particularly the Pareto approach of optimization considering that it is employed in most analyses for the present work related to the evaluation on suspension performance.

2.1 Inerter

Inerter is an element derived from the force-current analogy. This is a well-known electrical-mechanical analogy normally encountered in control engineering where the mechanical mass-spring-damper system is related to the electrical resistor-inductor-capacitor circuit. According to this analogy (Gopal, 2002; Smith, 2002), force is analogous to current, velocity is analogous to voltage, while kinetic and potential energies are respectively analogous to electrical and magnetic energies. On the

component side, spring is an analog of inductor, damper is an analog of resistor as they both dissipate energy, while mass is generally treated as an analog of capacitor.

The concept of inerter originated from a study by Smith (2002), when he pointed out the restriction of mass-capacitor analogy. As mentioned in the study, the acceleration of mass is relative to a fixed point in the inertial frame, which means one terminal of mass element is the ground while the other is the center of mass. This is strictly equivalent to a grounded capacitor in electrical circuits; however, there is no direct mechanical analog of a two-terminal capacitor, of which both terminals are connected to the circuit. Thus, in the study, Smith (2002) introduced the two-terminal mass concept known as the inerter, which is defined as 'a mechanical, two-node, one-port device with the property that the equal and opposite force applied at the nodes is proportional to the relative acceleration between the nodes' (Smith, 2002). This can be mathematically stated as follows:

$$F_{inerter} = b(a_2 - a_1) \tag{2.1}$$

in which $F_{inerter}$ is the equal and opposite force of the inerter, a_1, a_2 are the accelerations of the terminals or nodes, b is a constant of proportionality named the inertance and has the unit of kilogram. With this new element, there is now a complete mechanical analog of capacitor, as a two-terminal capacitor can also be represented in mechanical systems as a two-terminal mass. From the definition, it is also interesting to note that the inerter can be used as a replacement of mass when one of its terminals is fixed, as shown in the same study. In this case, the acceleration $a_1 = 0$, and b becomes the equivalent mass.

While the concept and the definition of inerter is direct and straight-forward, there are various means of realizing this element physically, as can be found in the related patent (Smith, 2008). Some of the presented methods include using rack-and-pinion, ball-screw and hydraulic mechanisms to achieve the effect of inerter. Many of the mechanisms have been developed and studied. For instance, Papageorgiou and Smith (2005), and Papageorgiou et al. (2009) have extensively tested two inerter prototypes: the first was a rack-and-pinion inerter and the second was a ball-screw inerter. Fundamentally, a rack-and-pinion inerter involves the simple approach of taking a plunger sliding in a cylinder which drives a flywheel through a rack, pinion and gears (Smith, 2002). In this type of realization, the relation between force and accelerations is generally as stated in equation (2.2):

$$F_{inerter} = (m)\left({}^{\gamma}/_{r_3}\right)^2 \left({}^{r_2}/_{r_1}\right)^2 (a_2 - a_1) \tag{2.2}$$

in which $F_{inerter}$, a_1, a_2 are as defined previously, m is the mass of flywheel, γ is the flywheel's radius of gyration which is related to the flywheel's inertia, r_1, r_2, r_3 are the radii of the pinions which determine the gear ratio. For a ball-screw inerter, the flywheel contained in the device is rotated by the ball-screw mechanism. In a study employing this type of inerter, Wang and Chan (2008) stated the equation governing the working principle of ball-screw inerter, as expressed in equation (2.3):

$$F_{inerter} = \left({}^{2\pi}/_{p}\right)^2 (J)(a_2 - a_1) \tag{2.3}$$

in which $F_{inerter}$, a_1, a_2 are again as defined before, p is the pitch of ball-screw, J is the mass moment of inertia of the flywheel. It is worth to note here that for both types of mechanical-based inerter, the rack-and-pinion and the ball-screw are responsible for the

conversion of translational motion at the terminals to the rotational motion of the flywheel, and although the effect of inerter (quantified by inertance) is fundamentally due to the inertia property of the rotating flywheel, it is the conversion ratios of the mechanisms that significantly scale the effect brought by the flywheel's inertia. In fact, from equations (2.2) and (2.3), one can see that a wide range of inertances is achievable by varying the gear ratio or the ball-screw pitch, while keeping the actual mass to be small.

Apart from these mechanical-based inerters, some other realizations of inerter were also studied. In 2011, Wang et al. (2011) proposed a novel hydraulic inerter device that was assembled from a hydraulic cylinder, a motor and pipes. The inertance of the hydraulic inerter can be designed or modified by tuning the parameters of flywheel (mass moment of inertia), hydraulic cylinder (piston's cross-sectional area) and the hydraulic motor. According to the study, this can be mathematically expressed as in equation (2.4):

$$F_{inerter} = (J)\left(A/D\right)^2 (a_2 - a_1) \tag{2.4}$$

in which J is the flywheel's inertia similar to that in the previous equation, A is the piston's cross-sectional area, while D is a constant related to the hydraulic motor. For this realization, the hydraulic flow enabled the rotational-to-translational motion conversion, and the term $\left(\frac{A}{D}\right)$ became the conversion ratio. In 2013, Swift et al. (2013) extended the use of hydraulic concept in inerter further by modeling and testing a fluid inerter. Unlike other types of realization which relied on the inertia of flywheel, the fluid inerter proposed in the study utilized the fluid's inertia directly to achieve advantages such as simplicity and durability of the device. Elsewhere, Wang and Chan

(2008, 2011) also tested a suspension strut comprising a ball-screw inerter and a permanent magnet electric machine (as generator) to give a mechatronic suspension with different mechanical impedance (representing suspension parameters).

So far, the discussion on inerter's definition and different physical realizations is based on the assumption that the inerter is ideal, which means that the actual mass of the device is insignificant compared to the inertance, and there is no non-linearity in the device (for instance, friction between contact surfaces). This is very similar to ideal assumptions applicable to other suspension elements like spring and damper, such as the massless assumption. However, in reality, such non-linearities are present, and these were studied by Wang and Su (2008a, 2008b). In the studies, they pointed out and investigated three types of non-linearity present in a ball-screw inerter device, namely friction, backlash and the elastic effect. From the analysis of the non-linear inerter model, they concluded that the non-linearities of inerter, in general, degraded the suspension performance; however, the overall performance was still better than traditional suspensions, especially when the suspension stiffness was large.

2.1.1 Applications of inerter

Since its introduction, the inerter has shown many possible suspension applications. In general, the use of inerter in these applications brings performance benefits when compared to conventional suspension systems. For example, in 2004, Smith and Wang (2004) studied the use of inerter in passive vehicle suspension. It was shown from the optimization results that there were performance benefits in passive vehicle suspension employing inerters. This will be elaborated later. Meanwhile, Evangelou et al. (2004, 2006, 2007) extended the use of inerter in motorcycle steering. In these studies, a mechanical steering compensator comprising a mechanical network of spring, damper

and inerter was intended to replace the conventional steering damper. The studies demonstrated, theoretically, that the steering compensator managed to improve wobble and weave modes of damping experienced in high-performance motorcycle.

Similar studies were also carried out on other types of vehicle suspension, such as train suspension (Wang et al., 2009; Wang et al., 2006). In these studies, a one-wheel train suspension was modeled, and two basic arrangements of inerter in the suspension (parallel and serial) were considered. The optimization of suspension based on passenger comfort and dynamic wheel load showed that the inerter in train suspension was capable of improving the former performance index, but not the latter. In the same study (Wang et al., 2006), it was pointed out that the suspension layouts were passive; in other words, no energy input was required to achieve those performance benefits. In addition, Wang and Liao (2010) extended the above studies which concentrated on vertical train dynamics, and instead investigated the lateral train dynamics with added inerter. In the study, the lateral stability of multi-body train model, in the form of attainable critical speeds, was assessed. Specifically, a 12-degree-of-freedom (DOF) model with fixed car body and a 16-DOF model with movable car body were added with inerters, and the possible improvement in critical speed was analyzed. From the study, it was found that the use of inerter with parallel layout in various suspension locations increased the critical speed, thus provided better lateral train stability.

There are also studies which concern the use of inerter in building suspensions for vibration isolation purpose (Wang et al., 2007; Wang et al., 2010). The studies investigated the potential benefits of building suspension systems employing inerter using one-DOF and two-DOF building models that were isolated from a fixed ground through suspensions. The analysis showed that inerters were effective in suppressing

vibrations from traffic and earthquakes. More recently, the study by Lazar et al. (2014) also demonstrated the use of inerter-based device for structural vibration suppression. The study similarly showed that vibration isolation can be achieved with low amount of added mass to the structure. In this aspect, the benefits due to an inerter are similar to those brought by a tuned mass damper which is also used in structures for vibration isolation. This can possibly be explained by the influence of inerter on the natural frequencies of vibration systems as studied by Chen et al. (2014). According to this study, like the use of mass damper, the inerter can reduce the natural frequencies of vibration systems by increasing the inertance. However, it is worth noting that an inerter is a two-terminal suspension element and has insignificant mass; this distinguishes it from a mass damper that is one-terminal and adds weight to the overall system, which is undesirable in certain applications such as in passenger vehicle suspensions.

2.1.2 Inerter in vehicle suspensions

From the various studies, it can be summarized that the capability of inerter in isolating vibration is general and is not only specific to a particular application. Nevertheless, the review shall now concentrate on the application of inerter in passenger vehicles, since this is undoubtedly the main focus of current research. Basically, the application of inerter in passenger vehicles is mostly on the suspension system, since the inerter is fundamentally a suspension element in the typical mass-spring-damper system. As one of the earliest studies in this area, the study by Smith and Wang (2004) claimed that performance benefits were possible in vehicle suspensions with inerters. The study investigated eight different suspension layouts, which included a conventional suspension without inerter, a suspension with simple parallel inerter arrangement, a suspension with simple serial inerter arrangement, and some other layouts with combinations of these arrangements. Both quarter and full vehicle models were used in

the analysis, and the suspensions were optimized based on three performance measures, namely ride comfort, tire load and suspension's ability to carry load. The optimization results showed that the tested suspensions improved the three performance measures (compared to conventional suspension without inerter) when the measures were independently optimized, although the improvements varied across different layouts. The study also showed theoretical improvement of both ride comfort and load carrying ability in multi-objective optimization with parallel and serial inerter suspension layouts.

In 2009, Scheibe and Smith (2009) extended the study by Smith and Wang (2004) by deriving analytical solutions for optimal suspension parameters instead of performing numerical optimization as in the earlier study. In this study, similar suspension layouts were considered; however, only ride comfort and tire grip (the tire load measure) were taken as performance measures. The analytical solutions proved that the optimization results in the earlier study were in fact global optima. Additionally, in multi-objective optimization involving the two performance measures, this study showed similar simultaneous improvements in both objectives when suspensions with inerter were considered.

In both studies (Scheibe & Smith, 2009; Smith & Wang, 2004), various types of suspension layout were analyzed and compared to the conventional suspension without inerter. However, although all layouts are theoretically possible, only the parallel and serial inerter arrangements can be easily implemented due to their simplicity and practicality. Consequently, passenger vehicle suspensions with these two layouts have generally received greater attention in researches. In 2012, C. Li et al. (2012a, 2012b) studied the use of a two-terminal flywheel (which is conceptually the same as inerter) in vibration suppression. In the first part of the study (C. Li et al., 2012a), a two-terminal

flywheel which used the inverse screw transmission was proposed, and the non-ideal factors of the device, such as the structure mass, stiffness, viscous damping, friction and backlash were incorporated during the modeling of the device. In the second part of the study (C. Li et al., 2012b), the application of the two-terminal flywheel in passive vehicle suspension was presented. The suspension model consisted of spring, damper and the flywheel arranged in parallel, and was designed with Chebyshev goal programming method for optimal passenger comfort, tire grip and suspension deflection. The study showed that the proposed flywheel in parallel layout had superior passenger comfort and tire grip, with equal suspension deflection compared to conventional passive suspension.

Similarly, in 2010, Nie et al. (2010) studied a vehicle suspension employing inerter in series to the spring and damper using quarter vehicle model, and concluded from the theoretical optimization result that the proposed suspension with serial inerter layout managed to improve passenger comfort to the maximum while ensuring or maintaining tire grounding performance and suspension working space. More recently, Wang et al. (2014) extended the study by Nie et al. (2010) by designing and testing a vehicle suspension system with inerter, and showed consistent outcome that passenger comfort can be greatly enhanced. In these two studies, the justification of performance advantage brought by serial suspension layout with inerter was also presented. As explained, the spring-damper combination can attenuate high-frequency vibration, while the inerter-damper combination can attenuate low-frequency vibration. Hence, a suspension incorporating a spring-damper combination in series to an inerter-damper combination will, theoretically, be capable of buffering and attenuating shock and vibration within a wider frequency domain.

Although both simple parallel and simple serial suspension layouts with inerter have been demonstrated to bring benefits to vehicle suspension, results from previous study (Smith & Wang, 2004) have suggested that the serial inerter arrangement has higher percentage improvement in ride comfort. However, it is also worth to point out that while spring and inerter are similar because they both store and release energy of the system, the inerter, unlike spring, cannot support static load. Therefore, although possible in theoretical analysis, the serial inerter arrangement might require an additional spring element to support the static load in physical implementation. The parallel inerter arrangement, on the other hand, does not encounter this limitation.

Finally, the adoption of inerter in passenger vehicles is not just limited to passive suspension system which has already been discussed. Some recent studies have also demonstrated the possibility of pairing an inerter with semi-active suspension system. For example, Zhang et al. (2010, 2012) have evaluated the benefits of semi-active suspensions with inerter. In the studies, the behavior of semi-active suspensions with inerter using common semi-active strategies such as Groundhook, Skyhook and hybrid control (which will be detailed in Section 2.2.2) was evaluated with quarter vehicle model and was compared to passive suspension with inerter. From numerical simulations, they concluded that the semi-active suspension with inerter gave much better performance than the passive suspension with inerter, especially with hybrid control strategy. In another recent study, Hu et al. (2012) investigated the potential improvements to suspension performance measures by pairing eight suspension configurations incorporating inerter with a parallel variable damper that was designed based on optimal control theory. With both inerter configurations and semi-active damper combined as suspension setups, it was determined that these setups generally improved ride comfort compared to conventional semi-active suspension. In general,

these studies have given an early indication that the inerter is useful in semi-active suspension system.

From the recent researches, it can be deduced that the current trend of inerter research is on combined implementation between inerter and semi-active suspensions. This research follows the direction of interacting an inerter with controllable suspension systems, for example by pairing it alongside different controllable suspension systems (as in Chapter 3), by incorporating switching algorithms to an inerter (as in Chapter 4), and by exploiting a fundamental feature from an inerter to realize a variable suspension (as in Chapter 5).

2.2 Controllable Suspension Systems and Control Strategies

Presently, most vehicles utilize passive suspension system which basically consists of passive spring and damper and has constant suspension characteristic. A passive suspension has the ability to store energy via a spring and to dissipate it via a damper. The parameters are generally fixed, being chosen to achieve a certain level of compromise between ride comfort and tire road holding ability (Paré, 1998). The continuous efforts for superior suspension performance have resulted in the introduction of some suspension solutions collectively known as controllable suspension systems, which can eliminate the compromise associated with passive suspensions due to the constant spring and damping characteristics. In general, controllable suspension systems are divided into active and semi-active suspensions. Fundamentally, an active suspension varies the suspension force using controllable force actuators and replaces the spring and damper setup, while a semi-active suspension varies the rate of energy dissipation by changing the damping coefficient and is used in parallel with a conventional spring (Maiorana et al., 2005). Both types of suspension system operate

based on certain control strategies which have been researched since the past decades. Thus, to gain an insight into controllable suspension systems, this section reviews the concepts, realizations and most importantly the control strategies associated with active and semi-active suspensions.

2.2.1 Active suspension system

Conceptually, a vehicle suspension is considered active when the suspension is capable of both dissipating and introducing energy to the system (in contrast to a passive suspension which can only dissipate system energy). In a typical active suspension system, a force actuator is used to replace the spring and damper found in passive system so that a control force can be applied to the suspension according to the implemented control strategy or controller, although some active suspensions might employ passive spring and damper as a fail-safe approach (for example as in the study by Ebrahimi et al. (2011)) or to reduce the required force to be generated by the actuator. Traditionally, active suspension system was realized using hydraulic actuators; however, recent researches on active suspensions mostly favored the use of linear permanent magnet electric machines as actuators. For instance, the study by Gysen et al. (2011) tested a prototype active suspension which employed a direct-drive tubular (linear) permanent magnet actuator functioning in both electrical motor and generator modes.

A look into the literatures on active suspension system shows several control strategies or controllers which can be implemented. A common approach is to apply the linear optimal control theory and solve the Ricatti's equation to obtain an expression of control force as feedback (Thompson, 1976, 1984; Wilson et al., 1986). According to the study by Wilson et al. (1986), there are two types of feedback, namely full-state

feedback and limited-state feedback. These are described in equations (2.5) and (2.6) respectively.

$$U = k_{f1}(z_u - z_g) + k_{f2}(z_s - z_g) + k_{f3}\dot{z}_u + k_{f4}\dot{z}_s \qquad (2.5)$$

$$U = k_{l1}z_u + k_{l2}z_s + k_{l3}\dot{z}_u + k_{l4}\dot{z}_s \qquad (2.6)$$

in which U is the control or actuator force, z_s, z_u and the respective derivatives are the displacement and velocity of the sprung and unsprung masses, z_g is the road displacement, while k_{f1}, k_{f2}, k_{f3}, k_{f4} are the optimal full-state feedback gains for a given set of weighting constants in the performance index (Wilson et al., 1986) and k_{l1}, k_{l2}, k_{l3}, k_{l4} are the limited-state feedback gains found through gradient search (Crolla & Whitehead, 2003).

Apart from the above strategy, another commonly adopted strategy is the well-established proportional-integral-derivative controller more commonly known as the PID controller. For example, the design of a hydraulic-based active suspension system using the PID controller is detailed by Mouleeswaran (2012). Generally, the controller has a form as shown in equation (2.7):

$$U = K_p e(t) + \frac{K_p}{T_i} \int_0^t e(t)dt + K_p T_d \frac{de(t)}{dt} \qquad (2.7)$$

in which U is the input (in this case the control current), $e(t)$ is the error, K_p is the proportional gain, while T_i and T_d are the integral and derivative time constants for the controller. To date, advancements in active suspension research have resulted in more comprehensive controllers, such as advanced fuzzy and sliding-mode controllers as

found in recent studies (H. Li et al., 2012; H. Li et al., 2013) which consider factors such as sprung and unsprung mass variations and actuator fault apart from suspension performance criteria.

However, although an active suspension is capable of achieving much superior suspension performance compared to the corresponding passive suspension, a commonly known disadvantage is that it requires significant power consumption for its operation (Cao et al., 2011). This is a major obstacle to its wide-spread adoption. More often than not, it is the semi-active suspension system, serving as a compromise between passive and active systems, that is employed. This will be elaborated in the section that follows.

2.2.2 Semi-active suspension system

Fundamentally, a semi-active suspension is similar to a passive suspension as they both employ a spring and a damper for their suspension configurations. However, a particular feature of semi-active suspension system is that the system involves variable damping characteristic as opposed to a passive system which has constant damping characteristic. Similar to active suspension system, the semi-active suspension system also provides superior performance; however, unlike the former, a semi-active suspension does not input energy to the system and only relies on variable rate of energy dissipation for its performance advantage. The capability of variable damping is usually achieved through the use of damper that is capable of varying its characteristic through adjustable orifices or through fluid with variable viscosity like the magnetorheological fluid (Goncalves, 2001) and the electrorheological fluid. Of the two methods, rheological fluid is more commonly adopted due to advantages such as the response time of within a few milliseconds (Yao et al., 2002) which is faster compared to the former. For

magnetorheological and electrorheological dampers, the variation of damping rate is achieved by directly changing the fluid viscosity in the presence of magnetic field (Bajkowski et al., 2008) and electric field (Choi et al., 1998) respectively.

Semi-active suspensions involving semi-active dampers can also be classified into two types: the continuously variable damper and the discrete two-state or multi-state switchable damper. Both types involve slightly different control algorithms, but the general strategies are the same. According to literature (Crolla & Whitehead, 2003), a continuously variable damper is theoretically capable of tracking a force demand signal independently of the velocity across the damper. In this type of semi-active damper, the control law as described previously for active suspension system can be adopted here. For example, assuming limited-state feedback control, the required damper force and the associated logical statement are stated in equation (2.8):

$$U = [k_{l1}(z_u - z_s) + k_{l2}\dot{z}_u + k_{l3}\dot{z}_s] - k(z_u - z_s),$$

if $(\dot{z}_u - \dot{z}_s)U > 0,$ demand signal $= U,$

else,   demand signal $= 0$ (2.8)

in which U in this case represents the required control force that will be provided by the variable damper after the exclusion of the spring force (the most ride-hand-side term where k is the stiffness), and other variables are as defined previously. Also, because a variable damper can only dissipate energy, the additional logical statement shows that when there is demand of power or energy input, the damper simply sets zero or negligible damping.

For semi-active suspension system, a widely researched control strategy is the well-known Skyhook strategy, which was first proposed by Karnopp et al. (1974). The basic idea of this strategy is to control the sprung mass response by a damper connected to a fixed point in the sky, hence the name 'Skyhook' which is a conceptual implementation and is physically not possible. For a semi-active suspension with variable damper, an approximation to ideal Skyhook strategy is given by the following control law (Guglielmino et al., 2008):

$$\text{if } \dot{z}_s(\dot{z}_s - \dot{z}_u) > 0, \qquad F_{damper} = c_{sky}\dot{z}_s,$$
$$\text{else}, \qquad F_{damper} = 0 \tag{2.9}$$

in which F_{damper} is the required damping force and c_{sky} is the Skyhook damping coefficient. This algorithm can be realized for a variable damper assuming that the damper can adjust its damping characteristic within its range of maximum and minimum damping rates, c_{max} and c_{min} to match the required force term, F_{damper} determined by Skyhook damping coefficient. In mathematical terms, the required damping coefficient, c can be determined from equation (2.10) (Liu et al., 2005):

$$\text{if } \dot{z}_s(\dot{z}_s - \dot{z}_u) > 0, \qquad c = max\left[c_{min}, min\left[\frac{c_{sky}\dot{z}_s}{(\dot{z}_u - \dot{z}_s)}, c_{max}\right]\right],$$
$$\text{else}, \qquad c = c_{min} \tag{2.10}$$

In practice, though, Skyhook control strategy's implementation is also studied for discrete switchable semi-active dampers, for example a simple two-state switchable damper. When a two-state switchable damper is used, the modified control law becomes a switching algorithm as shown in equation (2.11):

if $\dot{z}_s(\dot{z}_s - \dot{z}_u) > 0,$ $c = c_{max},$

else, $c = c_{min}$ (2.11)

For the implementation of Skyhook control strategy in two-state switchable damper, the physical interpretation is as follows: when the sprung mass is moving in the same direction as the relative motion between sprung and unsprung masses, maximum damping rate, c_{max} is set to resist sprung mass motion. Conversely, if both have opposite directions, then minimum damping rate, c_{min} is set. Thus, excessive sprung mass response is controlled at the expense of deteriorating unsprung mass response (Levesley et al., 2007). Besides the usual switching algorithm, other variants of Skyhook strategy have also been researched before. For instance, a study (Savaresi et al., 2003) explored the Skyhook strategy which considered sprung mass acceleration as the decision criterion rather than sprung mass velocity as in the usual implementation. Also, another study (Shen et al., 2006) evaluated, among others, a modified semi-active Skyhook control strategy which was dependent on jerk of the sprung mass instead.

As Skyhook damping is a relatively straight-forward concept (that is, attaching a damper between a fixed point and the targeted mass to control its response), it can be used with modifications to derive other conceptually similar strategies, namely the Groundhook and the hybrid control strategies. For Groundhook control strategy, instead of attaching a damper to the sky to control sprung mass movement, a ground-mounted damper is used to control unsprung mass movement. The control law for Groundhook strategy is stated in equation (2.12) (Goncalves & Ahmadian, 2003):

$$\text{if} - \dot{z}_u(\dot{z}_s - \dot{z}_u) > 0, \qquad F_{damper} = c_{gnd}\dot{z}_u,$$

$$\text{else,} \qquad F_{damper} = 0 \tag{2.12}$$

in which c_{gnd} is the Groundhook damping coefficient. Note that apart from the different philosophies, equation (2.12) actually resembles equation (2.9). Meanwhile, the hybrid control strategy combines both concepts from Skyhook and Groundhook to take advantage of the benefits of the two strategies. Specifically, hybrid control strategy operates based on equations (2.13) to (2.15) (Goncalves & Ahmadian, 2003):

$$\text{if} \ \dot{z}_s(\dot{z}_s - \dot{z}_u) > 0, \qquad \sigma_{sky} = \dot{z}_s,$$

$$\text{else,} \qquad \sigma_{sky} = 0 \tag{2.13}$$

$$\text{if} - \dot{z}_u(\dot{z}_s - \dot{z}_u) > 0, \qquad \sigma_{gnd} = \dot{z}_u,$$

$$\text{else,} \qquad \sigma_{gnd} = 0 \tag{2.14}$$

$$F_{damper} = G[\alpha\sigma_{sky} + (1 - \alpha)\sigma_{gnd}] \tag{2.15}$$

in which σ_{sky} and σ_{gnd} represent Skyhook and Groundhook components, α is a relative ratio or weightage between the two strategies and G in this case is a constant gain.

Apart from the well-known Skyhook strategy and the various Skyhook-derived alternatives, another commonly employed control strategy is the force cancellation strategy. Fundamentally, the working principle of this control strategy is that the force produced by the suspension is controlled such that it opposes and thus cancels the oscillating force produced by the spring (Yeh & Tsao, 1992). The force cancellation strategy can be used in active suspensions just like the Skyhook strategy; however, more

practically, it is used in a semi-active suspension system employing a switchable or variable damper. When applied to a switchable damper, the idea of this strategy is to balance the spring force by means of the damper force as long as these forces act in opposite directions, and to set damper force either to zero or to a minimum value when the forces have the same direction (Guglielmino et al., 2008). Hence, if a two-state switchable damper is used, the switching algorithm can be represented as equation (2.16):

$$\text{if } (z_u - z_s)(\dot{z}_u - \dot{z}_s) \geq 0, \qquad c = c_{min},$$

$$\text{else}, \qquad c = c_{max} \tag{2.16}$$

Finally, another strategy that is worth discussing here is the semi-active control based on limited relative displacement method. Generally, for this type of control strategy, the switching between damping states is based on criterion associated with the relative displacement between sprung and unsprung masses. According to Shen et al. (2006), the control law can be expressed in the form of equation (2.17):

$$\text{if } |z_u - z_s| \geq a, \qquad c = c_{max},$$

$$\text{else}, \qquad c = c_{min} \tag{2.17}$$

in which a is the limit of the relative displacement between sprung and unsprung masses. Following the same study, in the application to a semi-active switchable damper, high damping is set when the relative displacement is greater than a specific value to control sprung mass movement, while low damping is set otherwise. This explains the principle of limited-relative-displacement-based control strategy.

2.2.3 Comparison of control strategies

From the descriptions above, there are clearly various control strategies that can be applied to active and semi-active suspension systems to give improvement in suspension performance. Comparison among the suspension systems as well as the control strategies provides some remarks that are worth discussing. Firstly, it is generally accepted that the active suspension system is superior to the semi-active suspension system, although it should be noted that suspension performance advantage also depends on the directions of the design and optimization for these systems. To illustrate, the study by Ben et al. (2014) compared the ride performance of passive, semi-active and active suspension systems for off-road vehicles, and determined that the response of linear quadratic regulator active suspension was better than that of the hybrid semi-active suspension (both superior to the passive suspension). Meanwhile, evaluations among the semi-active control strategies mentioned in the previous section showed that different semi-active strategies have different characteristics. For example, the study by Faris et al. (2010) investigated Skyhook, Groundhook and hybrid control strategies by comparing them to passive suspension. From the study, it was concluded that the Skyhook strategy generally improved sprung mass responses but also increased the unsprung mass responses, while the Groundhook strategy did the opposite. Hybrid control, as already described previously, achieved better compromise among the performance criteria than the other two strategies. Similarly, another comparative study (Dong et al., 2010) also demonstrated that the performance of a semi-active suspension based on magnetorheological damper is highly dependent on the choice of employed strategy. For instance, judging from the results, certain strategies like the Skyhook control maintained the ride and road holding compromise (improved ride at the expense of road holding ability) while others such as sliding mode control, fuzzy control and hybrid control that were tested improved both ride and road holding criteria, showing

that the above mentioned compromise can be eliminated. Finally, it is worth to mention that some control strategies (like the linear optimal control) are model-based algorithms for which the controllers are designed around the system parameters, while others (such as Skyhook, its derivatives and the force cancellation strategy) are model-free algorithms for which prior knowledge of the system parameters is not essential (Cao et al., 2011). Therefore, even though all controllable suspension systems in general are superior to the passive counterpart, the selection of a particular control strategy to be implemented still requires careful consideration.

To summarize, this part of review has highlighted several control strategies that are commonly studied, and these algorithms become the basis of several parts of current research. For example, in Chapter 3, the Skyhook strategy for two-state switchable damper, and the linear optimal control for both continuously variable damper and active suspension were used to analyze the effect with parallel inerter, while modifications of the force-cancellation-based and displacement-based strategies were adopted directly in the inerter in Chapter 4. Additionally, in Chapter 5, a switching algorithm derived from the two-state switchable Skyhook strategy was used in the assessment of a modified suspension layout incorporating concept borrowed from the inerter.

2.3 Electromagnetic Damping

From the energy point of view, a damper in suspension system functions as an energy dissipater as it dissipates the unwanted vibrational kinetic energy of the system to the surrounding. For a regular fluid or viscous damper, the kinetic energy is converted to thermal energy due to the resistance or viscosity of the fluid in the damper. Apart from viscous damping, another way of achieving damping effect is to utilize electromagnetic induction to convert the kinetic energy from the system's vibration or movement to

electrical energy before harnessing it for energy regeneration purpose. This type of damping is commonly known as electromagnetic damping. Physically, electromagnetic damping can be realized through the use of permanent magnet electric machines like an electric generator. In fact, the use of permanent magnet electric machines as dampers for suspensions has already been proposed very early in studies such as that by Karnopp (1989); however, it was in the past decade that extensive studies on electromagnetic damper were carried out as the matter of energy conservation and regeneration became more important.

In general, studies on electromagnetic suspension have shown several approaches in realizing an electromagnetic damper. A fundamental approach is to add a rotary generator to a fluid damper for a combined damping device. To illustrate, in the study by Choi et al. (2009), a rotary generator which was driven by a rack-and-pinion mechanism was attached to an electrorheological viscous damper to realize a regenerative as well as variable damper. However, a more common approach among the studies is to use a linear electromagnetic device directly as the suspension damper, since the suspension movement is translational by nature. For instance, studies by Mirzaei et al. (2001) and Mirzaei (2007) introduced an electromagnetic shock absorber or damper to be used in vehicles. The proposed electromagnetic damper used a current-carrying primary winding to generate the magnetic flux density, while a secondary winding was used to induce electromotive force. In the studies, the characteristic of the proposed damper model was represented mathematically as in equation (2.18):

$$F_{damper} = \left(\frac{2\pi ahdB^2}{\rho}\right)(\Delta \dot{x}) \tag{2.18}$$

in which F_{damper} is again the damper force, $\Delta\dot{x}$ represents the relative velocity of the damper, a, h, d in this case are the dimensional parameters of the cylindrical secondary winding, B is the radial magnetic flux density of the air gap due to the primary winding, and ρ in this equation is the resistivity. Also, in the studies, it was mentioned that the damping coefficient represented by the combined term in equation (2.18) can be adjusted by varying the field current to vary the external magnetic field. Another example to the research on linear electromagnetic damper is the study by Zuo et al. (2010). In the study, the electromagnetic damper, named as electromagnetic energy harvester, was designed and analyzed. From the analysis, it was expected that the system would be able to harvest 16 – 64 W of power at typical suspension velocity. From these studies, it can be seen that electromagnetic damping is very closely associated with regenerative suspensions. This is mainly because the vibrational kinetic energy has to be converted to an extractable and usable form before being reused.

2.3.1 Eddy current damping

In the simplest description, eddy currents are currents induced in a conductive material in the presence of a magnetic field. Due to the electrical resistance, the induced currents will be dissipated into heat at the rate of I^2R (Sodano et al., 2005a) where I is the current and R is the resistance of the conducting material. Dynamically, the interaction of eddy current with the magnetic field will result in a force that opposes the initial motion (Gay, 2005) as described in equation (2.19), which serves as the damping force.

$$\boldsymbol{F} = \boldsymbol{J} \times \boldsymbol{B} \tag{2.19}$$

in which *F* is the Lorentz force opposing the motion, *J* is the current density which is representative of the induced eddy current and *B* is the magnetic flux density of the externally applied magnetic field.

Conceptually, an eddy current damper has the same working principle as an electromagnetic damper as both of them involve the conversion of kinetic energy to electrical energy by means of electromagnetic induction. However, for an eddy current damper, the resulted electrical energy is not harnessed; instead, the induced electrical current, in this case the eddy current, simply flows in the conductor, causing the electrical energy to be dissipated through resistive heating. Thus, an eddy current damper can be considered as a specific type of electromagnetic damper which does not regenerate the converted energy.

In comparison to electromagnetic damper or suspension, the eddy current damper generally receives less attention as it lacks the regenerative capability of an electromagnetic counterpart. Yet, there are still fundamental studies regarding its use as an additional source of passive damping. In 2005, Sodano et al. (2005a) investigated damping caused by eddy current in a vibrating cantilever beam. The study employed a permanent magnet that was placed close to a conducting sheet attached to a cantilever beam to evaluate the beam's response. From the findings, it was determined that the presence of eddy current damping increased the damping ratio by up to 150 times compared to the structure's initial damping and thus provided sufficient damping force to quickly suppress the beam's vibration. In a latter study, Sodano et al. (2006) improved the eddy current damping model by using two permanent magnets with like poles facing each other instead of relying on only one permanent magnet for the magnetic flux. They concluded that this had significantly outperformed the previously

studied model with only single magnet. For both studies mentioned above, the resulted eddy current damping effect acted as passive damping, since the externally applied magnetic field (due to the permanent magnets) was constant. However, several studies have shown that variable damping for an eddy current damper is possible when the magnetic field is varied. For example, in 2005, Sodano et al. (2005b) proposed a semi-active eddy current damping concept for the same cantilever beam vibration system. Essentially, the damper functioned by allowing the position of the magnet to change relative to the beam, thus maximizing the relative motion or velocity and significantly increasing the damping force. Also, studies by Sodano and Inman (2007, 2008) demonstrated the use of similar active eddy current damper. In the studies, the active damping was realized by utilizing electromagnet to replace the permanent magnet as in the earlier study by Sodano et al. (2005a), and then dynamically modifying the current flowing through the coil to generate a time-varying magnetic field. By this way, the damping force could be controlled.

In practice, the use of eddy current damping in vehicles is actually more widely investigated in the form of electromagnetic braking system. Although suspension and braking represent two distinct vehicle sub-systems, it should be noted that the implementation of eddy current retarder involves the same concept of converting kinetic energy to eddy current (electrical energy) before dissipating the energy as heat. For braking system, eddy current is induced in a rotating conductor in the presence of magnetic field, and the rotational motion is slowed down by the generated opposing torque. In a related research (Gay, 2005), a magnetic brake was analyzed by simulations and experiments to determine its possible application in vehicles. In the study, it was mentioned that some benefits of eddy current braking include its contactless nature and the brake force controllability by controlling the magnitude of flux source. To elaborate

on eddy current braking system slightly further, another study (Long et al., 2009) simulated the braking torque of an eddy current retarder which employed excitation coils rather than permanent magnets, while the study by Ying et al. (2010) explored the use of eddy current braking device in high-speed train braking system.

Perhaps one of the most related researches regarding eddy current damper's application in vehicle suspensions is the recent study by Ebrahimi et al. (2009). In the study, they proposed and tested a linear eddy current damper consisting of a mover, slotted with permanent magnets, which slid inside a hollow cylindrical conductor. More importantly in this study, the prototype of the eddy current damper was compared to existing dampers to analyze its applicability in vehicle suspensions, and it was shown that a full-scale eddy current damper attained comparable damping force in compression but less in extension compared to fluid dampers. In addition, the study also proved its robustness to demagnetization in a theoretical heat transfer analysis. These findings primarily pointed to possible application of linear eddy current dampers in vehicle suspensions. Actually, prior to the study, Ebrahimi et al. (2008) had already proposed a design of magnetic shock absorber based on eddy current damping effect. According to the study, the magnetic shock absorber utilized two permanent magnets with like poles facing each other to provide the springing effect and adopted a conductive aluminum plate, positioned around the strut, to generate eddy current damping effect. In addition to the analysis of the shock absorber model, the study also pointed out some advantages of the damping part (which was essentially an eddy current damper), including its non-contact and oil-free nature. In 2011, Ebrahimi et al. (2011) extended the previous study on linear eddy current damper (Ebrahimi et al., 2009) by adopting such damper as a source of passive damping in addition to an active electromagnetic damper to form a hybrid electromagnetic damper. According to the study, the presence of passive eddy

current damping provided reliability to the active electromagnetic damper in the case of power breakdown. The study stated that by introducing eddy current damping to the active part, a passive damping typical of passenger vehicle application (approximately 1570 Nsm^{-1} as stated in the study) can be achieved to act as fail-safe guarantee to the active part.

From the review above, it can be seen that the capability of eddy current to provide damping or generally motion retarding effect has been proven fundamentally, as well as specifically to vehicle suspension application. However, it is worth mentioning that the applicability of eddy current damping in vehicle suspensions has only been explored for linear damper, while rotary eddy current damper has only been studied as eddy current brakes rather than as damper. The rotary eddy current damper design will be considered in Chapter 3 (Section 3.3) when assessing the practicality of a realization of parallel inerter layout in which the inerter is made to incorporate eddy current damping to form a combined device.

2.4 Multi-objective Optimization

In many instances, the design and analysis of engineering problems, including vehicle suspension design and assessment, require optimization work. In general terms, optimization is simply the determination of the best solution for an engineering problem under certain circumstances. Mathematically, according to literature, optimization can be defined as the process of finding the conditions that give the maximum or minimum value of a function (Rao, 2009). As a general representation, an optimization problem has the fundamental form as in equation (2.20):

$$f_{optimum} = \min[f(\boldsymbol{X})],$$

subjected to constraints:

$$g_i(\boldsymbol{X}) \le 0, i = 1, 2, 3, \dots, n,$$

$$h_i(\boldsymbol{X}) = 0, i = 1, 2, 3, \dots, r \qquad\qquad (2.20)$$

in which $f_{optimum}$ is the optimum objective, $\boldsymbol{X}$ is the vector containing the design variables, $f(X)$ is the function to be minimized which is also known as the objective function, $g(X)$ and $h(X)$ are the inequality and equality constraints while n and r are the corresponding number of constraints. In general, optimization problems can be classified as single-objective and multi-objective. Single-objective optimization problems involve only the minimization of single objective function, as described in equation (2.20). Conversely, in multi-objective optimizations, several objective functions need to be considered. For this type of optimization, the general mathematical formulation becomes equation (2.21):

$$f_{optimum} = \min[f_1(\boldsymbol{X}), f_2(\boldsymbol{X}), \dots, f_n(\boldsymbol{X})] \qquad\qquad (2.21)$$

There are two approaches when dealing with multi-objective optimization problems. The first approach is to consider only one objective function by either combining the individual functions into a single composite function or by moving all but one objective to the constraint set (Konak et al., 2006). However, there are some inherent challenges in optimization when considering this approach: the former method with aggregated objective function requires suitable weightages for individual objectives which can be difficult to determine (Konak et al., 2006), while the latter method only evaluates one objective at a time and does not consider the interaction among the objectives. Besides the first approach, the other approach in multi-objective

34

optimization is to determine a set of equally optimal solutions rather than coming to a particular single solution as in previous approach. This approach is known as the Pareto optimization.

2.4.1 Pareto optimization

As mentioned above, Pareto optimization is the approach of solving multi-objective problems with the intention of returning a set of equally non-dominated solutions called the Pareto optimal solutions. In this approach of optimization, a solution to multi-objective problem is considered Pareto optimal if and only if there does not exist another solution that dominates it. In other words, a solution is non-dominated if there is no other solution that can improve at least one of the objectives without the degradation of any other objective (Ngatchou et al., 2005). Then, the non-dominated Pareto optimal solutions form the Pareto set, and the corresponding optimal values of the objective functions form a frontier in the design space which is known as the Pareto front.

An important advantage of the Pareto approach over the aggregated objective function approach is that by obtaining a set of optimal solutions, the trade-off among the different individual objectives is better reflected. This makes it suitable to be used in problems involving conflicting design objectives or criteria. A quick look at the related past studies demonstrates the usefulness of Pareto optimization in various situations. For instance, Van Sickel et al. (2008) applied this approach in a power plant model by examining the relevant Pareto fronts, as well as evaluated different optimization techniques which generated the fronts. Meanwhile, Johnsson et al. (2012) opted for the Pareto approach to optimize railway bogie suspension damping considering safety, ride comfort and rate of wear on the wheels and rails as the objectives. The optimized passive damping in the bogie suspension successfully enhanced safety and comfort,

which in turn allowed higher train speeds. Elsewhere, in another study (Maciejewski et al., 2011), the Pareto approach was used in the optimization of non-linear seat suspension system for an earth-moving machinery. In addition, another common application area of Pareto optimization is the road vehicle suspension design, since the typical performance measures, namely ride comfort, road holding and suspension travel are naturally conflicting. For example, Bagheri et al. (2011) employed Pareto optimization in a two-DOF vehicle model to obtain Pareto optimal suspension design solutions, and selected some solutions for subsequent assessment on the suspension responses using the same vehicle model. Also, Crews et al. (2011) used the Pareto approach to analyze several controllers for semi-active suspension system by comparing them to the Pareto optimal semi-active control solutions.

In general, Pareto multi-objective optimization offers a suitable method in the design of vehicle suspensions as well as in the evaluation of performance among different vehicle suspension systems. In this research, the approach was employed in several comparative studies to assess the superiority of a suspension case to another, for instance in the evaluation of performance benefits brought by passive inerter (Chapter 3), the analysis of suspension cases employing switchable inerter (Chapter 4), and the assessment of suspension performance for a modified suspension layout (Chapter 5).

Overall, this chapter has presented a comprehensive review on the inerter (Section 2.1) and has also provided descriptions on the concepts and method involved in this research (Sections 2.2 to 2.4). Moving back to the core area of this research, critical judgment can be made based on the review on inerter studies. In general, it can be seen that although past studies have demonstrated the benefit of using inerter in various suspension applications, most of them only concentrated on proving the possibility of

36

having performance advantage, while several other aspects which also contribute to the overall applicability, such as practicality in terms of versatility and realization, suitability of the achievable performance and potential of concept utilization have not been evaluated. In addition, most studies adhered to the conventional implementation of inerter by considering only the passive suspension context. In the subsequent chapters, these aspects of applicability of inerter in passenger vehicle suspensions will be evaluated for the new implementations involving interaction between inerter and controllable suspension systems.

CHAPTER 3 APPLICATION OF INERTER IN PASSENGER VEHICLE SUSPENSIONS

From the literature review of inerter in Section 2.1, it can be seen that the inerter has already been theoretically proven to be capable of providing performance benefits to passive vehicle suspensions. However, as first pointed out in Chapter 1, certain limitations which affect its use in passenger vehicle suspensions still exist. For instance, regarding the practical consideration, although various suspension layouts employing inerter are possible in theoretical analysis, their actual implementation is not particularly practical because of the limited design space around a passenger vehicle suspension. Thus, the work in Chapter 3 attempts to examine the practicality of implementing inerter as an additional element in passenger vehicle suspension systems. The workflow of this part of research is as follows: in the first part, the interaction of inerter with both passive and several controllable vehicle suspension systems was studied to assess the versatility of an inerter to be applied in vehicle suspensions and secondarily also to determine possible further suspension performance improvement when the inerter was paired with controllable suspensions instead of passive suspensions. This involved the use of a two-DOF, mathematical-based quarter vehicle model with typical passenger vehicle parameter values as the medium of study. The versatility in terms of performance consistency was evaluated by simulating vehicle responses when subjected to ground excitations, namely step and random profiles as the road inputs, using the co-simulation approach. Meanwhile, in the latter part, the practical aspect of a physical implementation of parallel inerter arrangement was studied by investigating the feasibility of an inerter incorporating eddy current damping to be applied in passenger vehicle suspensions. In this part, the achievable inertance was determined by mathematical design of inerter based on the governing equations for both ball-screw and

rack-and-pinion designs, while the suitability of eddy current damping was assessed based on electromagnetic transient simulation. These are discussed comprehensively in Sections 3.1 and 3.2 for the former, and Section 3.3 for the latter.

3.1 Working Principle of Inerter

Fundamentally, both inerter and spring are similar elements in a suspension system because they are energy storing elements as opposed to a damper which is an energy dissipater. In an early study of inerter, Smith (2002) considered the inerter as a mechanical-dual of spring. However, a difference between the two is that spring reacts to relative displacement while inerter reacts to relative acceleration. Hence, although similar, these two elements actually complement each other in a suspension system. For example, a recent study (Nie et al., 2010) highlighted a complementary property of inerter in an effort to justify the working principle of a serial inerter. According to the study, spring is good at attenuating high-frequency vibration, while inerter excels at isolating low-frequency vibration. Therefore, a suspension incorporating a spring-damper combination in series to an inerter-damper combination will theoretically attenuate vibration for a wider frequency range (Nie et al., 2010). While this rationale is true for serial inerter layout, it does not justify the performance improvement of suspensions with parallel inerter reported in previous studies since a parallel arrangement between spring and inerter, following the proposed explanation, will worsen the vibration isolation instead. This suggests that there exist other justifications to the effectiveness of a parallel inerter.

One way of explaining the vibration isolating capability of a suspension with parallel inerter is through the dynamical reasoning because the suspension performance (for instance, the measure of ride comfort) is associated to the acceleration of sprung

mass which, in turn, is dependent on the suspension force acting on the sprung mass. To investigate the complementary behavior between spring and inerter from the dynamical point of view, consider a simple suspension setup made up of the two elements with one terminal grounded or fixed and the other subjected to a sinusoidal displacement input as in Figure 3.1. Due to the input, forces are generated by both the spring and the inerter following equations (3.1) and (3.2) respectively. The resultant of forces forms the suspension force which is shown in equation (3.3):
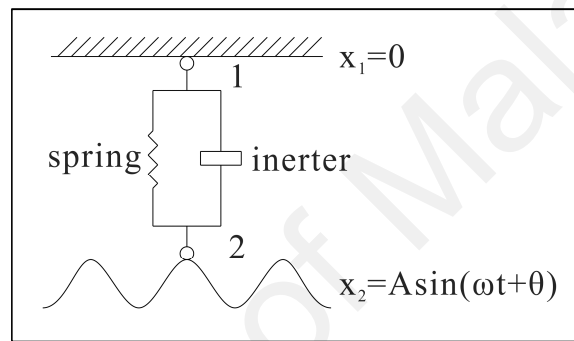
Figure 3.1: Simple suspension setup with spring and inerter in parallel layout

$$F_{spring} = k(x_2 - x_1) = k[A\sin(\omega t + \theta)] \tag{3.1}$$

$$F_{inerter} = b(\ddot{x}_2 - \ddot{x}_1) = b[-\omega^2 A\sin(\omega t + \theta)] \tag{3.2}$$

$$F_{resultant} = F_{spring} + F_{inerter} = (k - b\omega^2)[A\sin(\omega t + \theta)] \tag{3.3}$$

in which F_{spring}, $F_{inerter}$, $F_{resultant}$ are the spring, inerter and resultant (or suspension) forces, k is the spring stiffness, b is the inertance, x_1, x_2 are the displacements at terminals 1 and 2, $\ddot{x}_1$, $\ddot{x}_2$ are the corresponding accelerations, $A\sin(\omega t + \theta)$ is the sinusoidal input with amplitude A, frequency ω and phase angle θ. The complementary property between inerter and spring can be seen in equation (3.3). It is known that

acceleration is anti-phase to displacement since it is the double derivative of the sinusoidal input. Because inerter reacts to relative acceleration while spring reacts to relative displacement, the forces due to them are also anti-phase to each other. Due to the opposition of forces, the resultant force is lowered, if not eliminated at specific frequency, thus contributing to superior vibration isolation to a sprung mass. The force cancellation scenario is illustrated in Figure 3.2 which shows that the root-mean-squared (RMS) value of suspension force approaches zero under specific frequencies for stiffness, $k = 400$ Nm^{-1} and inertance, b ranging from 0 kg to 10 kg.
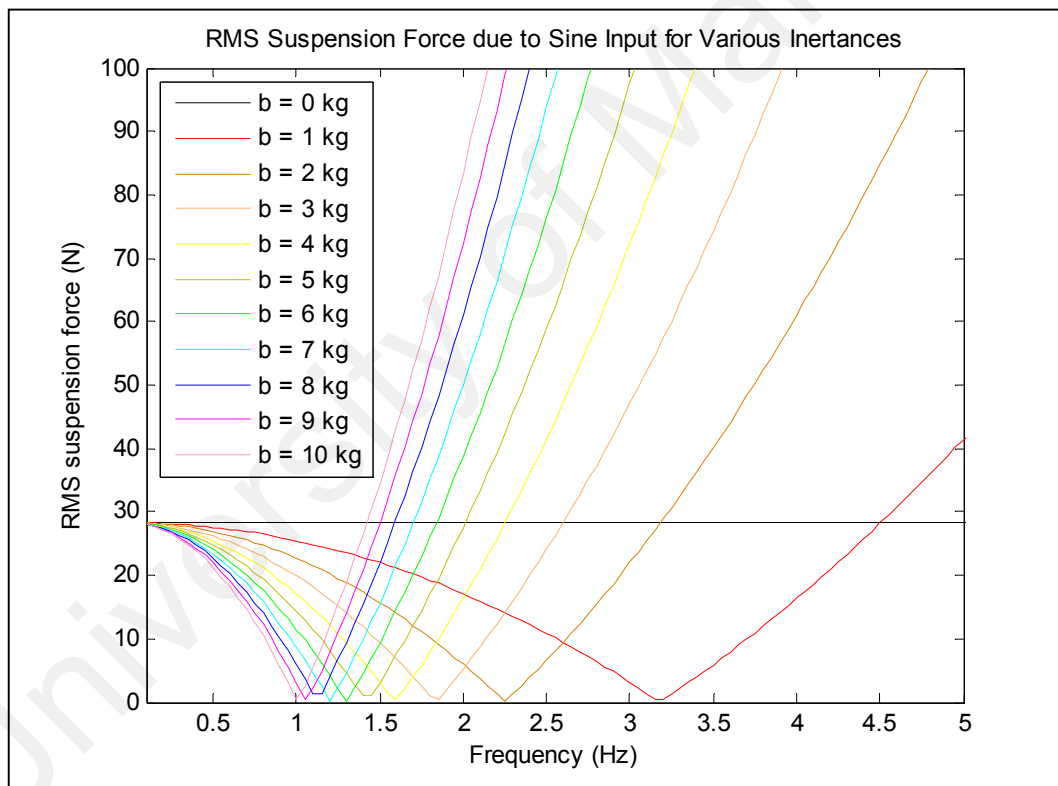
Figure 3.2: RMS value of suspension force for various frequencies of the sinusoidal input

It is worth noting the resemblance of this situation to resonance experienced by a typical mass-spring-damper system. During resonance, the spring force and the inertial

force of the mass eliminate each other, causing large oscillatory motion to the mass only to be limited by damping within the system. Meanwhile, for suspension setup with parallel inerter, similar elimination occurs between spring and inerter forces, leaving a sprung mass undisturbed and isolated.

As the dynamical complementary property of a parallel inerter is generally applicable, the interaction between spring and inerter forces can be used to justify the effectiveness of parallel inerter in a specific application, namely passive vehicle suspension where its performance benefits have been proven in previous studies (C. Li et al., 2012b; Smith & Wang, 2004). Unlike typical suspension applications in which the sole objective is to provide isolation to a sprung mass, a vehicle suspension not just serves the purpose of isolating the vehicle body from roughness in the road, but also ensures tire-road contact with minimal load variation (Gillespie, 1992). The former is important to provide ride comfort especially for passenger vehicles, while the latter ensures good tire road holding ability which is indirectly related to vehicle handling and safety. This part of work generally focuses on the justification of ride comfort, that is, vibration isolation achieved by a vehicle suspension with parallel inerter which is primarily measured by the RMS sprung mass acceleration when the vehicle is under road excitation. A simple, two-DOF quarter vehicle model, which consists of sprung and unsprung masses representing vehicle body and wheel, is used in the following analysis, as well as in most analyses throughout the research. According to a study by Georgiou et al. (2007), this model is commonly used in the prediction of dynamic response as well as the performance of parameter identification, optimization and control studies of ground vehicles. In a related study by Verros et al. (2005), it was pointed out that this is mostly due to the model's simplicity in representing a vehicle and the qualitatively correct information it provides especially for ride and handling

studies. The use of mathematical vehicle model in this research is also consistent with earlier studies on the inerter element (Kuznetsov et al., 2011; C. Li et al., 2012b; Smith & Wang, 2004).

In the analysis, considering parallel suspension layout, the inerter was added in parallel to existing suspension setup comprising of both a spring and a damper which were also parallelly arranged as in most actual vehicle suspensions. This is shown in Figure 3.3. The system can be conveniently solved to obtain suspension response by solving the equations of motion (equations (3.4) and (3.5)) derived from the system's free-body diagram.

$$m_s\ddot{z}_s = k(z_u - z_s) + c(\dot{z}_u - \dot{z}_s) + b(\ddot{z}_u - \ddot{z}_s) \tag{3.4}$$

$$m_u\ddot{z}_u = k_t(z_g - z_u) - k(z_u - z_s) - c(\dot{z}_u - \dot{z}_s) - b(\ddot{z}_u - \ddot{z}_s) \tag{3.5}$$
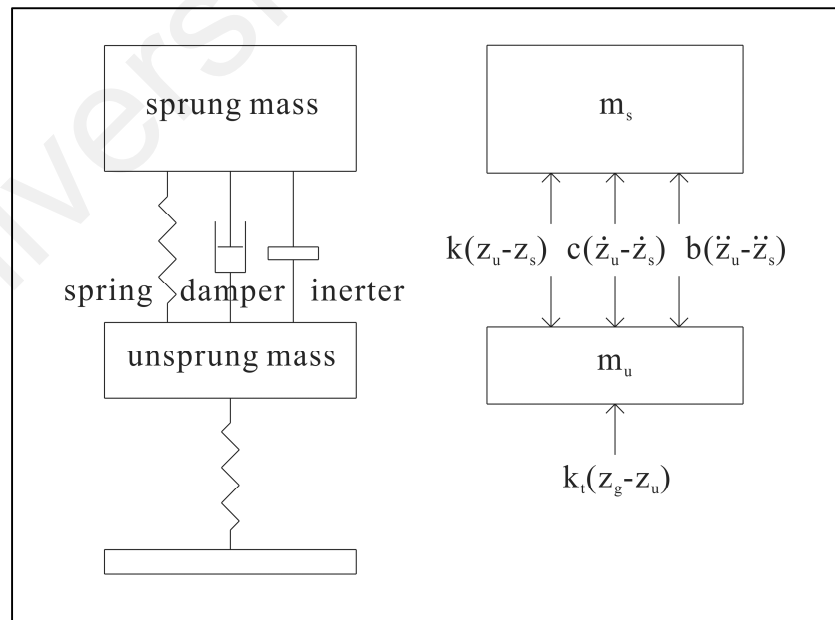
Figure 3.3: Quarter vehicle model with parallel inerter and its free-body diagram

in which m_s, m_u are the sprung and unsprung mass values, z_s, z_u are the sprung and unsprung mass displacements, $\dot{z}_s$, $\dot{z}_u$, $\ddot{z}_s$, $\ddot{z}_u$ are the corresponding velocities and accelerations, z_g is the vertical road displacement, k_t, k, c, b, are the tire stiffness, suspension stiffness, damping rate, and inertance respectively. Since ride was the primary focus in the analysis, the vehicle parameters in the equations of motion had values typical of a passenger vehicle, as stated in Table 3.1.

Table 3.1: Relevant parameters of the quarter vehicle model (Crolla & Whitehead, 2003)

Parameter	Value
Sprung mass, m_s (kg)	317.5
Unsprung mass, m_u (kg)	45.4
Suspension stiffness, k (Nm^{-1})	22000
Damping coefficient, c (Nsm^{-1})	1500
Tire stiffness, k_t (Nm^{-1})	192000

Input to the system came from the vertical road displacement, z_g which had a simple step profile with 0.1 m height in the study. Step input is commonly used in analyses involving quarter vehicle model, and it also allows the sprung and unsprung masses to oscillate at their natural frequencies, namely the body bounce and wheel hop frequencies. The system was solved iteratively for an inertance range of 0 kg $\leq b \leq$ 320 kg using mathematical software (MATLAB®/Simulink®, see Figure A1, Appendix A for the model's structure), and the suspension component forces were evaluated for the case with optimum inertance, which was determined based on the objective of minimizing RMS sprung mass acceleration (hence maximizing ride improvement). From the results obtained, the time history of spring, damper and inerter forces due to the step input for the optimum case of $b = 6$ kg is illustrated in Figure 3.4 for further evaluation.
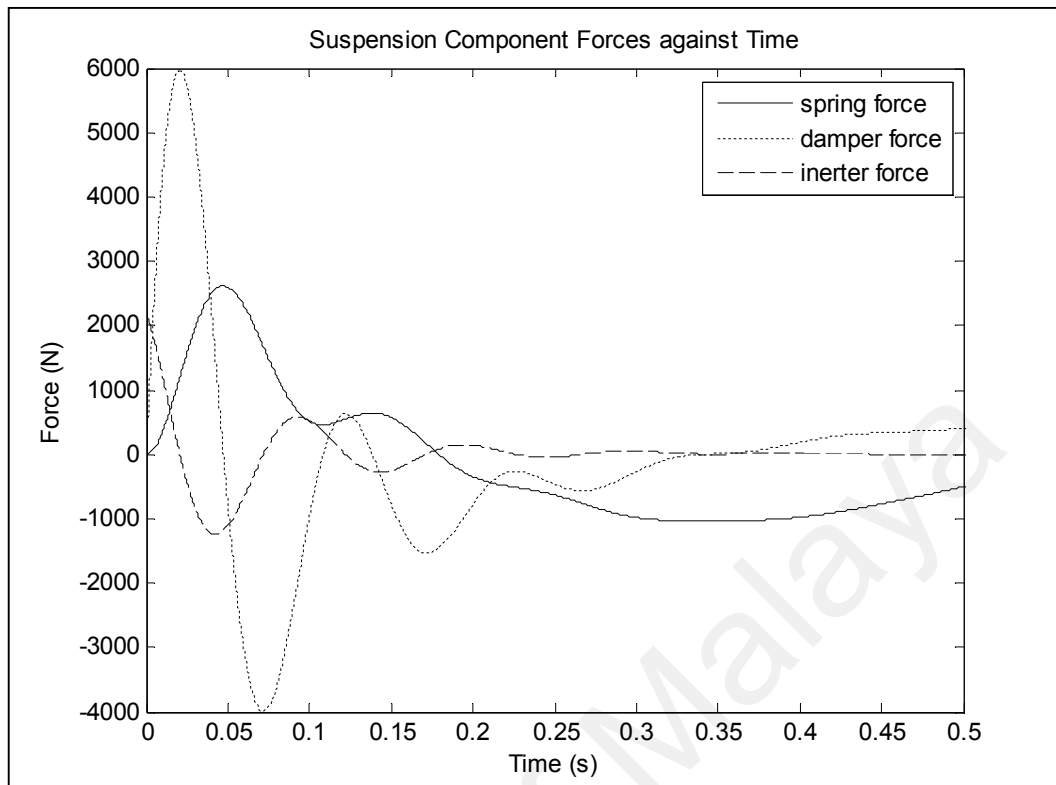
Figure 3.4: Spring, damper and inerter forces due to 0.1 m step input for optimum case

Figure 3.4 clearly illustrates the complementary or anti-phase property between a spring and an inerter. From the dynamical point of view, the opposition between these two suspension component forces resulted in reduced total suspension force acting on the sprung mass which, in turn, lowered the RMS sprung mass acceleration and led to improvement in ride comfort. The observation provided a fundamental explanation to the effectiveness of a parallelly-arranged inerter in providing better vibration isolation or better ride performance in terms of vehicle suspension application. However, although effective, the result of RMS sprung mass acceleration from the analysis showed only slight decrease from 2.0046 ms^{-2} (reference case with $b = 0$ kg) to 1.9640 ms^{-2} (optimum case with $b = 6$ kg) which was considered to be insignificant (2.03 %), when the parallel inerter was treated as an 'add-on' device to existing spring and damper associated with existing suspension parameters. This was because the damping

45

rate used in the study became unsuitably high after considering the addition of inerter, thus generating high damping force (Figure 3.4). Considering that the total suspension force in parallel suspension layout is the resultant of all component forces, the decrease in resultant force due to spring-inerter force cancellation became insignificant relative to the high damping force, inferring that both damping rate and inertance need to be simultaneously optimized in a suspension employing parallel inerter.

3.1.1 Delving into quarter vehicle model's validity

In the work presented above, it can be seen that the analysis used a two-DOF mathematical model as a representation of the dynamics of an actual vehicle. It was also mentioned that the quarter vehicle model would be used in most studies throughout the research. Considering its extensive adoption as the medium of study in the present research, it seems reasonable to delve deeper into this vehicle model as well as the numerical representation of the model in computational software to gain a better understanding on the model's usability, accuracy and validity.

In general, the use of quarter vehicle model, especially in suspension analyses, has received mixed and conflicting views. On one hand, this type of lumped-mass, mathematical-based model with only the essential DOFs representing the vehicle sprung and unsprung masses can be considered as being widely used in vehicle and suspension researches. As already pointed out previously, the model is commonly used in studies related to the dynamics of basic suspension element like the inerter (Kuznetsov et al., 2011; C. Li et al., 2012b; Smith & Wang, 2004), in controllable suspension studies (for instance, the study by Sharma et al. (1992)), and also in optimizations of vehicle parameters (such as the study by Georgiou et al. (2007)). Typically, the use of quarter vehicle model is because of its simplicity and also the fundamentally correct vehicle

response it predicts, particularly in the ride aspect (Verros et al., 2005). However, on the other hand, a quarter vehicle model does not include the representation of the vehicle details like the suspension kinematic effects, making the prediction of realistic vehicle response challenging. To illustrate, in the study by Maher and Young (2011), it was cited that although this model captures the most basic features of a real vehicle problem, when the detailed vehicle motion is required, more elaborate models which take account of features omitted from the quarter vehicle model must be used (ElMadany & Abduljabbar, 1999). Considering the views from the past researches, it is observed that a quarter vehicle model most suitably finds its use in studies concerning the evaluation of fundamental suspension concepts or implementations, so that a clear comparison with a reference setup is made possible. Thus, the current research, which deals with interactions between inerter and controllable suspension systems, logically favors the use of quarter vehicle model.

It is known that a quarter vehicle model consists of two DOFs which enable the prediction of vertical response for the sprung mass, which represents the vehicle body, as well as that for the unsprung mass, which represents the wheel and suspension assembly. For a typical model which involves only a spring and a damper as the suspension setup (that is, without the inerter component as in other parts of the current research), the equations of motion governing the two responses are stated in equations (3.6) and (3.7):

$$m_s \ddot{z}_s = k(z_u - z_s) + c(\dot{z}_u - \dot{z}_s) \tag{3.6}$$

$$m_u \ddot{z}_u = k_t(z_g - z_u) - k(z_u - z_s) - c(\dot{z}_u - \dot{z}_s) \tag{3.7}$$

which are almost identical to equations (3.4) and (3.5), apart from the omission of the inerter force term. Note that these are ordinary differential equations which contain the derivatives of the sprung mass response, z_s and the unsprung mass response, z_u. From the relevant literature (Crolla & Whitehead, 2003), it is known that if the model is entirely linear, then the system can be solved analytically, for instance directly in the frequency domain to obtain the responses as well as the suspension performance measures such as the RMS sprung mass acceleration. Conversely, if the model contains some forms of non-linearity, for example variable damping (or, in the case of Chapter 4 as will be seen later, a switchable inerter force), then the solution has to be computed numerically. Consequently, considering the non-linear elements like the semi-active damper and the inerter incorporating switching algorithm that are present in various analyses, the quarter vehicle model employed in the research was represented in MATLAB®/Simulink® and was numerically solved in the software environment with its solver (the ODE5 solver) to obtain the vehicle response in the form of sprung and unsprung mass displacements. However, even though the mathematical vehicle representation, in the general form of equations (3.6) and (3.7), is only a simple set of differential equations, it is still worth to carry out validation work on the model in MATLAB®/Simulink® prior to any meaningful result analysis, for example by checking the accuracy of the employed solver and by comparing it with a physical two-DOF system.

In the first part of validation work, it is desirable to have an idea on the accuracy of the numerical integration performed in MATLAB®/Simulink® by the selected ODE5 (Dormand-Prince) solver. The check on accuracy is best carried out by comparing the numerical solution of a quarter vehicle model against the analytical solution which can be determined for a linear system. In the study, this was done by determining the

transfer functions for both the sprung and unsprung mass responses due to the ground input, and then substituting the parameter values and solving the equations for the responses. Firstly, the two equations of motion (3.6) and (3.7) can be rewritten and combined in the matrix form:

$$\begin{bmatrix} m_s & 0 \\ 0 & m_u \end{bmatrix}\begin{bmatrix} \ddot{z}_s \\ \ddot{z}_u \end{bmatrix} + \begin{bmatrix} c & -c \\ -c & c \end{bmatrix}\begin{bmatrix} \dot{z}_s \\ \dot{z}_u \end{bmatrix} + \begin{bmatrix} k & -k \\ -k & k+k_t \end{bmatrix}\begin{bmatrix} z_s \\ z_u \end{bmatrix} = \begin{bmatrix} 0 \\ k_t \end{bmatrix} z_g \tag{3.8}$$

Applying Laplace transform to equation (3.8) results in equation (3.9):

$$\begin{bmatrix} (m_s s^2 + cs + k) & -(cs + k) \\ -(cs + k) & (m_u s^2 + cs + k + k_t) \end{bmatrix}\begin{bmatrix} z_s(s) \\ z_u(s) \end{bmatrix} = \begin{bmatrix} 0 \\ k_t \end{bmatrix} z_g(s) \tag{3.9}$$

The transfer functions for sprung mass displacement, z_s and unspsrung mass displacement, z_u due to the input, z_g can be obtained by solving the simultaneous component equations in the combined equation (3.9) using substitution or Cramer's method. Thus, after the necessary algebraic manipulations and eventually simplifications, the transfer functions for sprung and unsprung mass responses for a typical quarter vehicle model are shown in equations (3.10) and (3.11) respectively:

$$\frac{z_s(s)}{z_g(s)} = \frac{(ck_t)s + (kk_t)}{(m_s m_u)s^4 + (m_u c + m_s c)s^3 + (m_u k + m_s k + m_s k_t)s^2 + (ck_t)s + (kk_t)} \tag{3.10}$$

$$\frac{z_u(s)}{z_g(s)} = \frac{(m_s k_t)s^2 + (ck_t)s + (kk_t)}{(m_s m_u)s^4 + (m_u c + m_s c)s^3 + (m_u k + m_s k + m_s k_t)s^2 + (ck_t)s + (kk_t)} \tag{3.11}$$

Finally, by replacing the vehicle parameters with the values employed in the research (see Table 3.1), using the 0.1 m step input as in Section 3.1, and solving the

transfer functions by performing partial fraction (to obtain the standard equation form) before applying inverse Laplace transform, the analytical expressions for sprung and unsprung mass displacements as functions of time are shown in equations (3.12) and (3.13):

$$z_s(t) = 2e^{-16.9403t}(0.0021\cos(65.5784t) - 0.0026\sin(65.5784t)) +$$
$$2e^{-1.9418t}(-0.0521\cos(7.7529t) + 0.0133\sin(7.7529t)) + 0.1 \qquad (3.12)$$

$$z_u(t) = 2e^{-16.9403t}(-0.0458\cos(65.5784t) - 0.0124\sin(65.5784t)) +$$
$$2e^{-1.9418t}(-0.0042\cos(7.7529t) + 0.0039\sin(7.7529t)) + 0.1 \qquad (3.13)$$

Being expressions of time, equations (3.12) and (3.13) enabled the determination of time histories of the sprung and unsprung mass motions due to the step input, which served as the reference solution to check the accuracy of the ODE5 solver used in the MATLAB®/Simulink® model at a reasonably small time resolution of 0.001 s. Figure 3.5 shows the sprung and unsprung mass responses that were solved analytically as well as numerically.

From a qualitative point of view, it is directly observable from Figure 3.5 that both the analytical method and the numerical method of solving a linear quarter vehicle model produce solutions which are very close to each other with only very slight difference. To quantify the deviation of numerical solution from the analytical solution, comparison of the displacement values between them revealed that the maximum percentage difference for the sprung mass is 0.24 % while that for the unsprung mass is 1.52 %. Hence, judging from the closeness of the responses, although MATLAB®/Simulink® has higher order ODE solver (namely ODE8) which should give

better prediction theoretically, for the case of a quarter vehicle model, the use of ODE5 solver at a resolution of 0.001 s is sufficiently accurate in solving the equations of motion. It can be said that the model in MATLAB®/Simulink® can represent the equations of motion almost perfectly.
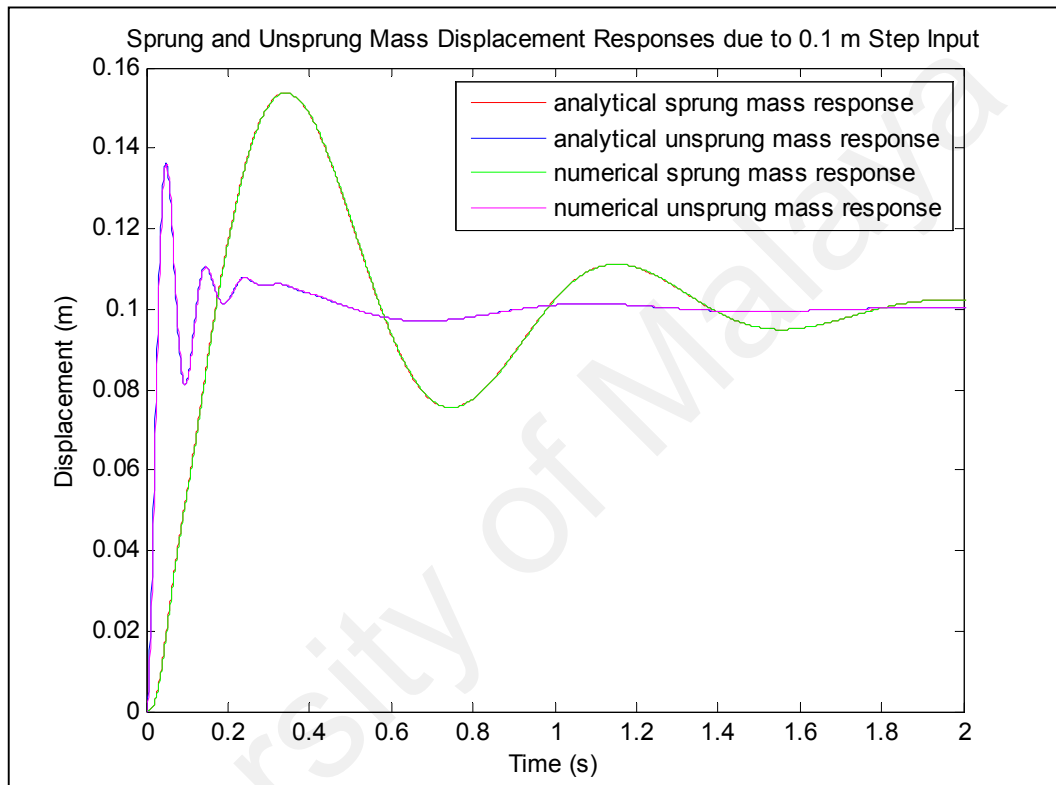
Figure 3.5: Sprung and unsprung mass responses due to 0.1 m step input determined analytically and numerically

At this point, it is already determined that the two equations of motion which form the basis of a quarter vehicle model can be confidently modeled and solved in computational software like MATLAB®/Simulink® to obtain close prediction of sprung and unsprung mass responses compared to the actual solution. With this in mind, it is then logical to evaluate further the validity of such an ideal quarter vehicle representation (the two fundamental equations of motion) by comparing it with a similar

physical mechanical system. In the subsequent part of this work, it is desirable to observe the closeness between a mathematical model in MATLAB®/Simulink® and an actual representation of this mass-spring-damper system. This is important because although the set of ideal equations of motion by no means resembles a realistic vehicle which is significantly more detailed and complicated, it should at least be capable of emulating an actual lumped-mass two-DOF system closely in order to be confidently used in subsequent comparative studies. To enable this validation work, an experimental rig, which provided the physical representation of a two-DOF quarter vehicle model, was built and tested. The structure of this experimental rig and the descriptions of its components are shown in Figure 3.6.
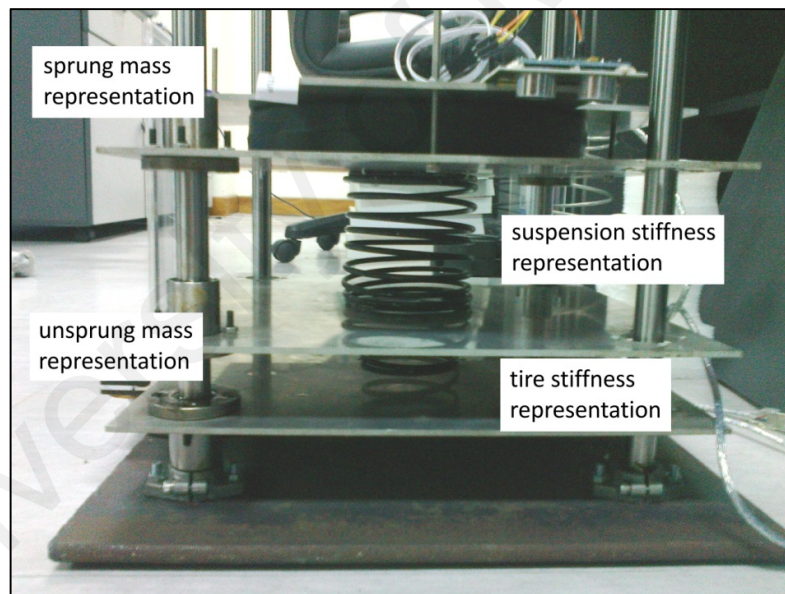
Figure 3.6: The physical representation of a two-DOF quarter vehicle model

Physically, as illustrated in the figure, the experimental rig was essentially a quarter vehicle model with its core components: the upper platform (together with the standard mass) served as the sprung mass, while the lower platform with its own mass became the unsprung mass. Meanwhile, the suspension stiffness and the tire stiffness

were respectively represented by a coil spring positioned between the platforms and a similar but harder spring located beneath the lower platform and supported by a base. Finally, the linear shafts and the sliding collars or bearings gave rise to the two DOFs of a quarter vehicle model, and the same sliding mechanism also provided a source of frictional damping, an approximation of viscous damping which will be explained later.

Quantitatively, the physical two-DOF model was designed around vehicle parameter values to ensure meaningful sprung and unsprung mass responses when the system was tested with inputs. However, while not particularly apparent in Figure 3.6, this physical system was actually scaled down from the actual values of a quarter vehicle model. This should not lead to irrelevant responses between the scaled model and the corresponding full-sized model, since it can be theoretically proven that the sprung and unsprung mass responses will not be affected by a consistent scaling factor applied to all vehicle parameters. From the earlier theoretical derivation to obtain analytical solution for the two equations of motion, it is obvious that the responses of sprung and unsprung masses depend on the transfer functions (assuming identical input from the ground). Judging from equations (3.10) and (3.11), it is directly observable that the transfer functions have a mathematical form such that the evaluated expressions remain identical if a consistent proportionality factor is applied to all the vehicle parameters in the equations, namely m_s, m_u, k, c and k_t. In other words, an entirely scaled physical quarter vehicle model is still as valid as a full-sized physical model because they produce the same responses when subjected to the same input, although the suspension forces, being proportional to the vehicle parameters, will be scaled accordingly. As an additional note, this justification is also applicable to a system with inerter (for instance, in the parallel layout) as the same deduction can be made for the transfer functions involving sprung and unsprung masses. For the case of parallel inerter

53

layout, the equations of motion (3.4) and (3.5) are used. By the same derivation (Laplace transform and solving the resulted simultaneous equations), the two transfer functions are stated as equations (3.14) and (3.15):

$$\frac{z_s(s)}{z_g(s)} = \frac{(bk_t)s^2+(ck_t)s+(kk_t)}{(m_sm_u+m_sb+m_ub)s^4+(m_uc+m_sc)s^3+(m_uk+m_sk+m_sk_t+bk_t)s^2+(ck_t)s+(kk_t)} \tag{3.14}$$

$$\frac{z_u(s)}{z_g(s)} = \frac{(m_sk_t+bk_t)s^2+(ck_t)s+(kk_t)}{(m_sm_u+m_sb+m_ub)s^4+(m_uc+m_sc)s^3+(m_uk+m_sk+m_sk_t+bk_t)s^2+(ck_t)s+(kk_t)} \tag{3.15}$$

Hence, by considering a scaling factor which consequently normalized the unsprung mass to maintain the possibility of adjusting the sprung to unsprung mass ratio by varying only the sprung mass, the scaled parameter values were determined. These values, as well as the corresponding actual values adopted from Table 3.1, are stated in Table 3.2.

Table 3.2: Full-sized and scaled values for the relevant quarter vehicle parameters

Quarter vehicle parameter	Actual value	Scaled value
Sprung mass, m_s (kg)	317.5	6.99
Unsprung mass, m_u (kg)	45.4	1.00
Suspension stiffness, k (Nm^{-1})	22000	484.58
Damping rate, c (Nsm^{-1})	1500	33.04
Tire stiffness, k_t (Nm^{-1})	192000	4229.07

The scaled parameter values as stated in the table provided the general basis for the mathematical design of the scaled-down physical quarter vehicle model, since the physical model needed to emulate a real-sized model. However, the specific parameter values were slightly different from the targeted values in the table due to variations in the eventual setup and would require determination to enable subsequent validation work. Another matter worth discussing is the damping rate requirement determined to

be approximately 33 Nsm^{-1}. It was noted that while the targeted mass and stiffness properties could be realized relatively easily through proper design, the realization of viscous damping with low damping rate proved to be more difficult. Furthermore, it was also apparent that the dampening effect to the response brought by kinematic friction became relatively more significant when the physical system was scaled down sufficiently. Consequently, for the model in this part of validation work, frictional damping originated from the surface contact of the bearings was taken as an approximation of the required viscous damping for the quarter vehicle model.

In order to get meaningful comparison between the response computed by MATLAB$^{®}$/Simulink$^{®}$ and that from the real situation of the experimental rig, the specific values of the relevant vehicle parameters for the scaled physical model needed to be determined before being adopted in the computational or mathematical model for an equivalent system. Such parameter estimation work is commonly performed for studies involving quarter vehicle test rig. For instance, a relevant study (Taskin et al., 2013) demonstrated lumped parameter identification of a quarter vehicle test rig by analyzing the frequency response functions obtained from acceleration signals for both sprung and unsprung masses. Moving back to the parameter determination work of the present research, the parameters were either obtained directly by measurement (sprung and unsprung mass values) or estimated from tests using common methods (suspension stiffness, tire stiffness and damping rate).

For the former, both the upper and lower platform assemblies were taken out and weighed. The masses were therefore determined directly. Also, for both sprung and unsprung masses, the two springs which represented suspension stiffness and tire stiffness were treated as part of the upper and lower platform assemblies respectively

and were weighed together. Consequently, the mass of the springs was included as part of the sprung mass or unsprung mass, hence maintaining the ideal massless assumption for suspension elements. Meanwhile, for the latter, the stiffness values and the approximated viscous damping rate were estimated from system responses due to static load test and dynamic load test. For suspension stiffness and tire stiffness, the two representative spring rates were determined from the force-displacement characteristics of the springs which were obtained by sequentially adding static loads (standard masses) and determining the resulted sprung mass displacements corresponding to the spring deflections. For damping rate estimation, using the upper platform assembly (including the suspension spring) and loaded with fixed standard mass, a transient input was applied to the system to result in transient sprung mass oscillation. Then, using the sprung mass displacement measurements obtained from an ultrasonic type non-contact distance sensor, the linearized damping rate due to frictional damping was derived by using the logarithmic decrement method which is a common way of estimating damping of an underdamped system from the time domain data. As an additional note, for both stiffness and damping determination work, estimations were done multiple times to obtain average values in an effort to minimize the effect of randomly occurred errors, therefore ensuring the estimated parameter values to be as precise as possible. From the estimations, the specific parameter values for the scaled quarter vehicle model are shown in Table 3.3.

Table 3.3: Specific parameter values for the scaled physical quarter vehicle model

Scaled model parameter	Specific value
Sprung mass, m_s (kg)	6.7443
Unsprung mass, m_u (kg)	0.9755
Suspension stiffness, k (Nm^{-1})	563.7100
Damping rate, c (Nsm^{-1})	10.0134
Tire stiffness, k_t (Nm^{-1})	3369.5964

The detailed estimations of the suspension parameters (suspension stiffness, tire stiffness and damping rate) using their respective individual sets of data are shown collectively in Appendix B. Judging from the result sets, some comments regarding the correctness of estimations can be made. For the suspension and tire stiffness estimations, it can be seen, from Figures B1 and B2, that the individual result sets for both cases mostly resulted in estimations with high R^2 (coefficient of determination) values that were in the region of 0.9 when the result sets were linearly curve-fitted. Mathematically, this showed that the linearly-fitted equations, from which the stiffness values were derived, were sufficiently accurate in representing the force-displacement characteristics behind the result sets. Moreover, the generally high R^2 values across most result sets, especially for the case of suspension stiffness estimation, indicated that the repetitions in estimating the two stiffness parameters were very consistent. Consequently, both the estimated stiffnesses could be confidently adopted in the MATLAB®/Simulink® model to emulate the physical model. For damping rate estimation, however, the logarithmic plots of peak displacements of the transient oscillations (Figures B3(a) to B3(j)) resulted in relatively lower (although still acceptable) R^2 values when linearly curve-fitted. This is mainly caused by the use of frictional damping, which is actually non-linear with respect to velocity of movement, as an approximation of viscous damping characteristic used in a typical quarter vehicle model. While the estimated damping rate was still considered as a valid adoption in the MATLAB®/Simulink® model because the curve-fitted equation considered the average decay in such a transient oscillation, in the subsequent response comparison work, deviation in some aspects of the response related to damping, like the settling behavior, should be anticipated.

With the knowledge on these specific parameter values, meaningful comparative analysis can be carried out to evaluate the closeness between a mathematical quarter

vehicle and the corresponding physical model by judging the computed and the measured transient responses due to an input. In the validation work, both upper and lower platform assemblies were included in the experimental rig to obtain the physical representation of a two-DOF system. To generate a transient response which would be used in comparison, a transient input was applied to the unsprung mass by compressing the lower platform for a finite displacement (limited by the solid length of the lower spring) before releasing it quickly. In the test setup, this displacement input was determined to be 0.0185 m by the difference between the spring's length at static equilibrium and the solid length. This is mathematically equivalent to subjecting the MATLAB®/Simulink® model with an upward step input of the same height acting from the ground. For the physical test system, the sprung mass response due to the displacement input acting on the unsprung mass was taken using displacement measurement system with the same ultrasonic non-contact distance sensor as used previously. Again, similar to the work associated with stiffness and damping estimations, the measurement of transient response was repeated several times, and the averaged sprung mass response was determined from the individual displacement data sets. This approach was taken because it was observed during the test that there were sources of error in the rig which prevented smooth oscillatory response, such as the presence of static friction which resulted in ragged movement after a significant decay of the response and abruptly stopped the oscillation at positions deviating from the final, steady-state equilibrium position. As the errors were random in nature, taking averaged response from a large number of trials mitigated them to a certain extent. Therefore, the averaged sprung mass displacement response was taken for comparison against the computed response from MATLAB®/Simulink® model. This is shown in Figure 3.7.

At first glance, the two responses do not seem to correlate closely. Specifically, while the responses are similar in the initial part, there is a significant difference for the latter part of the responses. However, this is actually expected. As explained when commenting on the damping rate estimation, due to the non-linear nature of frictional damping with respect to velocity, when used as an approximation of the viscous damping, there will be some deviations in the response, particularly the settling characteristic of a transient oscillation. For frictional damping, the relative significance of dampening effect increases as the velocity of movement decreases. Consequently, as can be seen from Figure 3.7, for the sprung mass response of the physical model, the decay of oscillation became increasingly more significant as the transient response continued to settle.
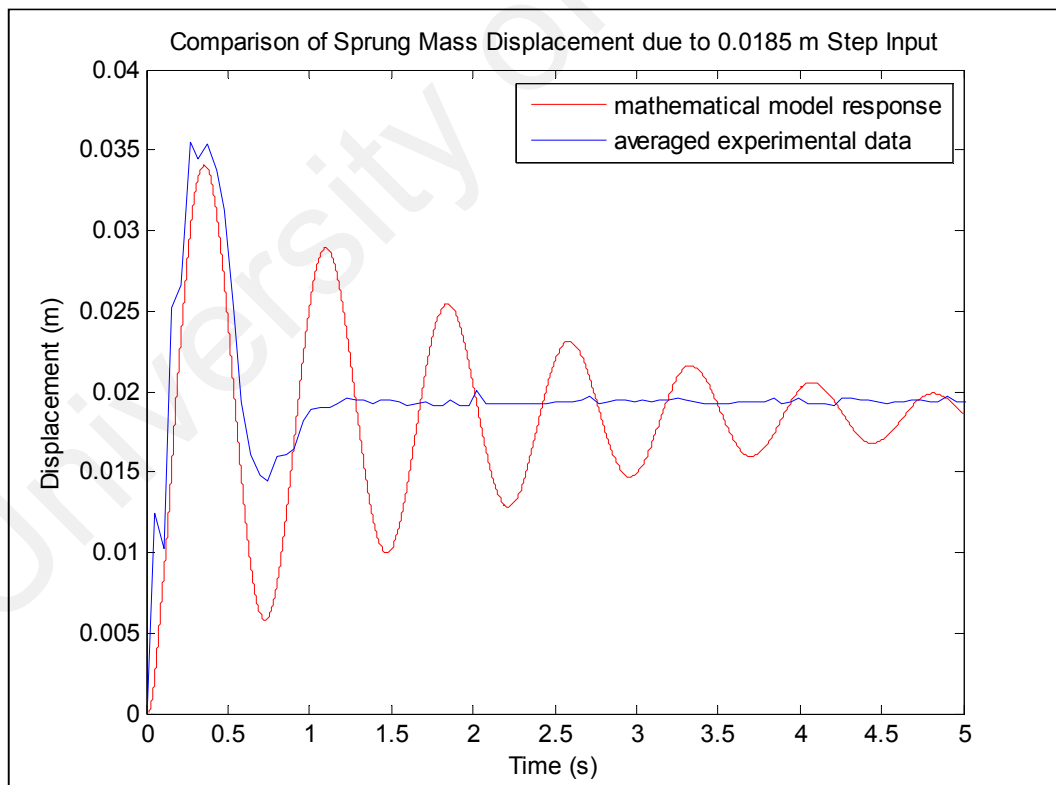
Figure 3.7: Comparison between sprung mass response from MATLAB®/Simulink® model and that from the physical model

However, although in certain aspects the computed and physical responses were quite distinct due to the deficiencies in the setup, the closeness between the ideal quarter vehicle representation and the real situation can still be evaluated by examining the first part of the responses. Several common transient response parameters related to the initial part of the responses, namely the rise time (time taken from 10 % to 90 % of the final response), peak or maximum value, first overshoot (difference between peak value and final value of response) and the corresponding maximum percent overshoot were employed to quantify the deviation between the two cases. From the analysis of both sets of parameters, the percentage differences were determined to be 9.30 %, 3.94 %, 3.11 % and 1.27 % for the respective transient response parameters. Considering the deficiencies of the experimental rig which gave rise to several errors specific to the existing setup, the differences can be deemed acceptable. Therefore, this analysis has shown that a quarter vehicle model that is mathematically represented in computational software (in this case, in MATLAB$^{®}$/Simulink$^{®}$) can correlate acceptably with a similar lumped-mass physical model. This gives confidence in using the mathematical quarter vehicle model in subsequent studies involving various implementations of inerter for suspension performance analyses.

3.2 Interaction of Inerter with Passive and Controllable Suspensions

This part of research begins with an analysis on the response of a quarter vehicle model with passive suspension incorporating inerter. By analyzing the response of vehicle suspension employing inerter, one can obtain greater understanding on the advantages brought by the addition of inerter to existing suspension setup comprising of only spring and damper. As with many previous studies, this analysis considered two basic inerter layouts, namely the parallel arrangement and the serial arrangement, for which their

fundamental working principles have already been discussed in Section 3.1. For the analysis, the same quarter vehicle model as in the previous section was employed, and its two equations of motion (equations (3.4) and (3.5)) as well as the vehicle parameter values (Table 3.1) can be referred in Section 3.1.

For the study, two types of road profile were considered as the road input to the system. The first was a step profile with step height of 0.1 m as used earlier. Step profile can be treated as the emulation of a vehicle striking a curb or accidentally hitting an obstacle, which can occur occasionally during driving. Moreover, step profile is commonly used as an input to control system to evaluate the transient response of the system. Apart from this, in the analysis, an additional input, namely the random road profile, was also considered. Random road profile is used in simulations primarily to emulate ground excitation experienced under normal driving conditions. The use of both road inputs in the study ensured comprehensiveness as well as closeness to the reality, since a typical road is generally characterized by the presence of large isolated irregularities such as potholes and curbs in combination with continuously distributed profile irregularities (Verros et al., 2005).

Relevant to the latter input, road profiles are typically represented in the form of spectral density curves. The ISO 8608:1995 (1995), for example, classifies road profiles into several classes with each class having its average roughness coefficient. The spectral density curves can be mathematically represented as equation (3.16):

$$s(f_{sp}) = G \left(\frac{f_{sp}}{f_{sp0}} \right)^{-n} \tag{3.16}$$

in which s is the density in the unit of $m^2(cycle.m^{-1})^{-1}$, f_{sp} is the spatial frequency in cycle.m^{-1} which is related to frequency, f in Hz by multiplying with velocity of travel, v in ms^{-1} ($v = 20$ ms^{-1} in this study), $f_{sp0} = 0.1$ cycle.m^{-1} is the reference frequency as used in a similar study (Gubitosa et al., 2009), n is a non-dimensional index ($n = 2$ in this study), and G is the roughness coefficient in $m^2(cycle.m^{-1})^{-1}$. Table 3.4 shows the roughness coefficients for different road classes found in ISO 8608:1995 (1995). From this data, a single track can be generated by adding together a discrete number of sine waves; the amplitudes are derived from spectral density data, while the phase angles are determined through a random number generator (Crolla & Whitehead, 2003). In mathematical terms, this is shown in equations (3.17) and (3.18):

$$z_g(t) = \sum_{i=1}^{n} A_i \sin(2\pi f_i t + \theta_i) \tag{3.17}$$

$$A_i = \sqrt{2 \cdot s(f_i) \cdot \Delta f} \tag{3.18}$$

in which $z_g(t)$ is the time dependent ground displacement or road profile, while A_i, θ_i and $s(f_i)$ are the amplitude, phase angle and density value at specific frequency, f_i. This method was used in the study to create a random road profile of class A, which is shown in Figure 3.8 together with the simpler step profile.

Table 3.4: Degree of roughness of road profiles classified by ISO 8608:1995 (1995)

Road classification	Range ($\times 10^{-6}$ $m^2(cycle.m^{-1})^{-1}$)	Geometric mean ($\times 10^{-6}$ $m^2(cycle.m^{-1})^{-1}$)
A (very good)	< 8	4
B (good)	8 – 32	16
C (average)	32 – 128	64
D (poor)	128 – 512	256
E (very poor)	512 – 2048	1024
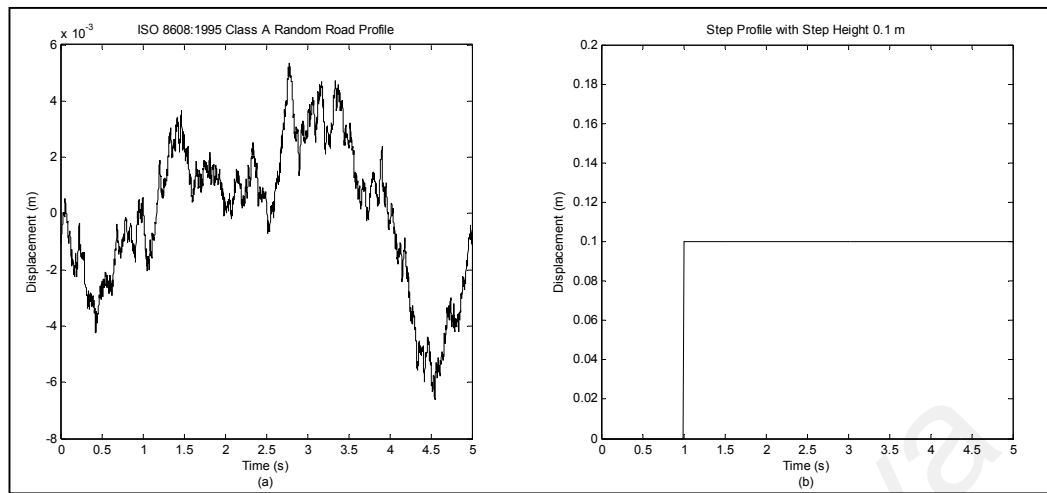
Figure 3.8: Representation of (a) class A random road profile and (b) step profile with

step time shifted from 0 s to 1 s for clarity

As a two-DOF vehicle model was used in the analysis, both the sprung and unsprung mass responses due to road inputs could be obtained by solving the equations of motion. Thus, two important but conflicting performance criteria could be assessed, namely the RMS sprung mass acceleration and the RMS dynamic tire load which respectively measured ride comfort and tire road holding ability. Basically, the RMS sprung mass acceleration is the primary measure of ride as the acceleration of vehicle body is directly experienced by the passengers. Therefore, smaller RMS sprung mass acceleration value generally indicates more comfortable ride. Meanwhile, the RMS dynamic tire load affects the road holding ability and also affects indirectly the generation of lateral and longitudinal tire forces which govern the handling performance. A lower value is again desirable as it represents less variation in the tire normal load.

A good way to evaluate both ride and road holding criteria simultaneously is to analyze the Pareto front involving the two objectives for a given suspension system, for example as done in the study by Scheibe and Smith (2009). Referring to the description in Section 2.4, it is known that in typical multi-objective situations, a Pareto front shows

the relationship among multiple design objectives, and corresponds to the set of all Pareto optimal solutions which are non-dominated by other solutions. As mentioned in the section, a solution is non-dominated and belongs to the Pareto set if there is no other solution that can improve at least one of the objectives without degradation of any other objective (Ngatchou et al., 2005). Therefore, specific to this study which involved only the two conflicting objectives, a solution is Pareto optimal and its objective values contribute to part of the Pareto front if there is no other solution that can reduce the RMS sprung mass acceleration without increasing RMS dynamic tire load. With the use of multi-objective optimization function in MATLAB$^{®}$, the system was solved considering damping rate and inertance as the variables in optimization. The results are presented in the form of Pareto fronts for original passive suspension, suspension with parallel inerter and suspension with serial inerter to enable comparison. These are shown in Figure 3.9 for step input and Figure 3.10 for class A random road input (with the detailed Pareto solutions and objective values shown in Appendix C).

As multi-objective optimization algorithms only return Pareto optimal set that approximates the true Pareto front because not all solutions are evaluated, results in Figures 3.9 and 3.10 were compared with similar work in a previous analytical study (Scheibe & Smith, 2009) as an attempt to verify its validity. By comparison, the trend of the Pareto fronts is the same as that from the previous study: the Pareto front for the case with parallel inerter is wider but shows only slight improvement over the Pareto front for the reference case with original passive spring and damper in the region of low RMS sprung mass acceleration, while the Pareto front for the case with serial inerter shows better improvement of the two arrangements. This observation also shows agreement to the point that the serial inerter arrangement offers greater performance benefit compared to the parallel inerter arrangement, mentioned in the study by Smith

and Wang (2004) based on percentage improvement obtained from the optimization work. However, although a serial inerter results in greater combined performance improvement in sprung mass acceleration and dynamic tire load, this layout may be less practical in an actual implementation. This is because the inerter does not support static load, and in physical implementation a serial connection between inerter and damper as employed in the simple serial layout will require an additional spring element to maintain equilibrium at the point of connection between the two. On the other hand, for parallel arrangement, even though the achievable improvement is small, it can be physically implemented with relative ease since in the most basic implementation the inerter is only added onto other suspension elements. Consequently, considering that practicality is one of the main concerns of the research, subsequent analyses will focus solely on parallel inerter layout.
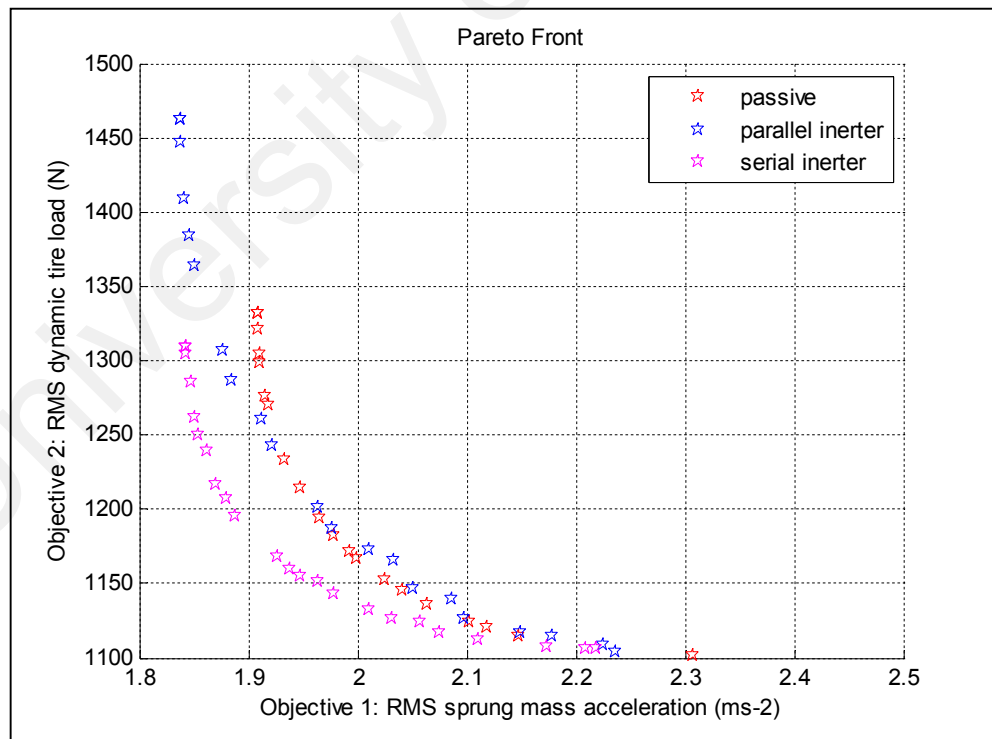
Figure 3.9: Pareto fronts for optimization of system subjected to step input
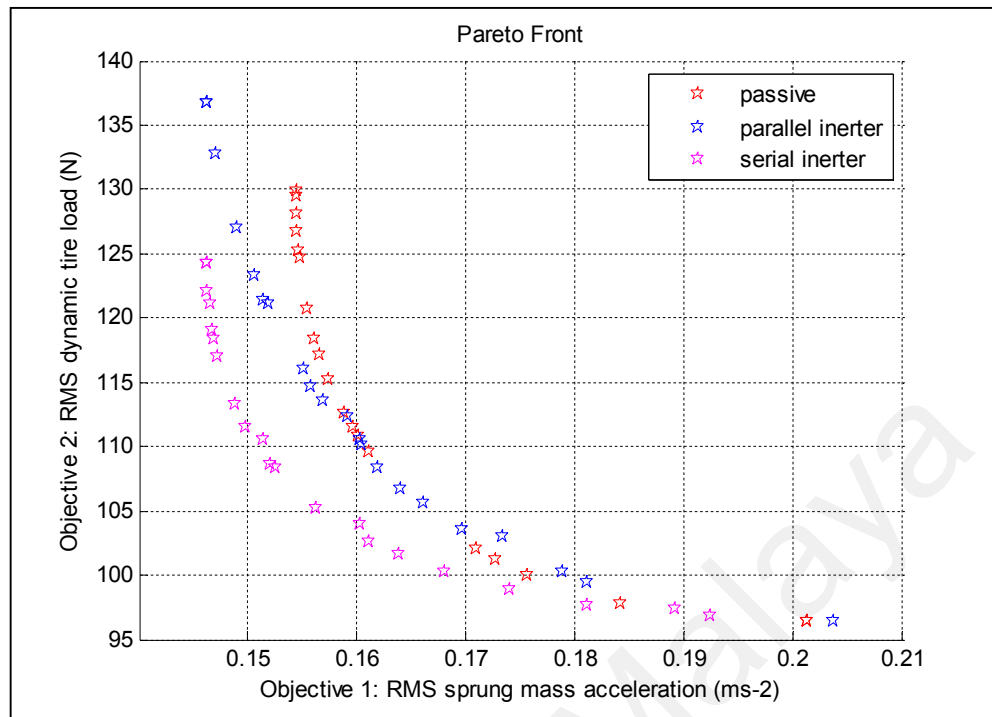
Figure 3.10: Pareto fronts for optimization of system subjected to class A random road

input

3.2.1 Effectiveness of parallel inerter in controllable suspension systems

Based on the outcome in Section 3.1, it is already known that the effectiveness of a parallel inerter in achieving ride improvement is due to the opposition and cancellation between spring and inerter forces which reduce the RMS sprung mass acceleration. Since the pairing between a parallel inerter with passive suspension is already well explored, it is then interesting to discover the interaction between a parallel inerter with controllable suspension systems instead. This is because a controllable suspension system is also capable of providing superior ride performance, and there is a possibility that simultaneous implementation of the two will, in accumulation, bring even greater ride improvement. Furthermore, it is also the intention of this study to evaluate inerter's versatility in passenger vehicle suspension systems as part of determining its practicality. In this part of the study, the inerter was again employed as an 'add-on' device in parallel

to several controllable suspension systems to determine its effectiveness in ride improvement so as to judge its application in various types of passenger vehicle suspension system. The controllable suspension systems that were considered included the semi-active switchable damper using discrete, two-state switchable Skyhook control strategy, semi-active continuously variable damper and fully-active suspension using linear optimal control method. The relevant control strategies have been described and stated as equations (2.11), (2.8) and (2.5) in Section 2.2 respectively. Referring to the relevant equations, for the parameters related to the control strategies, c_{max} and c_{min} are the maximum and minimum damping rates in a two-state switchable damper ($c_{max} = 1500$ Nsm^{-1} and $c_{min} = 900$ Nsm^{-1} in this study), while $k_{l1,2,3}$ and $k_{f1,2,3,4}$ represent the sets of feedback gains that were determined based on a previous study on linear optimal control theory (Wilson et al., 1986).

In the analysis, a technique of solving control-related problems, known as co-simulation method, was employed. This simulation method was naturally considered when analyzing a system comprising an inerter and different controllable suspension systems, since the situation involved solving two distinct systems, namely the dynamical system and the control system. However, it is important to mention that for simplified engineering problems, if both the dynamical and the control systems can be represented conveniently within a single software environment, then co-simulation might not give significant advantage in terms of modeling convenience and accuracy. Conceptually, co-simulation is the method of simulating an engineering system by the use of multiple software programs. It is also called 'software-in-the-loop' as the process involves passing variable values from a software program to another during each simulation time step. In the study, the simulation of the dynamic behavior of a quarter vehicle model that contained a controllable damper or actuator called for the use of

MSC.ADAMS, which served as a multi-body dynamic analysis software, and MATLAB®/Simulink®, which acted as the control application. This concept is outlined by Figure 3.11(a), while the actual model is shown in Figure 3.11(b) which displays the block diagram used in the co-simulation of passive suspension system that served as the reference case.
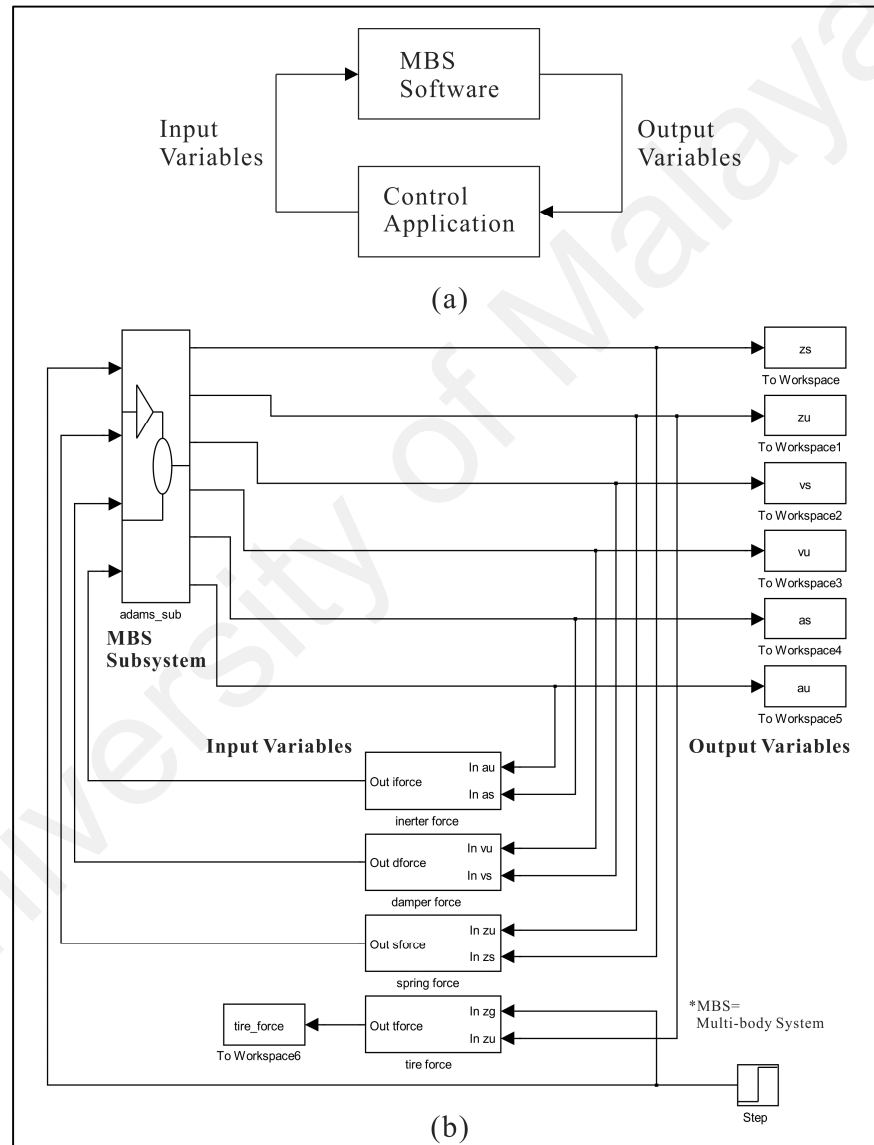
Figure 3.11: Representation of co-simulation in (a) schematic diagram and (b) the actual MATLAB®/Simulink® model

During co-simulation, ADAMS/Controls was used to create communication between the software. The computation of MSC.ADAMS and MATLAB®/Simulink® models was performed by their respective solvers. At every time interval MSC.ADAMS solved and sent the specified variables, such as the displacements and velocities of the parts to MATLAB®/Simulink®. The control forces were then calculated in MATLAB®/Simulink® and were fed back to MSC.ADAMS for the implementation of the next time step.

In the study, both step and random road inputs were considered again. While the definition of step input remained the same, for random road input, three different types of road data in ISO 8608:1995 (1995) were considered, namely class A (smooth), class C (average) and class E (poor) power spectral density data for a more comprehensive study and also to determine the inerter's effectiveness under different road conditions. With these, co-simulations of the test systems or models were performed to enable determination of relevant performance measures, namely the RMS sprung mass acceleration and the RMS dynamic tire load. As explained earlier, both lower RMS sprung mass acceleration and RMS dynamic tire load are favorable, hence reductions of these two criteria were considered as performance improvements. For the analysis of results, firstly, Figure 3.12 shows the plots of RMS sprung mass acceleration and RMS dynamic tire load against inertance due to step input excitation for the tested suspension systems employing parallel inerter.

It can be observed that there was an optimum inertance for each of the tested vehicle suspension systems which resulted in a minimum RMS sprung mass acceleration, and this was true not just for passive suspension system, but also for controllable suspension systems. Basically, this inferred that the addition of parallel

inerter was consistently effective in improving ride, showing versatility in the application of vehicle suspensions as its benefit was independent on the types of suspension system. Clearly, for passive and semi-active vehicle suspension systems, the inerter force only opposed the spring force; therefore, the cancellation of forces, as discussed in Section 3.1, existed regardless of the types of damper used in the suspensions. Meanwhile, for the specific active suspension system employed in the study, although the system involved the use of an actuator to replace the spring and damper combination altogether, the controller as stated in equation (2.5) actually consisted of an implicit spring force term which can be shown by rearranging the equation. Hence, mathematically, the parallel inerter also demonstrated ride improvement for the tested active suspension system. Additionally, it is also worth to note that the optimum points occurred at relatively low values of inertance.
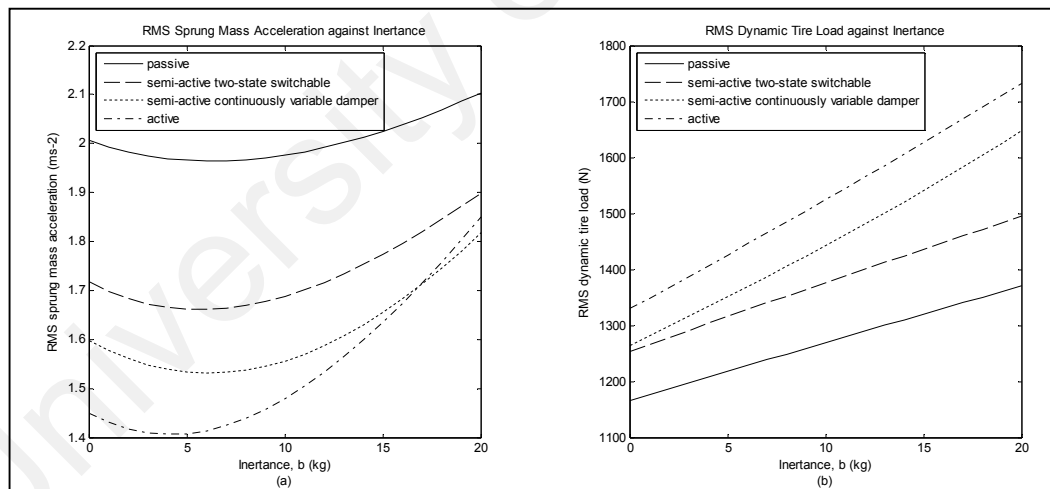
Figure 3.12: Graph of (a) RMS sprung mass acceleration and (b) RMS dynamic tire load against inertance for various tested suspension systems

On the contrary, results from simulations did not show any optimum inertance for improvement in RMS dynamic tire load. In fact, the RMS dynamic tire load increased along with inertance, and this is an indication of reduced road holding ability

70

as greater tire load variation results in greater variation of the tire contact area as well as the lateral and longitudinal tire forces (in the presence of handling maneuvers). This observation is supported by referring to the derivation of analytical solutions for optimal ride and road holding criteria in the relevant study by Scheibe and Smith (2009), which mentioned that the optimum inertance for road holding is zero when the suspension stiffness is less than a certain critical value determined from the sprung mass, unsprung mass and the tire stiffness (applicable to parallel layout only). The vehicle parameter values used in this study fulfilled the condition, as the stiffness, $k = 22000$ Nm^{-1} is less than the critical value computed to be 94498 Nm^{-1}. Consequently, any presence of inertance in the parallel layout, specifically to the tested passenger vehicle in this study, will increase the road holding criterion which is the RMS dynamic tire load.

From Figure 3.12, the ride performance improvement that a parallel inerter brought was relatively small. The ride improvement was less than that provided by a semi-active or an active suspension alone. However, it still acted as an enhancement in ride criterion for the controllable suspensions. To be specific, Table 3.5 shows the comparison of RMS sprung mass accelerations between the reference case and the cases with optimum inertance.

From Table 3.5, the ride improvement due to a parallel inerter ranged from 2 % to 4 % for the suspension systems of interest. Note that the vehicle parameter values used in the simulations belong to those of a typical passenger vehicle; therefore, this range of ride improvement is the expectation of implementing a parallel inerter in a vehicle of this type. Additionally, the improvement was consistent across the various road profiles that were considered in the analysis. In other words, both inerter and the

tested controllable suspension systems offered consistent ride improvement across various road conditions.

Table 3.5: Comparison of RMS sprung mass accelerations due to step and random road profiles

Type	RMS sprung mass acceleration (ms^{-2})		Percent difference (%)
	Reference case ($b = 0$)	With best b value	
Step profile			
Passive	2.0061	1.9639 ($b = 6$ kg)	-2.1036
Semi-active two-state switchable	1.7176	1.6610 ($b = 6$ kg)	-3.2953
Semi-active continuously variable damper	1.5973	1.5313 ($b = 6$ kg)	-4.1320
Active	1.4484	1.4063 ($b = 4$ kg)	-2.9067
Random class A profile			
Passive	0.1712	0.1675 ($b = 6$ kg)	-2.1612
Semi-active two-state switchable	0.1548	0.1503 ($b = 6$ kg)	-2.9070
Semi-active continuously variable damper	0.1398	0.1339 ($b = 6$ kg)	-4.2203
Active	0.1265	0.1229 ($b = 4$ kg)	-2.8458
Random class C profile			
Passive	0.6879	0.6728 ($b = 6$ kg)	-2.1951
Semi-active two-state switchable	0.6229	0.6046 ($b = 6$ kg)	-2.9379
Semi-active continuously variable damper	0.5629	0.5389 ($b = 6$ kg)	-4.2636
Active	0.5102	0.4957 ($b = 4$ kg)	-2.8420
Random class E profile			
Passive	2.7351	2.6771 ($b = 6$ kg)	-2.1206
Semi-active two-state switchable	2.4743	2.4025 ($b = 6$ kg)	-2.9018
Semi-active continuously variable damper	2.2333	2.1390 ($b = 6$ kg)	-4.2225
Active	2.0200	1.9634 ($b = 4$ kg)	-2.8020

In summary, the implementation of inerter as an additional element to both passive and controllable suspension systems gave consistent improvements in ride quality to the tested passenger vehicle as its working principle was unaffected by the types of suspension system in use. Simulations on inerter with controllable suspension systems resulted in optimum inertances which gave greatest reduction in RMS sprung mass acceleration, however there was no optimum inertance for the RMS dynamic tire load. In fact, similar to some other ride improvement methods, the RMS dynamic tire

load increased and this became the compromise in an effort to reduce sprung mass movement. Comparison from a different perspective indicated that the ride improvement brought by a parallel passive inerter was only slight relative to that offered by the tested semi-active and active suspension systems, and this will be dealt with in Chapter 4. Nevertheless, it can be said that the pairing of inerter and controllable suspensions in this layout still enhances the ride performance as it does with passive suspension, demonstrating that the inerter has versatility in the application of passenger vehicle suspensions.

3.3 Feasibility of Implementing Vehicle Suspension Layout with Parallel Inerter

Up to present moment, it has been shown in the preceding sections that an inerter, arranged in parallel to spring and damper, is capable of improving ride comfort as indicated by a reduction in RMS sprung mass acceleration. However, as pointed out in the beginning of this chapter, an important issue is that while various suspension layouts employing inerter are possible in theoretical analysis, their implementation does not seem to be very practical on passenger vehicle suspensions. For instance, with parallel inerter arrangement, it is not very realistic to directly mount an inerter device in parallel to existing spring and damper because there is typically not much space within the wheel-house area of a vehicle. Consequently, if the suspension layout is to be practically implemented, then it is favorable that the damper and the inerter be combined to make a damper-inerter device so that, together with a concentric spring, a parallel suspension layout as theoretically studied previously can be practically realized.

Following the discussion above, the motivation of this part of research work is basically to assess the practicality of the parallel inerter suspension layout by looking

into the feasibility of incorporating damping in an inerter. One way of achieving damping in an inerter is to exploit the fact that the rotating flywheel which contributes to the inerter force is also a conductor, since it is usually made of metallic material. Theoretically, in the presence of a magnetic field, for instance due to permanent magnets, eddy current will occur in the rotating flywheel, and the flow of eddy current will cause resistive heating, therefore dissipating the system's kinetic energy. Hence, it acts as a damper. As already explained in Section 2.3, for passenger vehicle suspension application, currently only linear eddy current damper has been researched (Ebrahimi et al., 2009), although the electromagnetic or eddy current brake, which is conceptually identical but has different requirements, has been widely explored (Gay, 2005). Since rotary eddy current damper for vehicle suspension application has not been studied before, the suitability of the achievable damping rates and inertances for passenger vehicles needs to be investigated. This justifies the purpose of present work, which is to study the fundamental feasibility of a combined parallel damper-inerter setup for application in passenger vehicle suspensions.

For this study, the general workflow is as follows. The first part of the work involved mathematically designing an inerter to assess the feasibility of meeting the typical inertance range for a parallel layout, especially the desirable or optimum inertance determined in Section 3.2. This was done by performing design optimization to achieve the optimum value using typical ranges for the involved design parameters. Secondly, the feasibility study was extended to include the analysis on the achievable damping rates due to the incorporation of eddy current damping in an inerter. In this part of work, a base design was modeled in electromagnetic software and was simulated to obtain the damping characteristic, and the suitability of achievable damping for use in passenger vehicle suspensions was evaluated. In addition, some electromagnetic-related

design parameters were varied in parametric analysis to determine their effects on the achievable damping. Finally, the last part of the work looked into the possibility of achieving variable damping for the damper-inerter setup by utilizing current-carrying coil with variable currents instead of permanent magnets which gave only passive damping. The details of these analyses are described in Sections 3.3.1, 3.3.2 and 3.3.3 respectively.

3.3.1 Mathematical design of inerter

The feasibility study begins with analyzing the inerter part of the proposed damper-inerter setup by means of mathematical design. The main objective of this design work is to demonstrate the achievement of the desirable inertance for parallel suspension layout as studied in Section 3.2. Generally, the design methodology is as explained: firstly, the expression for equivalent inertance, b_{eq} of an inerter was determined, and from there the design parameters that affected inertance, such as the dimensions of the flywheel and its density, could be identified. Secondly, design optimization was performed with typical ranges for the involved parameters, and the set of design parameters that resulted in desired b_{eq} was selected. This also formed the dimensional basis for subsequent eddy current damping analysis in the latter sections.

This part of study considered two types of inerter design, namely the ball-screw inerter and the rack-and-pinion inerter. Both types of inerter are mechanically-based and have been tested extensively in past studies (Papageorgiou et al., 2009; Papageorgiou & Smith, 2005). For both designs, the core element (flywheel) which provides the inerter effect is the same; the only difference is on the methods used to achieve the conversion between rotational and translational motions (the former uses ball-screw mechanism while the latter uses rack-and-pinion mechanism). For the ball-screw inerter, the

equivalent inertance can be obtained from the following derivation. Firstly, equation (3.19) provides the fundamental expression of the inertia of a cylindrical flywheel. Meanwhile, in rotational motion, torque is related to the product of inertia and the derivative of rotational velocity. By considering that for ball-screw mechanism, force and torque (as well as linear and rotational velocities) are related by the conversion ratio $\left(\frac{2\pi}{p}\right)$ in which p is the pitch, equation (3.20) is derived. Finally, by representing the inertia in the fundamental expression form, the final form of relation between force and acceleration is shown in equation (3.21), and the expression which represents the inertance can be identified as equation (3.22).

$$J = \frac{1}{32}(\pi)(\rho)(t)\left(d_o{}^4 - d_i{}^4\right) \tag{3.19}$$

$$F_{inerter} = \frac{2\pi}{p}\left(J\frac{d\omega}{dt}\right) \tag{3.20}$$

$$F_{inerter} = \left(\frac{\pi^3 \rho t\left(d_o{}^4 - d_i{}^4\right)}{8p}\right)\left(\frac{dv}{dt}\right) \tag{3.21}$$

$$b_{eq} = \frac{\pi^3 \rho t\left(d_o{}^4 - d_i{}^4\right)}{8p} \tag{3.22}$$

in which d_o is the flywheel's outer diameter, d_i is the inner diameter, ρ is the density, t is the thickness of flywheel, p is the pitch of ball-screw. Note that most of the design parameters are dimensional parameters.

The desirable inertance, $b_{desired}$ was taken to be 6 kg, as this was the optimum value obtained from previous theoretical analysis in Section 3.2 which gave greatest ride improvement to the tested quarter vehicle model. So, the design problem is to find

the set of $[d_o, d_i, t, p, \rho]$ such that $b_{eq} = 6$ kg (minimum inertance error, e_b), and also that

the mass, m is minimum or is at least sufficiently small to be negligible (since in ideal

definition, inerter is considered massless, similar to an ideal spring and damper). The

expression of flywheel mass is shown in equation (3.23). For the design parameters,

their values followed the ranges as specified in Table 3.6. These represented the usual

ranges in the design of damper-inerter device for use in passenger vehicle suspensions.

For example, the outer diameter's range of the flywheel was selected by considering the

reasonable outer diameters for typical suspension struts as well as the need of

incorporating a cylindrical flywheel to the setup. Similarly, the pitch values considered

in the design analysis was in the range of millimeters, and the values were found in

common ball-screws. Additionally, the flywheel's density is material-based, and

therefore the parameter took the approximated or general values corresponding to

Aluminum, Copper and steel respectively. Both Aluminum and Copper were considered

in the study because they are the most commonly employed materials for eddy current

dampers (due to their high conductivities), while steel was also selected to complement

the analysis, considering that it is a commonly available conducting material.

$$m = \frac{\pi \rho t (d_o{}^2 - d_i{}^2)}{4}$$ (3.23)

Table 3.6: Ranges of design parameters for ball-screw inerter design

Parameter	Range of values
Outer diameter, d_o (m)	[0.100 – 0.150]
Inner diameter, d_i (m)	[0.010 – 0.020]
Thickness, t (m)	[0.005 – 0.020]
Pitch, p (m)	[0.002 – 0.010]
Density, ρ (kgm^{-3})	[2700, 8900, 7800]

With these, the exploration of design space was carried out. Since equations

(3.22) and (3.23) were simple to compute, enumeration of every combination of the

parameter values within the ranges for a sufficiently small resolution could be determined, and optimization algorithms were not needed in this case. As only two criteria were involved, the design points can be plotted as two-dimensional scatter plot for visualization (Figure 3.13).
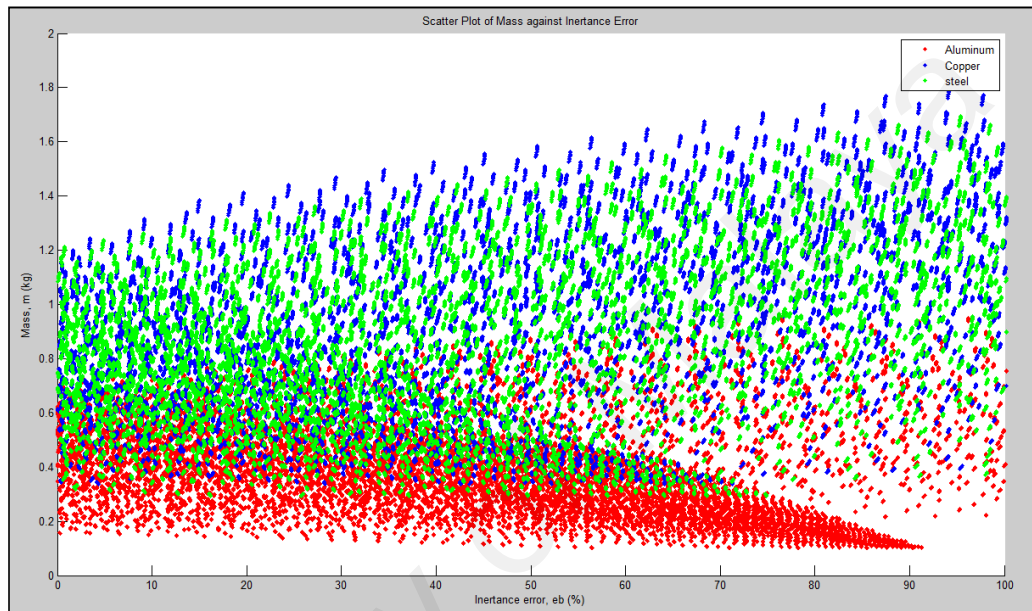
Figure 3.13: Scatter plot showing all possible design points for ball-screw inerter design

From the results, it was noted that $b_{eq\_min} = 0.5224$ kg, while $b_{eq\_max} = 174.6249$ kg, which was determined based on the minimum and maximum values of all the enumerations using MATLAB®. This stated range of achievable inertances due to the specific ranges of design parameter values is the typical inertance range for parallel inerter layout (for example, in this case, $b_{desired} = 6$ kg which is within the range). For design selection, the goal is primarily to select a point that has inertance error close to 0 % (b_{eq} close to 6 kg) and secondarily to also obtain a small mass. Specifically, the design selection process was performed through qualitative assessment which involved manual judgment based on achieving desirable inertance without compromising the additional small mass requirement as opposed to using additional algorithm to identify the design

point. The exact procedures are described here: Firstly, the Pareto approach was considered by using simple MATLAB® sorting program to obtain the Pareto optimal set. This eliminated the design points that were inferior to the non-dominated solutions. Then, from the Pareto optimal solutions, the design points associated with negligible inertance error were identified, and the point which gave minimum mass was eventually selected as the design point. Based on this design philosophy, the selected point has the following values: outer diameter, d_o = 0.123 m, inner diameter, d_i = 0.017 m, thickness, t = 0.005 m, pitch, p = 0.002 m, density, ρ = 2700 kgm^{-3} (Aluminum) which resulted in the following: inertance error, e_b = 0.2359 %, mass, m = 0.1573 kg, inertance, b_{eq} = 5.9858 kg.

Meanwhile, for the analysis employing rack-and-pinion inerter design, the workflow remained the same, and the difference between the two cases was only on the expression governing the equivalent inertance, b_{eq} and the design parameters (as well as their ranges of values) involved in the analysis. For a simple rack-and-pinion inerter design which uses only a single pinion along with the rack to convert the rotational motion of the flywheel to the translational motion of the strut and vice versa, the inertance expression can be derived. The derivation is the same as that for the ball-screw design, except that the conversion ratio for this simple rack-and-pinion design is $\left(\frac{2}{d_p}\right)$, in which d_p is the pinion diameter.

$$J = \frac{1}{32}(\pi)(\rho)(t)\left(d_o{}^4 - d_i{}^4\right) \tag{3.24}$$

$$F_{inerter} = \frac{2}{d_p}\left(J\frac{d\omega}{dt}\right) \tag{3.25}$$

$$F_{inerter} = \left(\frac{\pi\rho t\left(d_o{}^4 - d_i{}^4\right)}{8d_p{}^2}\right)\left(\frac{dv}{dt}\right) \tag{3.26}$$

$$b_{eq} = \frac{\pi\rho t\left(d_o{}^4 - d_i{}^4\right)}{8d_p{}^2} \tag{3.27}$$

in which d_p is the pinion diameter of the rack-and-pinion mechanism while the other variables remain the same, namely the flywheel's outer diameter d_o, inner diameter d_i, density ρ and the thickness of flywheel t. Also, note that because only the rotational-to-translational conversion method had changed, the flywheel remained conceptually the same and therefore had the same mass expression as equation (3.23). With these two design equations, the analysis of achievable inertance was repeated with the parameter ranges stated in Table 3.7. Basically, as can be observed from the table, the ranges relevant to the flywheel's parameters, namely the outer diameter, inner diameter and thickness remained the same as in the previous case involving the ball-screw design. Meanwhile, the pinion diameter took a range of centimeters, an order of magnitude larger than the range of pitch for the ball-screw design. For the rack-and-pinion design, again, enumeration of all possible design points were carried out, and the results are illustrated in Figure 3.14.

Table 3.7: Ranges of design parameters for rack-and-pinion inerter design

Parameter	Range of values
Outer diameter, d_o (m)	[0.100 – 0.150]
Inner diameter, d_i (m)	[0.010 – 0.020]
Thickness, t (m)	[0.005 – 0.020]
Pinion diameter, d_p (m)	[0.020 – 0.040]
Density, ρ (kgm^{-3})	[2700, 8900, 7800]
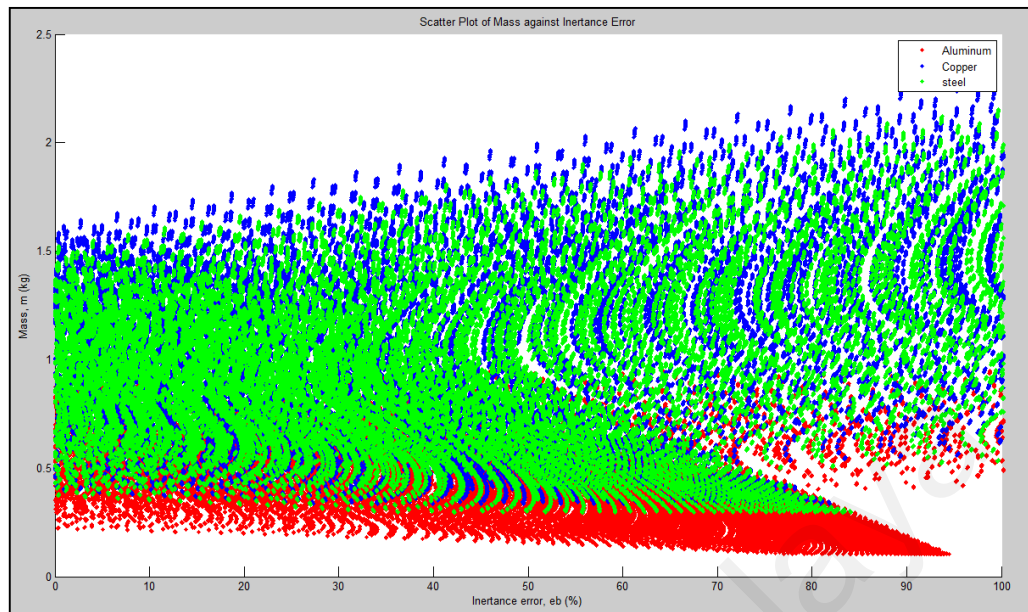
Figure 3.14: Scatter plot showing all possible design points for rack-and-pinion inerter
design

From the results, this time, it was noted that $b_{eq\_min} = 0.3308$ kg, while $b_{eq\_max} = 88.4660$ kg which resulted in a narrower achievable inertance range. Similarly, this was also determined based on the minimum and maximum values from all enumerations. However, the range is generally still suitable for the parallel layout, considering that the optimal inertance requirement for this layout is typically lower compared to other layouts like the serial layout (Smith & Wang, 2004). Hence, the suitability in terms of achievable inertance was again demonstrated. The selected point has the following values: outer diameter, $d_o = 0.146$ m, inner diameter, $d_i = 0.020$ m, thickness, $t = 0.005$ m, pinion diameter, $d_p = 0.020$ m, density, $\rho = 2700$ kgm^{-3} (Aluminum) which resulted in the following: inertance error, $e_b = 0.3323$ %, mass, $m = 0.2218$ kg, inertance, $b_{eq} = 6.0199$ kg. Note that the selection of the design point was based on the same design philosophy, that is, the attainment of desirable inertance was prioritized over the mass criterion. The design parameter values for both cases, particularly the flywheel's

dimensional parameter values, would then be used for subsequent work involving eddy current damping analysis.

Overall, results from the design analysis on inerter have shown that the desirable inertances for typical passenger vehicle suspensions in the parallel layout can be easily achieved through proper selections of the design parameter values, regardless of the types of conversion mechanism used in the inerter device. However, for the proposed combined damper-inerter setup involving the incorporation of damping in an inerter, the feasibility study should consider the achievable damping along with the achievable inertance. This is elaborated in Section 3.3.2.

3.3.2 Achievable eddy current damping in parallel damper-inerter setup

After looking into the feasibility of achieving typical inertance range for parallel suspension layout as well as obtaining desirable inertance for the specific passenger vehicle considered in the research, in the second part, it was the damping component of the proposed damper-inerter concept that was evaluated. For this part of the feasibility analysis, the achievable eddy current damping incorporated in an inerter was judged to determine its suitability to be used in passenger vehicle suspensions. Basically, this was done by solving the situation of eddy current damping due to the presence of permanent magnets in an electromagnetic simulation software, namely ANSYS® Maxwell, to obtain the rotational damping characteristics for some design configurations before deriving the corresponding linear damping characteristics for analysis. However, being a finite-element analysis software, it can generally be expected that various simulation settings such as the choice of solver, the size of mesh elements and the simulation time resolution (for transient response computation) do affect the accuracy and thus the reliability of the predicted outcomes. Because of this, prior to the feasibility analysis,

validation work needed to be carried out to determine the reliability of the computed response in a typical eddy current damping situation. This is an important prerequisite considering that the subsequent feasibility analysis would depend on the computationally determined damping rates for assessment.

For the validation work, a general rotary eddy current damping scenario was emulated with an appropriate setup, and comparison was made between the actual rotational transient response due to damping (as determined experimentally using the setup) and the predicted response by modeling and simulating the scenario in ANSYS$^{®}$ Maxwell environment. The setup which resembled an eddy current damping situation consisted of a freely rotatable flywheel assembly to act as the moving conductor for eddy current induction, and a cylindrical, axially magnetized Neodymium permanent magnet placed near the flywheel to provide the external magnetic field. Additionally, in the test, a standard mass (0.5 kg), tied to a sufficiently long thread (0.5 m), was utilized to initiate the rotation of flywheel by exerting an initial torque to the setup. Overall, Figure 3.15(a) illustrates the entire eddy current damping setup, while Figure 3.15(b) details the important dimensions of the setup.

Essentially, the test setup represented the typical situation of rotary eddy current damping in which a rotating conductor was acted by an opposing damping torque that affected the rotational response dynamically. Observing from Figure 3.15(b), the setup was dimensionally different from the eventual eddy current damper model which adopted the flywheel dimensions as determined in the preceding section; however, the general scenario to be simulated remained the same: both cases involved the computation of damping torque due to eddy current induction in the presence of an externally applied magnetic field. Consequently, if the computational response for the

tested case is shown to correctly represent the actual test setup, then the validity of the simulation can be extended to the situation involving the eddy current damper model used for feasibility analysis.
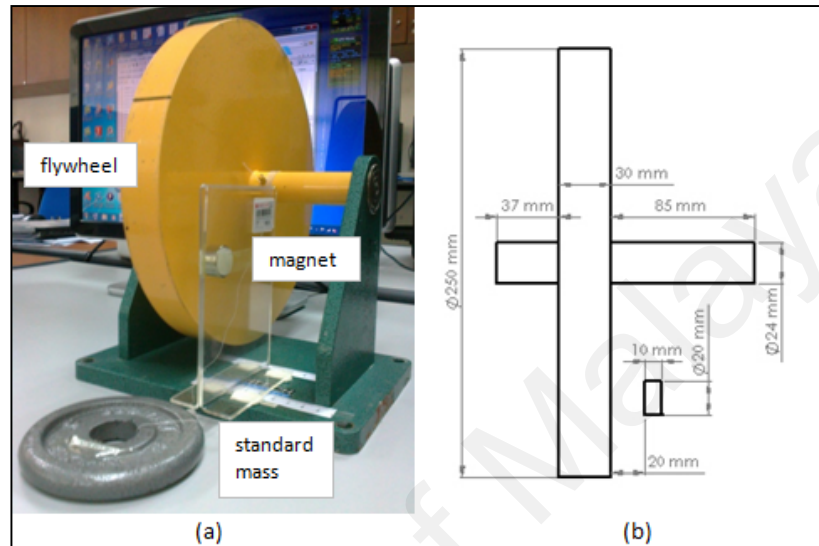
Figure 3.15: (a) Test setup used in eddy current damping validation work and (b) some relevant dimensions of the setup

The validation work proceeded as follows. The work involved measuring the transient, deteriorating response of the flywheel (in the form of rotational speed) due to eddy current damping, and then comparing it with that predicted by ANSYS® Maxwell in which the setup was replicated. This was done to observe the closeness between the two responses. For the test setup, firstly, without the permanent magnet, the flywheel's rotational motion was initiated by winding a 0.5 m thread around the shaft of the flywheel assembly and then by using the attached 0.5 kg mass to provide a consistent initial torque. This would accelerate the flywheel for a period determined by the length of the thread so that it reached an initial rotational speed before beginning to slow down. Then, the flywheel's rotational speed was measured indirectly by measuring the successive time taken for each revolution until the flywheel stopped completely.

Basically, this preliminary run was meant for the determination of the base damping of the setup (for instance, the damping effect due to friction of the rolling element bearings) which would then be approximately modeled in ANSYS® Maxwell as a base damping coefficient value. This approximated coefficient value was pinpointed using a curve-fitting approach with the aid of multi-body dynamic analysis software. Specifically, MSC.ADAMS was employed to compute the relevant damped response for an appropriate range of damping coefficients (0 – 0.0020 Nm.srad^{-1}). Following this, the response curve which gave rise to the least sum of square of errors was treated as the closest representation of the actual response due to base damping, and the associated damping coefficient value was taken into consideration in ANSYS® Maxwell as base damping modeling.

After the quantification of the base dampening effect, the test was then repeated in the presence of permanent magnet. With the permanent magnet in position according to the dimension stated in Figure 3.15(b), the flywheel was again subjected to the same motion initiation due to the weight of the standard mass. Similarly, the damped rotational response was determined by noting the successive time taken for each revolution. The obtained flywheel response, in the form of time trace of the rotational speed, would then serve as the reference for comparison with the simulated response. Finally, the same eddy current damping situation was modeled in ANSYS® Maxwell environment and was simulated using appropriate settings to obtain the computed flywheel response. The main simulation settings included the mesh element size (5 mm) which needed to be finer than the limiting dimensional parameter of the flywheel, as well as the simulation time resolution (0.001 s) determined by judging the convergence of the computed result parameters based on a number of preliminary trials. With both responses available, comparison between the responses would indicate the validity of

the simulation. First of all, the relevant responses in the tests described above, including those due to base damping and eddy current damping, are shown in Figure 3.16.
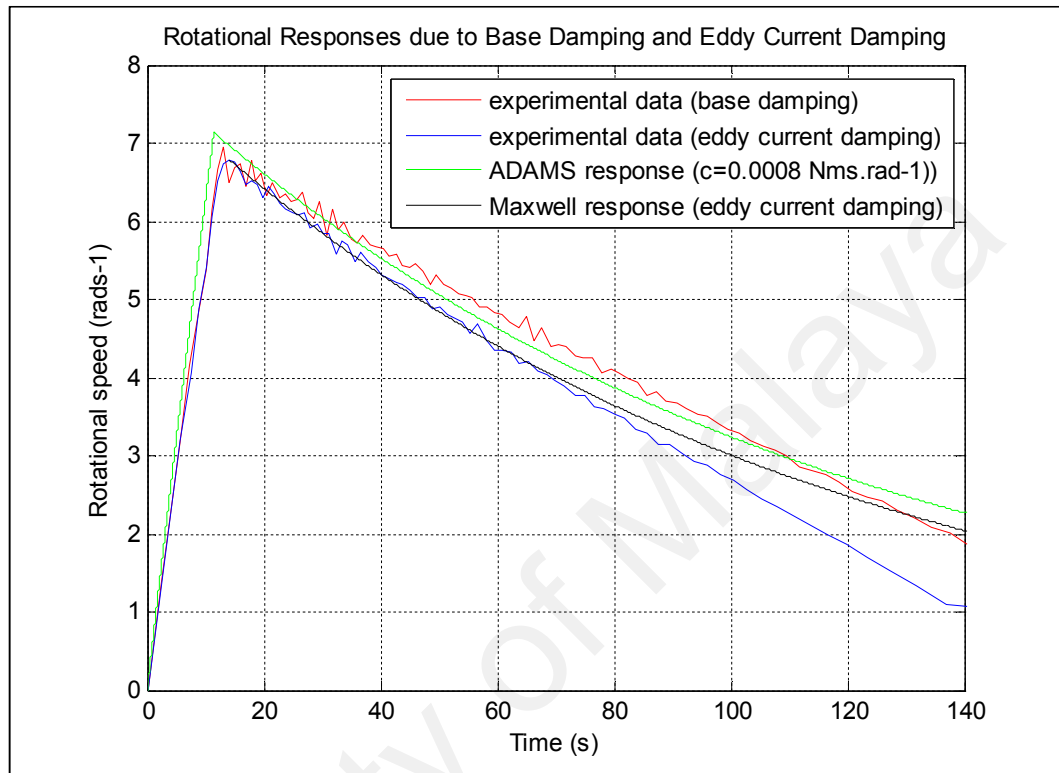
Figure 3.16: Measured and simulated flywheel responses due to base damping and eddy current damping

For the preliminary work involving the approximation of base dampening effect, it was determined that the rotational damping coefficient value of 0.0008 Nm.srad^{-1} produced the response with the least sum of square of errors. Hence, this value subsequently became the approximated representation of the base dampening effect for the flywheel assembly. The approximation using the base damping coefficient approach can be seen in Figure 3.16. Meanwhile, in the same figure, observation from the two plots representing the ANSYS® Maxwell simulated response and the actual flywheel response (both involving eddy current damping) showed some findings on the simulation's validity that are worth discussing. From the figure, it can be seen that the

responses can generally be divided into two parts: in the first part (ranging from plot time of 0 s to about 80 s), both simulated and actual responses were very close to each other; conversely, in the second part (ranging from plot time of about 80 s to the end of plots), the simulated response deviated quite significantly from the actual response. This can be justified by the following explanations. Basically, the first part of the flywheel response was associated with relatively high rotational speeds, and the deterioration of the response was mainly due to eddy current damping, as high rotational speeds gave rise to large opposing damping torques. In this region, the ANSYS® Maxwell model closely resembled the actual scenario. However, in the second part of the flywheel response, it can be deduced from the relatively low rotational speeds that the deterioration of response was dominated by the base dampening effect (mostly from frictional damping) which continued to slow the flywheel down until its motion was completely halted. The ANSYS® Maxwell model considered this with the inclusion of a base damping coefficient, but the approach did not accurately represent the situation, hence the obvious deviation of the second part of simulated response from the actual response. However, considering that the subsequent eddy current damping feasibility analysis involved the computation of damping torques at constant rotational speeds which were generally higher than the range of speeds relevant to Figure 3.16, the first part of the flywheel response was relevant in this validation work. By calculating the percentage of largest difference between the computed response and the actual response within the first part, with a deviation not greater than 3.65 % for the first part of responses, it can be said that the eddy current damping situation modeled in the virtual environment can serve as a valid representation of an actual setup.

With the simulation of eddy current damping situation in ANSYS® Maxwell validated, the suitability of the achievable damping for the combined damper-inerter

setup in passenger vehicle suspension application can be assessed confidently by computing the damping characteristic of the relevant eddy current damper model in the same software environment. For this part of feasibility study, again, the simplified eddy current damping situation was modeled, in which the model consisted of a cylindrical or disc-shaped flywheel as the conductor based on the dimensional values determined earlier in the inerter design work, and two permanent magnets with the shape resembling a segment of the cylinder. Figure 3.17 shows the illustration of the model. Although the model by no means served as a detailed representation of a damper-inerter device, it still captured the fundamental working principle of the rotary eddy current damping part of the combined damper-inerter concept.
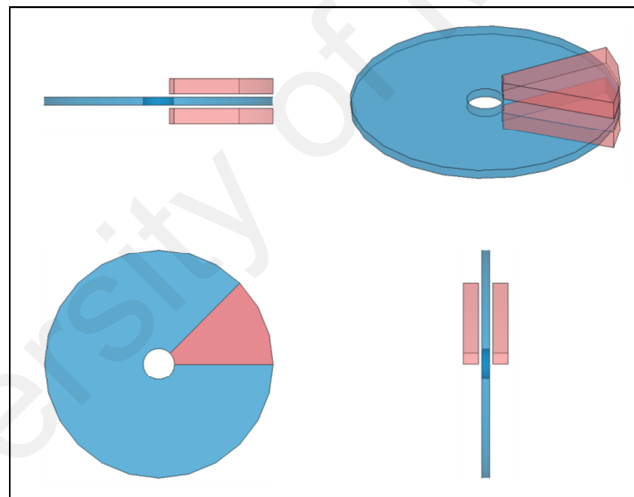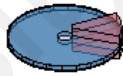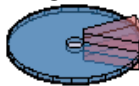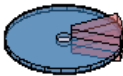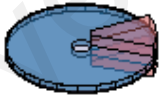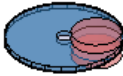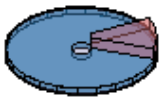
Figure 3.17: Illustration of the model used in eddy current damping simulation

Similar to the design analysis of inerter in Section 3.3.1, both the ball-screw and the rack-and-pinion designs were considered by adopting the flywheel's dimensional parameter values associated with both cases. The analysis first considered the parameter values for the ball-screw design. Basically, in the analysis, the model was repetitively solved to compute the opposing torques or damping torques acting on the flywheel when the flywheel was moving at a wide range of constant rotational speeds. This

88

enabled the determination of a comprehensive torque-speed characteristic across a wide range of speeds. Then, following the determination of rotational damping characteristic for a base design consisting of reasonable values or selections for some electromagnetic-related design parameters, these design parameters were taken into consideration for parametric analysis. In total, seven parameters were considered, namely (i) air gap, (ii) magnet configuration, (iii) coverage of magnet segment, (iv) magnet material, (v) height of magnet, (vi) number of magnet segment and (vii) magnet shape. Essentially, these were the design parameters which would affect the achievable damping, in addition to the flywheel's dimensional parameters which also affected the achievable inertance (and was therefore fixed during the design of inerter). In the parametric analysis, the parameters were varied individually as described in Table 3.8.

Table 3.8: Relevant variations of parameters for parametric analysis

Parameter						
(i)	(ii)	(iii)	(iv)	(v)	(vi)	(vii)
2 mm	Opposite poles	Partial	NdFeB	5 mm	1 segment	Arc
4 mm	Like poles	Complete	SmCo	10 mm	2 segments	Circular
6 mm	Single pole			15 mm	4 segments	
8 mm				20 mm		
10 mm						

For each parametric variation, the concerned parameter was varied while keeping other parameters at the base values or selections. In other words, these variations represented departures from the base design; consequently, evaluation on these variations enabled the analysis of the general range of achievable damping rates for the tested eddy current damper model.

With ANSYS® Maxwell simulations outputting the necessary results, the analysis on rotary eddy current damping feasibility can be carried out. Firstly, Figure 3.18 shows the plot of torque-speed characteristic due to eddy current damping for the base design. It should be noted here that the base design involved the following selections: (i) 2 mm air gap, (ii) opposite pole configuration, (iii) partial magnet segment, (iv) NdFeB magnet, (v) 10 mm height, (vi) single magnet segment and (vii) arc magnet shape.

Figure 3.18 describes the unique damping characteristic due to eddy current induction. Generally, such damping curve can be divided into two regions separated by a maximum point (maximum damping torque). In the first region, the damping characteristic is mostly linear as indicated by the almost linearly proportional relation between the damping torque and the rotational speed. This is because the current induced in the conductor under the presence of an external magnetic field varies proportionally with the magnitude of the conductor's motion. However, as the rotational speed increases, the reaction magnetic field due to eddy current itself can no longer be ignored. Therefore, the resulted damping torque increases with slower rates until it reaches a maximum value. Then, in the second region, at speeds higher than that of the maximum point, the interaction between the reaction magnetic field and the external magnetic field actually weakens the resulted flux density, hence a decrease in the

damping torque. This is consistent to the torque-speed characteristic of an electromagnetic brake (which is actually conceptually identical to an eddy current damper) as explained in a relevant past study (Gay, 2005). As the decreasing damping torque at high speeds is an undesirable damping characteristic for suspension application, only the first part of the computed results (from 0 rads^{-1} to 100 rads^{-1}), in which the linear relationship generally holds, was considered for the determination of damping rate. Similarly, subsequent simulations involved in the parametric analysis would consider only the same range of 0 rads^{-1} to 100 rads^{-1} as the damper's operating speed range.
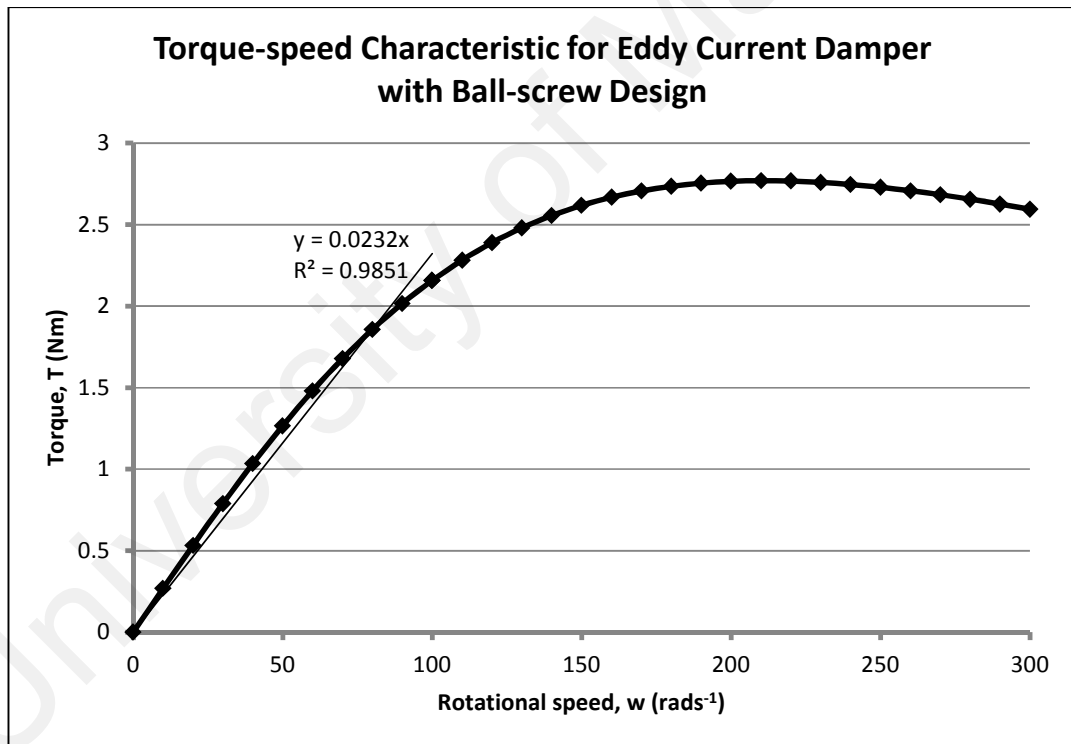
Figure 3.18: Torque-speed characteristic due to eddy current damping for ball-screw design

From the simple first order (linear) curve-fitting of the first part of computed damping characteristic, considering interception at the point of origin, the gradient value

obtained was 0.0232 Nms.rad^{-1} with an R^2 value of 0.9851. The high R^2 value fundamentally indicated that the torque-speed relationship was accurately captured by the equation of the fitted line. Meanwhile, the gradient value was equivalent to the estimated rotational damping rate for the base design used in simulation. Then, the achievable linear damping rate could be determined from the relation outlined in equation (3.28).

$$c_{translational} = \left(2\pi/p\right)^2 c_{rotational} \tag{3.28}$$

in which $c_{rotational}$ and $c_{translational}$ are respectively the rotational and translational damping rates. When converted back to the translational or linear motion, the linear damping rate is 228975 Nsm^{-1}, which is unsuitably high for the application of passenger vehicle suspensions. As a quick comparison, the linear damping rate of the specific passenger vehicle employed in the present research has a value of 1500 Nsm^{-1} (Table 3.1). To illustrate further, a previous research (Ebrahimi, 2009) also mentioned that for a passive damper in a midsize vehicle, the required mean damping coefficient in the range from 1500 Nsm^{-1} to 2000 Nsm^{-1} is acceptable.

Likewise, further analysis considering the variations in the electromagnetic-related parameters (described in Table 3.8) resulted in the same observation that the achievable linear damping rates were too high. The individual rotational damping characteristics are shown in Appendix D (Figure D1), while the derived damping rates are detailed in Table 3.9.

Table 3.9: Achievable rotational and linear damping rates for various parametric design

variations for ball-screw design

Parameter variation	Rotational damping rate, $c_{rotational}$ (Nms.rad^{-1})	Linear damping rate, $c_{translational}$ (Nsm^{-1})
Air gap		
2 mm	0.0232	228975
4 mm	0.0152	150018
6 mm	0.0101	99683
8 mm	0.0085	83892
10 mm	0.0051	50335
Magnet configuration		
Opposite poles	0.0232	228975
Like poles	0.0008	7896
Single pole	0.0077	75996
Coverage of magnet segment		
Partial	0.0232	228975
Complete	0.0005	4935
Magnet material		
Neodymium Iron Boron (NdFeB)	0.0232	228975
Samarium Cobalt (SmCo)	0.0188	185549
Height of magnet		
5 mm	0.0102	100670
10 mm	0.0232	228975
15 mm	0.0319	314840
20 mm	0.0408	402680
Number of magnet segment		
1 segment	0.0232	228975
2 segments	0.0499	492493
4 segments	0.0837	826086
Magnet shape		
Arc-segment	0.0232	228975
Circular	0.0222	219105

Being electromagnetic related, these additional design parameters (to the dimensional parameters which were already fixed due to the design of inerter) affected the generation of damping torque by affecting the externally applied magnetic field. Judging from the simulation outcomes (Figure D1, Appendix D), as a general observation, parametric variations which intensified the applied magnetic field, such as the reduction in air gap, the increase in magnet's height and greater number of magnet segments increased the achievable damping level. Apart from this, some specific observations are also worth discussing. For instance, it was noticed that although an

93

increase in coverage of the magnet segment (representing the coverage of magnetic field) should logically improve the achievable damping, the case with complete coverage (with magnetic field covering the entire flywheel) gave close to zero rotational damping rate. This is because the specific magnetic field for the case was symmetrical about the axis of rotation, and this prevented the flow of eddy currents. This justification is reversely in line with the explanation found in a past study (Montgomery, 2004) which mentioned that eddy current will be generated (in a Faraday disc setup) if the magnetic field is asymmetrical about the rotational axis. Elsewhere, it was also observed that the magnet configuration with opposite poles facing each other generated significant damping effect, but the reverse configuration with like poles facing each other resulted in negligible damping level. This is mainly because electromagnetic induction, in this case the induced current, is related to the vector product between the conductor's motion and the applied magnetic field which is favorable if the two components are perpendicular to each other. In the simulated damper model, the generated torque was maximized as well as acted in the desired opposite direction only in the presence of mostly axially-oriented magnetic field (the former configuration) instead of mostly radially-oriented magnetic field (the latter configuration). Finally, it is also interesting to note that both the arc-segment magnet shape and the circular or cylindrical magnet shape as investigated in the final parametric variation produced approximately the same achievable damping level. This was, however, only specific to the analyzed eddy current damper model with the fixed dimensional values. Nevertheless, the arc-segment shape had slightly higher damping characteristic. This is because a greater portion of the magnetic flux was applied near the outer edge of the flywheel, hence the slightly greater achievable damping torque.

Meanwhile, in terms of quantitative evaluation, results from Table 3.9 shows that the achievable linear damping rates ranged from 4935 Nsm^{-1} to as high as 826086 Nsm^{-1}, which is clearly not suitable for the application as damping in passenger vehicle suspension systems. It should be noted, however, that the unsuitability in vehicle suspension application was caused by the ball-screw design more than it was due to the eddy current damper concept. It can be seen from equation (3.28) that the expression of linear damping rate consists of a squared term involving the rotational-to-translational conversion factor of the ball-screw mechanism. As the typical ball-screw's pitch is small (in the range of millimeters as mentioned previously), this conversion factor becomes very large. Therefore, even though the eddy current damping produced in the model was reasonable in rotational motion, its effect was inappropriately enlarged by the conversion factor. Furthermore, the inappropriate magnitude of the conversion factor also resulted in a very narrow linear damper velocity working range. From the earlier explanation on Figure 3.18, it is already known that the favorable rotational operating speed range for the tested eddy current damper model is from 0 rads^{-1} to 100 rads^{-1}. However, after considering the rotational-to-translational conversion, this translated to a narrow working range of 0 ms^{-1} to 0.1 ms^{-1} (or ±0.1 ms^{-1} for both directions). This is significantly less than the common range of velocities for a damper which can reach ±1 ms^{-1} during operation. Considering these unfavorable outcomes, it is then logical to explore the other rotational-to-translational method commonly employed in an inerter, namely the rack-and-pinion mechanism.

In the repeated analysis involving the rack-and-pinion design, the eddy current damper model employed in the simulations remained fundamentally identical as shown in Figure 3.17. However, it was slightly different physically as it adopted the set of dimensional parameter values corresponding to the case of rack-and-pinion inerter

design. Following the same workflow, simulations in ANSYS® Maxwell using the base design parameter values related to this case gave the following outcome.

Torque-speed Characteristic for Eddy Current Damper with Rack-and-pinion Design

$y = 0.0464x$
$R^2 = 0.9735$

Torque, T (Nm)

Rotational speed, w (rads⁻¹)
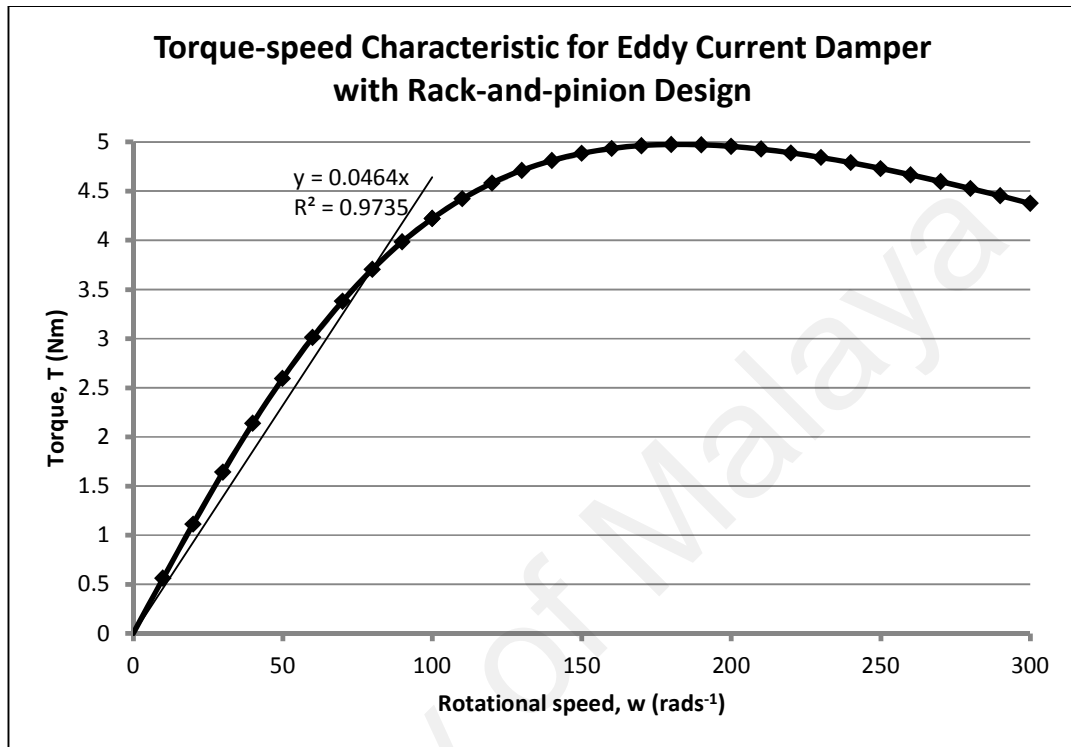
Figure 3.19: Torque-speed characteristic due to eddy current damping for rack-and-

pinion design

Similar to the outcome in the previous case (Figure 3.18), the torque-speed curve computed from the simulations can be separated into two regions, with the first region displaying almost linear relationship prior to a maximum point while the second region showing a deteriorating damping torque along with an increase in rotational speed. Also, the range of 0 rads⁻¹ to 100 rads⁻¹ was again adopted as the working speed range due to the region's linearity, and it was subsequently used in parametric analysis. From Figure 3.19, simple first order (linear) curve-fitting of the first part of damping curve, considering interception at the point of origin, resulted in a gradient value of 0.0464

Nms.rad^{-1} with a similarly high R^2 value of 0.9735. The gradient value can be converted to linear damping rate by the following relation:

$$c_{translational} = \left(2/d_p\right)^2 c_{rotational} \tag{3.29}$$

After conversion, this time the calculated linear damping rate is 464 Nsm^{-1}, which is lower than the typical requirement for passenger vehicle suspensions but still has similar order of magnitude compared to the requirement for the same application. Inferring from the calculated damping rate, it seems that a combined damper-inerter device is applicable in passenger vehicle suspensions using the rack-and-pinion design. From this point, it is then worth to evaluate whether or not parametric variations from the base design ensure that the original damping rate of 1500 Nsm^{-1} as stated in Table 3.1 can be realized. This was again done through parametric analysis considering variations of the same electromagnetic-related parameters, and the results are shown as damping rates in Table 3.10 (refer Figure D2, Appendix D for the individual damping characteristics).

Table 3.10: Achievable rotational and linear damping rates for various parametric

design variations for rack-and-pinion design

Parameter variation	Rotational damping rate, $c_{rotational}$ (Nms.rad^{-1})	Linear damping rate, $c_{translational}$ (Nsm^{-1})
Air gap		
2 mm	0.0464	464
4 mm	0.0343	343
6 mm	0.0208	208
8 mm	0.0148	148
10 mm	0.0117	117
Magnet configuration		
Opposite poles	0.0464	464
Like poles	0.0013	13
Single pole	0.0114	114

Coverage of magnet segment		
Partial	0.0464	464
Complete	0.0009	9
Magnet material		
Neodymium Iron Boron (NdFeB)	0.0464	464
Samarium Cobalt (SmCo)	0.0377	377
Height of magnet		
5 mm	0.0217	217
10 mm	0.0464	464
15 mm	0.0747	747
20 mm	0.0845	845
Number of magnet segment		
1 segment	0.0464	464
2 segments	0.0890	890
4 segments	0.1535	1535
Magnet shape		
Arc-segment	0.0464	464
Circular	0.0408	408

Due to the similarity of eddy current damper models used in both the ball-screw design and the rack-and-pinion design, the effects of these parameters on eddy current damping were the same, and the previous explanations are also applicable to the analysis involving the rack-and-pinion design. Based on the results in Table 3.10, variations in these parameters showed that a range from negligible damping to 1535 Nsm^{-1} for linear damping rate is achievable. It is noted that, due to the similarity in the dimensional parameter values between the two cases, the achievable rotational damping rates are actually quite similar. However, the particular factor that effects to a significant difference in terms of linear damping rate is the different conversion factors used in the repeated work. Using the rack-and-pinion method, with pinion diameter typically in the range of centimeters, the calculated conversion factor became desirable for the achievable damping rate, not to mention the achievable inertances as already explained in Section 3.3.1. Also, based on the same range of 0 rads^{-1} to 100 rads^{-1} for the usable rotary damping characteristic (Figure 3.19), the transformation back to translational motion using the conversion factor resulted in a linear damper velocity working range of 0 ms^{-1} to 1 ms^{-1} (or ±1 ms^{-1} for both directions), which closely matched the common

damper velocity operating range of about ± 1 ms^{-1}. Thus, to summarize, this part of work has demonstrated the practicality of implementing a parallel passive suspension layout with inerter by incorporating eddy current damping to an inerter.

3.3.3 Potential realization of semi-active suspension with variable eddy current damping

As already discovered in the study detailed in Section 3.2, the use of parallelly-arranged inerter is capable of providing performance benefits, particularly in terms of ride comfort, to typical passenger vehicles. This is not just applicable to passive suspension system, but to semi-active system as well. Up to this point, the study in this section (Section 3.3) has proven the fundamental feasibility of a parallel passive vehicle suspension layout through the incorporation of damping in an inerter for a combined parallel damper-inerter setup. However, while the suitability of a passive damper-inerter setup in passenger vehicle suspensions has been demonstrated in the form of achievable damping rates and inertances, it remains to be seen whether a variable damper-inerter setup, which relates to the pairing between semi-active suspension and inerter as studied in Section 3.2, is similarly suitable for passenger vehicle suspension application or not. Thus, to complement the previously discussed analyses, the final analysis serves as an extension to the feasibility study by looking into the possibility of achieving variable damping in an inerter as well as the suitability of the achievable damping levels for the realization of a semi-active suspension using the combined damper-inerter concept.

Like the previous analysis in Section 3.3.2, in this part of the study, the integration of damping element in an inerter was again considered to come from eddy current scenario. As explained in Section 2.3, eddy current is induced in a moving conductor when the conductor is subjected to an external magnetic field, and the dissipation of the generated resistive heat due to the flow of eddy currents contributes to

the damping effect. Therefore, in short, it can be said that the damping coming from an eddy current damper is the direct consequence of the externally applied magnetic field. In general, as discussed in the previous analysis, the greater the magnetic field (or, specifically, the flux density), the greater the resulted damping will be. Consequently, for each parametric variation examined previously, the achievable damping characteristic had a constant rate due to the constant magnetic field created by the permanent magnets. Deriving from this, it is conceptually possible to realize variable or discretely switchable damping in an inerter to form a variable damper-inerter device by applying variable magnetic field to the rotating conductor using, for example, electromagnets (current-carrying coils) instead of permanent magnets. However, in quantitative terms, it is presently not known whether the level of generated damping will fit the application of passenger vehicle suspensions or not, hence the need of feasibility analysis. Specifically, in this part of research, evaluations were carried out on a modified eddy current damper model comprising of the basic realization of the variable damping part of the damper-inerter setup. The model is illustrated in Figure 3.20.
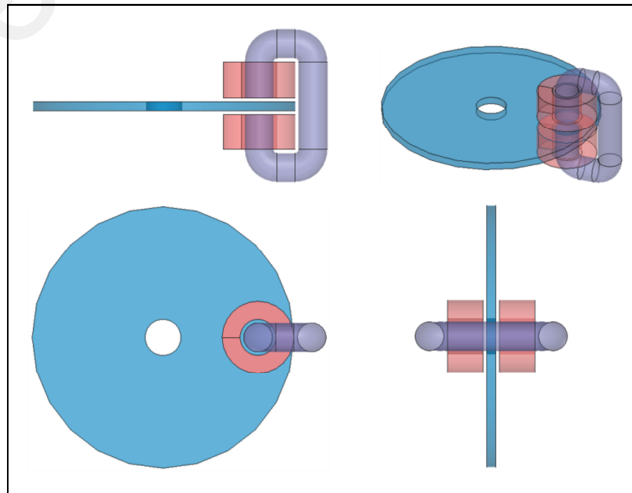
Figure 3.20: Illustration of the variable eddy current damper model

By comparing between the eddy current damper models used in the analyses (Figures 3.17 and 3.20), it is obvious that the modified damper model utilized current-carrying coils as replacement to the permanent magnets found in the initial damper model. Essentially, the use of current-carrying coils provided the capability of varying the achievable damping level, as the external magnetic flux density could be adjusted by varying the input coil current. However, despite the fundamentally different sources of damping (current coils as opposed to permanent magnets), the modified damper model still shared the same dimensional parameter values of the rotating flywheel conductor as the initial damper model. The adoption of the flywheel's dimensional parameter values as determined from the mathematical design of rack-and-pinion inerter, together with the use of the same rotational-to-translational conversion factor, ensured that the required inertance of $b_{desired} = 6$ kg was similarly achieved in this part of work. With the damper model conceptually and physically defined, the feasibility study was carried out by assessing the range of achievable damping rates as obtained from parametric analysis. In total, five design parameters related to the setup of current-carrying coils were considered for variations, including (i) input coil current, (ii) coil configuration, (iii) number of coil segment, (iv) core material and (v) coil-magnet combination. To be specific, the variations in these design parameters are stated in Table 3.11.

The analysis on the variations was done by again simulating the eddy current damper model in ANSYS® Maxwell to obtain the computed torque-speed relationships which represented the rotational damping characteristics. Consistent to the preceding section, for these damping characteristics, the region of 0 rads^{-1} to 100 rads^{-1} was considered as this would translate to a linear working velocity range of 0 ms^{-1} to 1 ms^{-1} (or ±1 ms^{-1} considering both directions) using the same rack-and-pinion conversion factor. Following this, the first order (linear) curve-fitting of the computed damping

characteristics gave the quantitative representation of the achievable rotational and translational damping for evaluation. These derived damping rates are stated in Table 3.12. Note that in this case the base selections included: (i) 2.0 A current, (ii) two coils with opposite pole configuration, (iii) single coil segment, (iv) iron core and (v) coil-only combination.

Table 3.11: Variations of parameters considered for the variable damper-inerter design
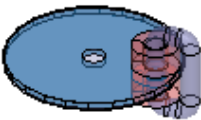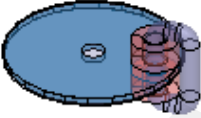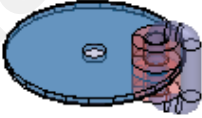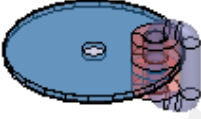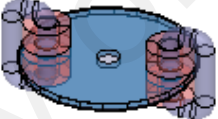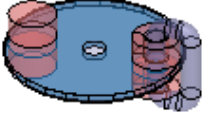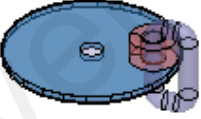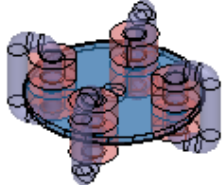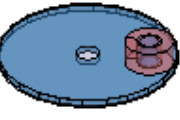
Parameter				
(i)	(ii)	(iii)	(iv)	(v)
0 A	2 coils opposite poles	1 segment	Iron	Coil
1.0 A	2 coils like poles	2 segments	Ferrite	Coil-magnet (opposite)
2.0 A	1 coil opposite poles	4 segments	Steel	Coil-magnet (adjacent)
3.0 A	1 coil single pole			
4.0 A				

Table 3.12: Achievable damping rates for parametric variations involving variable

damper-inerter design

Parameter variation	First rotational damping rate, $c_{rotational1}$ (Nms.rad^{-1})	Second rotational damping rate, $c_{rotational2}$ (Nms.rad^{-1})	First linear damping rate, $c_{translational1}$ (Nsm^{-1})	Second linear damping rate, $c_{translational2}$ (Nsm^{-1})
Input coil current				
0 A	0	0	0	0
1.0 A	0.0036	0.0012	36	12
2.0 A	0.0142	0.0047	142	47
3.0 A	0.0320	0.0105	320	105
4.0 A	0.0570	0.0186	570	186
Coil configuration				
2 coils opposite poles	0.0142	0.0047	142	47
2 coils like poles	0.0001	0.0001	0.8	0.6
Single coil opposite poles	0.0039	0.0012	39	12
Single coil single pole	0.0006	0.0003	6	3
Number of coil segment				
1 segment	0.0142	0.0047	142	47
2 segments	0.0279	0.0092	279	92
4 segments	0.0521	0.0170	521	170
Core material				
Iron	0.0142	0.0047	142	47
Ferrite	0.0133	0.0044	133	44
Steel	0.0120	0.0045	120	45
Coil-magnet combination				
Coil only	0.0142	0.0047	142	47
Coil-magnet (opposite)	0.0788	0.0456	788	456
Coil-magnet (adjacent)	0.0623	0.0394	623	394

In the analysis, it was found that the damping characteristics involved greater degree of non-linearity in the same range of 0 rads^{-1} to 100 rads^{-1} compared to the situation in the previous analysis. Consequently, to minimize the loss of accuracy in quantifying the achievable damping levels with a single linear damping coefficient value, the first order curve-fitting in this case took a slightly different approach by separating the damping curves into two regions (namely from 0 rads^{-1} to 50 rads^{-1}, and from 50 rads^{-1} to 100 rads^{-1}) and then fitting two different equations to obtain piecewise

functions. Each of the two-piece functions would then give two gradients or damping rates corresponding to the two regions of the damping characteristic, as in Table 3.12.

Results in the table clearly indicate that the use of current-carrying coils to provide the required magnetic field gave variability in terms of achievable damping to the proposed damper-inerter concept, as can be seen from the first parametric variation. This is because a current-carrying coil provides the flexibility of adjusting the applied magnetic field, hence the variability in damping characteristic. Generally, the outcome from the first parametric variation demonstrated that the damping level increased with input coil current. However, as observed from the same table, the overall range of achievable damping from 0 Nsm^{-1} to 570 Nsm^{-1} (considering the first four parametric variations) indicated that the tested current-carrying coil setup could not act as a standalone source of external magnetic field for the eddy current damper to be applied in typical passenger vehicle suspensions (recall that the passive damping requirement is typically from 1500 Nsm^{-1} to 2000 Nsm^{-1} (Ebrahimi, 2009) as discussed before; also, the study by Sharma et al. (1992) which used the same vehicle parameter values employed 900 Nsm^{-1} and 1500 Nsm^{-1} as the minimum and maximum damping rates for the discrete switchable damper). Despite the shortcoming, this did not stop a current coil setup to be utilized to provide an auxiliary, adjustable source of damping in addition to the main passive damping sourced from a permanent magnet setup. This is generally demonstrated by the final parametric variation, in which the combined use of permanent and variable magnetic sources significantly improved the total achievable damping rate, yet managed to provide certain level of variability in the damping characteristic. Considering that the permanent magnet setup has just been proven to be capable of generating the required damping level for typical passenger vehicle suspension application, it can therefore be deduced that the use of variable damper-inerter device in

the same application is also feasible by utilizing current-carrying coils to provide auxiliary but variable damping. Hence, in addition to the feasibility to be applied in passive suspensions, the idea of incorporating eddy current damping to an inerter is also effective in realizing a semi-active suspension (with parallel inerter) by applying variable damping to the combined damper-inerter device. Moving back to the main issue studied in the present section (Section 3.3), the feasibility as well as the practicality of implementing suspension layout with parallel inerter for passenger vehicles has therefore been proven.

CHAPTER 4 IMPLEMENTATION OF SWITCHING ALGORITHMS TO INERTER

The analyses carried out in Chapter 3 have demonstrated the practicality of inerter's implementation in passenger vehicle suspension systems in terms of its versatility and the achievable suspension parameter values for a realization of the parallel suspension configuration. However, the other issue, namely the non-prominent performance benefit first mentioned in Chapter 1, remains a limitation to be addressed. In fact, results from the study in Section 3.2 has shown that the degree of ride improvement due to passive inerter in parallel layout was rather small (although consistent) when it was applied to different vehicle suspension systems. Thus, Chapter 4 brings the matter of performance attainment into focus by examining modifications to the concept of inerter which can give rise to superior suspension performance. Considering that inerter and controllable suspension systems are two key areas of the current research, apart from pairing the inerter with existing controllable suspension systems as in the preceding chapter, another potentially advantageous implementation is to borrow the control strategies and allow the inerter element to be manipulated. This becomes the idea of Chapter 4. Specifically, this chapter deals with an in-depth study on the implementation of discrete on-off switching algorithms to an inerter: in Section 4.1, the switching algorithm derived from the commonly used semi-active force cancellation control strategy was theoretically applied to the inerter, and the potential performance improvement due to this semi-active suspension setup was analyzed. The method involved employing the same quarter vehicle model subjected to step and random road inputs as in the previous chapter. The analysis was comparative by nature, considering several suspension cases with switching algorithms in single-objective and multi-objective evaluations through numerical optimizations considering ride and road holding criteria. Meanwhile, in

Section 4.2, a switching algorithm which described the behavior of a passive but non-linear inerter was considered to determine its potential in improving vehicle sprung mass response. In this part, the comparative analysis involved the use of additional vehicle models, namely seven-DOF and ten-DOF full vehicle models, to investigate events due to ground disturbances initiated by the same road excitations as well as load disturbances initiated by typical step and sine steering maneuvers.

4.1 Performance Improvement of Suspension with Switchable Inerter

As seen in Chapter 2, researches for suspension performance improvement in terms of ride and handling have resulted in semi-active and active suspension systems that are capable of varying the suspension forces as well as a new suspension element that is the inerter which has been shown to be effective in providing improved ride and road holding ability when used with conventional passive suspension system (Smith & Wang, 2004). As both controllable suspension systems and the inerter are used with the same goal, it is interesting to evaluate the possibility of implementing the two concepts together to achieve even greater suspension performance. Apart from the pairing of passive inerter with semi-active and active suspensions as discussed previously, another possible implementation is to take the concept of switchable damper and apply it to the inerter to allow the inerter force to be switched and, therefore, manipulated.

This section deals with the use of inerter (in vehicle suspensions) which, theoretically, is capable of switching between on and off states based on semi-active force cancellation strategy to achieve superior ride comfort. In the study, the potential ride improvement brought by vehicle suspensions with switchable inerter force acting in parallel to spring and damper forces was determined and then compared against passive

suspension system with typical inerter to gage the additional suspension performance

gain. To begin, the switching algorithm applied to the inerter is shown by equation (4.1).

$$\text{if } (z_u - z_s)(\ddot{z}_u - \ddot{z}_s) \geq 0, \qquad b = b_{off},$$

$$\text{else,} \qquad b = b_{on} \tag{4.1}$$

in which b_{on} is the on-state inertance and b_{off} is the off-state inertance which was set to

be zero in this study, while other variables are as defined previously. It can be observed

that the switching algorithm outlined in equation (4.1) is adopted and modified from the

semi-active force cancellation strategy commonly applied to switchable damper

(equation (2.16)). The force cancellation control strategy was chosen in the study

considering that it was in line with the parallel inerter's inherent property of opposing

and cancelling the spring force as discussed in Section 3.1 when justifying its working

principle in vehicle suspensions.

In general, the implementation of discrete switching algorithms or other control

strategies require varying the inertance of a switchable or variable inerter. Although this

study is of theoretical nature, the realization of such variable-inertia device has been

shown possible in recent studies. For instance, the study by Li and Liang (2012)

demonstrated a realization of variable two-terminal mass device for which the

equivalent inertial mass was adjustable using an electro-hydraulic proportional valve.

Similarly, another study (Tsai & Huang, 2011) described the development of a variable-

inertia device employing planetary gearbox with variable gear ratio to control the

equivalent inertia of the device. Hence, conceptually, if the rack-and-pinion mechanism

is used to rotate the flywheel of an inerter, different inertances can be achieved by

varying the gear ratio of the mechanism as the inertance is dependent on this factor,

among others. Consequently, altering the gear ratio will enable the manipulation of inertance according to the switching algorithm. For the case of an on-off switchable inerter, the implementation can possibly be achieved by controlling the attachment and detachment of gears through actuator. As illustrated schematically in Figure 4.1, in the on state, the pinion is moved to mesh with the rack so that the effect of inerter is present. Conversely, in the off state, the pinion is detached, and the inerter's two terminals are free to move (off-state inertance, $b_{off} = 0$). For this switchable inerter, the on-state inertance can be designed similar to an ordinary passive inerter. For instance, the inertance of a rack-and-pinion inerter (Smith, 2008) is related to the mass or inertia property of the flywheel as well as the ratio of the gearing mechanism. For a simplified rack-and-pinion inerter as shown in Figure 4.1, the expression of on-state inertance is as derived in equation (3.27).
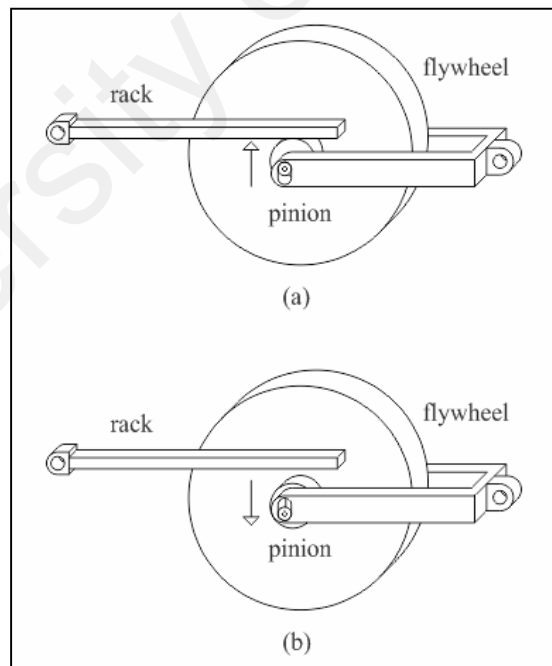
Figure 4.1: A possible physical realization of on-off switchable inerter in (a) the on state and (b) the off state

4.1.1 Test suspension cases and setup of analysis

In the study, simulations on mathematical vehicle model were carried out to determine the response of sprung and unsprung masses for several cases of suspension which included an ordinary passive suspension, suspensions with passive inerter, a system employing switchable inerter, and systems employing both switchable damper and inerter working on slightly different variants of force cancellation strategy. To clarify, the spring-damper-inerter combinations are summarized in Table 4.1.

Table 4.1: Combinations of suspension forces in the tests

Suspension case	Spring force	Damper force	Inerter force
1	Passive	Passive	-
2	Passive	Passive	Passive
3	Passive	Switchable	Passive
4	Passive	Passive	Switchable
5	Passive	Switchable	Switchable
6	Passive	Switchable	Switchable
7	Passive	Switchable	Switchable

As described in Table 4.1, seven cases were considered in the study; cases 1, 2 and 3 were treated as reference cases for comparison with the test cases employing switchable inerter (cases 4 to 7). For cases 3, 4 and 5 which involved switchable damper and inerter forces, the forces were determined based on the force cancellation strategy with switching algorithms as outlined in equations (2.16) and (4.1) respectively. However, slight modifications were made to the switching algorithms for cases 6 and 7. In case 6, when the directions of the relative displacement and relative velocity (or acceleration for inerter) were opposite to each other, a further decision was made according to which damper or inerter state was closer to the cancellation of the spring force. Similar logic was used in case 7; however, instead of allowing the damper and inerter to work independently, the control strategy would determine one of the four possible combinations of damping coefficient and inertance which gave rise to a

combined damper-inerter force that most closely canceled the spring force. When the direction criterion was not met, minimum damping state or off-state inertance, or both, was set. In logical statements, the switching algorithm for case 6 is represented by equations (4.2) and (4.3), while the switching algorithm for case 7 is described from equations (4.4) to (4.7), in which the variables are as defined previously. It can be seen from the equations that the algorithm for case 7 contains that for case 6, and case 7 differs from case 6 only in equation (4.7) where the decision logic between the two cases is different.

if $(z_u - z_s)(\ddot{z}_u - \ddot{z}_s) \geq 0,\ b = b_{off},$

elseif $|-k(z_u - z_s)| \leq \left| b_{off}(\ddot{z}_u - \ddot{z}_s) + \frac{1}{2}\left[b_{on}(\ddot{z}_u - \ddot{z}_s) - b_{off}(\ddot{z}_u - \ddot{z}_s) \right] \right|, b = b_{off},$

else, $b = b_{on}$ (4.2)

if $(z_u - z_s)(\dot{z}_u - \dot{z}_s) \geq 0,\ c = c_{min},$

elseif $|-k(z_u - z_s)| \leq \left| c_{min}(\dot{z}_u - \dot{z}_s) + \frac{1}{2}\left[c_{max}(\dot{z}_u - \dot{z}_s) - c_{min}(\dot{z}_u - \dot{z}_s) \right] \right| c = c_{min},$

else, $c = c_{max}$ (4.3)

Switch case (1),
$(z_u - z_s)(\dot{z}_u - \dot{z}_s) \geq 0$ and $(z_u - z_s)(\ddot{z}_u - \ddot{z}_s) \geq 0, b = b_{off}, c = c_{min}$ (4.4)

Switch case (2),
$(z_u - z_s)(\dot{z}_u - \dot{z}_s) \geq 0$ and $(z_u - z_s)(\ddot{z}_u - \ddot{z}_s) < 0,\ c = c_{min},$

if $|-k(z_u - z_s)| \leq \left| b_{off}(\ddot{z}_u - \ddot{z}_s) + \frac{1}{2}\left[b_{on}(\ddot{z}_u - \ddot{z}_s) - b_{off}(\ddot{z}_u - \ddot{z}_s) \right] \right|,\ b = b_{off},$

else, $b = b_{on}$ (4.5)

Switch case (3),

$$(z_u - z_s)(\dot{z}_u - \dot{z}_s) < 0 \text{ and } (z_u - z_s)(\ddot{z}_u - \ddot{z}_s) \geq 0, \ b = b_{off},$$

$$\text{if } |-k(z_u - z_s)| \leq \left| c_{min}(\dot{z}_u - \dot{z}_s) + \frac{1}{2}[c_{max}(\dot{z}_u - \dot{z}_s) - c_{min}(\dot{z}_u - \dot{z}_s)] \right|, \ c = c_{min},$$

$$\text{else, } c = c_{max} \tag{4.6}$$

Switch case (4),

$$(z_u - z_s)(\dot{z}_u - \dot{z}_s) < 0 \text{ and } (z_u - z_s)(\ddot{z}_u - \ddot{z}_s) < 0,$$

$$\text{if } \left| [-k(z_u - z_s)] - [b_{off}(\ddot{z}_u - \ddot{z}_s) + c_{min}(\dot{z}_u - \dot{z}_s)] \right| = \min, \ [b, c] = [b_{off}, c_{min}],$$

$$\text{elseif } \left| [-k(z_u - z_s)] - [b_{off}(\ddot{z}_u - \ddot{z}_s) + c_{max}(\dot{z}_u - \dot{z}_s)] \right| = \min, [b, c] = [b_{off}, c_{max}],$$

$$\text{elseif } |[-k(z_u - z_s)] - [b_{on}(\ddot{z}_u - \ddot{z}_s) + c_{min}(\dot{z}_u - \dot{z}_s)]| = \min, \ [b, c] = [b_{on}, c_{min}],$$

$$\text{else } |[-k(z_u - z_s)] - [b_{on}(\ddot{z}_u - \ddot{z}_s) + c_{max}(\dot{z}_u - \dot{z}_s)]| = \min, \ [b, c] = [b_{on}, c_{max}]$$

$$\tag{4.7}$$

The analysis of on-off switchable inerter for various cases was carried out mathematically using quarter vehicle model with two DOFs represented by the two equations of motion stated in Section 3.1. While equations (3.4) and (3.5) can be solved analytically for passive suspension system with fixed values of tire stiffness, spring stiffness, damping coefficient and inertance, for systems involving controllable suspensions, the results are obtained by solving the model numerically through simulations because these systems have damping coefficients and inertances which vary according to the control strategy. In this study, similar to other parts of the research, the mathematical vehicle model was solved numerically in MATLAB®/Simulink® to obtain sprung and unsprung mass responses. Also, the parameter values used in the study were again adopted from Crolla and Whitehead (2003) for consistency throughout the entire research.

To ensure consistency in the results, for all cases involving switchable damper, the maximum damping coefficient, c_{max} was set to be 1500 Nsm^{-1}, which is identical to the passive damping coefficient of the reference case (Table 3.1). The minimum damping coefficient, c_{min} was set to be approximately half of the passive damping coefficient value, hence the value of 900 Nsm^{-1}, which is the same as that used in a similar study (Sharma et al., 1992). On the other hand, the determination of passive and on-state inertance values took a different approach. While the off-state inertance was meant to be zero as there should be no inerter force acting on the system whenever it was switched off, the passive inertances in cases 2 and 3, and the on-state inertances from cases 4 to 7 were determined by iteratively experimenting each system with inertance values ranging from 0 kg to 320 kg. The selection of this range is actually similar to another study (C. Li et al., 2012b) which considered a range from zero to one for the ratio between inertance and sprung mass during analysis. For this part of analysis, a simple exploration on the design space was already sufficient, since the system which involved only two DOFs and single design variable could be solved quickly. In the study, evaluations were carried out in two ways. For evaluation based on single objective of ride only, in each case the inertance that gave minimum RMS sprung mass acceleration was chosen as optimum passive or on-state inertance, and the response due to the optimum inertance was analyzed. Meanwhile, for evaluation considering multiple objectives (ride and road holding ability), responses due to all inertances within the range were obtained from simulations, and the non-dominated Pareto solutions were determined to assess the relationship between RMS sprung mass acceleration and RMS dynamic tire load. These will be further detailed in Sections 4.1.2 and 4.1.3.

Again, the input to the quarter vehicle model was the vertical tire force generated due to ground excitation in the form of vertical road displacements, z_g. In the

study, the same class A smooth random road profile as described in Chapter 3 was employed. In addition, for single-objective evaluation, after the optimum inertances were determined, for each case the quarter vehicle model with optimum inertance was solved again using step profile with a step height of 0.1 m instead of random road profile to obtain the corresponding step response.

4.1.2 Evaluation based on single objective of ride criterion

By repetitively simulating the mathematical vehicle model with various inertances and keeping other parameters constant, there was an optimum inertance for each suspension case which gave lowest RMS sprung mass acceleration, similar to the outcome of analysis in Section 3.2. Note that case 1 did not require the determination of optimum inertance as the suspension setup consisted of only spring and damper. Also, whenever switchable inerter was involved, the off-state inertance was set to be zero; hence, only the optimum on-state inertance was determined. The complete set of results, which consist of several RMS suspension performance parameters and some transient characteristics due to step input, are summarized in Table 4.2.

Firstly, results from Table 4.2 shows that for the inerter to work and result in an improvement in ride, the suitable inertances occurred at a low value range for the passenger vehicle parameter values considered in this study. Particularly, the optimum inertances for suspension cases involving passive inerter were lower than the optimum on-state inertances for cases involving switchable inerter. This low inertance range shows agreement to earlier research (Smith & Wang, 2004) which noted that the parallel arrangement requires lower value of inertance than other arrangements such as the serial arrangement when it is optimized for ride quality.

114

Table 4.2: Summary of results due to random road input and the corresponding transient

characteristics due to step input

Parameter	Case 1	Case 2	Case 3	Case 4	Case 5	Case 6	Case 7
Random road response							
Optimum inertance (kg)	-	6	5	14	8	13	15
RMS sprung mass acceleration (ms^{-2})	0.1719	0.1682	0.1470	0.1600	0.1429	0.1291	0.1305
RMS dynamic tire load (N)	101.569	107.242	114.220	110.539	115.897	124.412	126.240
RMS suspension deflection ($\times 10^{-3}$ m)	1.248	1.246	1.291	1.158	1.232	1.337	1.514
Transient response							
Rise time (s)	0.1181	0.1211	0.1560	0.1642	0.2002	0.1996	0.1826
Peak time (s)	0.3418	0.3448	0.3990	0.4003	0.4533	0.4605	0.4467
Percent overshoot (%)	53.7161	52.9458	46.3617	36.2294	37.1956	41.7085	51.4270
Settling time (s)	2.0307	2.0469	2.1975	1.7715	2.2251	2.6287	2.6634
RMS sprung mass acceleration (ms^{-2})	2.0046	1.9633	1.6748	1.7616	1.5541	1.4813	1.5081
RMS dynamic tire load (N)	1164.2	1226.4	1316.0	1244.5	1327.2	1476.5	1540.6
RMS suspension deflection (m)	0.0156	0.0156	0.0165	0.0149	0.0168	0.0179	0.0190

Since the optimum inertances occurred at low values for all cases involving inerter (both passive and switchable, that is, from cases 2 to 7), it is worth analyzing the degree of variation in RMS sprung mass acceleration for each of the mentioned cases when the inertance is varied from zero to the optimum value. The purpose of performing this assessment is to determine whether or not the switchable inerter implementation is a worthwhile replacement to the passive inerter implementation, since the former has to show greater rate of performance parameter improvement than

the latter to be considered as superior. The outcome of analysis is shown in Table 4.3. Judging from the percentage difference and the average rate of change of performance parameter (variation in RMS sprung mass acceleration per inertance), it can be observed that the improvement in ride performance for cases with switchable inerter was more sensitive to the variation of inertance than that for cases with passive inerter. In other words, switchable inerter achieved greater ride performance than passive inerter for the same application of inertance. Specifically, cases 4 and 5 showed greater degree of improvement in RMS sprung mass acceleration per inertance than cases 2 and 3 respectively.

Table 4.3: Variations of RMS sprung mass acceleration from zero to optimum inertance

Parameter	Case 2	Case 3	Case 4	Case 5	Case 6	Case 7
RMS sprung mass acceleration at zero inertance (ms^{-2})	0.1719	0.1507	0.1719	0.1507	0.1517	0.1517
RMS sprung mass acceleration at optimum inertance (ms^{-2})	0.1682	0.1470	0.1600	0.1429	0.1291	0.1305
Percent difference (%)	-2.1397	-2.4595	-6.8899	-5.1811	-14.9441	-14.0069
Average rate of change of parameter ($\times 10^{-3}$ ms^{-2}kg^{-1})	-0.613	-0.741	-0.846	-0.976	-1.744	-1.417

Once the optimum inertances were known, the model was then simulated using those values to obtain sprung and unsprung mass responses due to random road input, followed by step input. When tested with random road input, the results showed that the RMS sprung mass acceleration of all cases with inerter were reduced and there were increases in RMS dynamic tire load. As mentioned previously, a reduction in RMS sprung mass acceleration implies ride improvement, as lower acceleration or lower resultant force is experienced by the passengers in the vehicle body. On the other hand, an increase in RMS dynamic tire load is generally undesirable as this means greater tire normal load variation which results in less road holding ability. Therefore, in the

implementation of passive as well as switchable inerter, an increase in RMS dynamic tire load became the compromise in an effort to reduce vertical body movement, since maintaining a smooth ride for the body invariably caused greater wheel movement. From Table 4.2, treating case 1 as reference, it can be seen that the case with passive inerter (case 2) brought only slight decrease in RMS sprung mass acceleration, cases with either switchable damper or inerter (cases 3 and 4) gave greater reduction in that parameter, while cases with both switchable damper and inerter (cases 5 to 7) resulted in the most reduction. Note that cases 6 and 7 gave similar reductions in RMS sprung mass acceleration due to the similarity of their switching algorithms.

In addition to RMS sprung mass acceleration and RMS dynamic tire load, the RMS suspension deflection is also an important performance parameter to consider. Even though the RMS suspension deflection obtained from the analysis was due to ground disturbance, it can still serve as an indirect indication on the performance of different cases when subjected to load disturbances. From the results, cases 1 and 2 had almost identical RMS suspension deflection values. This is consistent to a study (C. Li et al., 2012b) which mentioned that paralleling a two-terminal flywheel cannot improve the deflection performance of the suspension. Meanwhile, for most cases involving force cancellation strategy (case 3 and cases 5 to 7), the RMS suspension deflections were greater than the values corresponding to passive suspension cases. This has indirectly led to an inference of worsen performance for load disturbances, since greater RMS suspension deflection typically reflects a more softly sprung suspension which is favorable to the ride aspect but is known to deteriorate the performance in situations involving load transfer. Case 4, however, was an interesting exception in that it had lower RMS suspension deflection than reference case 1. While other suspension cases with force cancellation strategy attempted to minimize the resultant force acting

117

between the sprung and unsprung masses, the cancellation of spring force due to switchable inerter in case 4 left behind the damper force which acted between the masses, causing the oscillations of the masses to be controlled. Because suspension deflection is a measure of relative motion between sprung and unsprung masses, its RMS value was lowered.

When simulated using step input, the results were consistent to those due to random road input. The use of inerter, both passive and switchable, resulted in reductions in RMS sprung mass acceleration and increases in RMS dynamic tire load, indicating better ride but greater tire normal load variation. This shows that the use of passive and switchable inerter could be beneficial not just in normal driving situations but also in transient events which are less frequently encountered.

Apart from the RMS parameters, for simulations with step input, the sprung mass response (Figure 4.2) was also analyzed to determine the transient characteristics of the systems. The transient parameters have the following definitions. The rise time is the time taken for a body to rise from 10 % to 90 % of the final value of response which, in this study, referred to the final sprung mass displacement. The peak time is defined as the time for the body to reach the maximum value, and the corresponding overshoot, which is normally calculated as percentage, is the percent overshoot. The settling time used throughout the study is the time taken for the body response to settle down and remain within 2 % of the final value (Nise, 2008). Generally, for a comfortable ride, longer rise time and peak time are desirable as these mean less impact is experienced by the passengers. Conversely, lower percent overshoot and shorter settling time are preferred as these indicate less oscillatory response, hence less bumpy ride. From Table 4.2, with ordinary passive suspension (case 1) as reference, the use of inerter, both

passive and switchable, gave better effect to sprung mass response. From cases 2 to 7, the respective rise times and peak times were longer, and there was reduction in percent overshoot for each case when compared to reference case 1. These represented ride improvement. The only observed disadvantage of having the inerter force came in the form of increased settling time, with case 4 being the only exception.
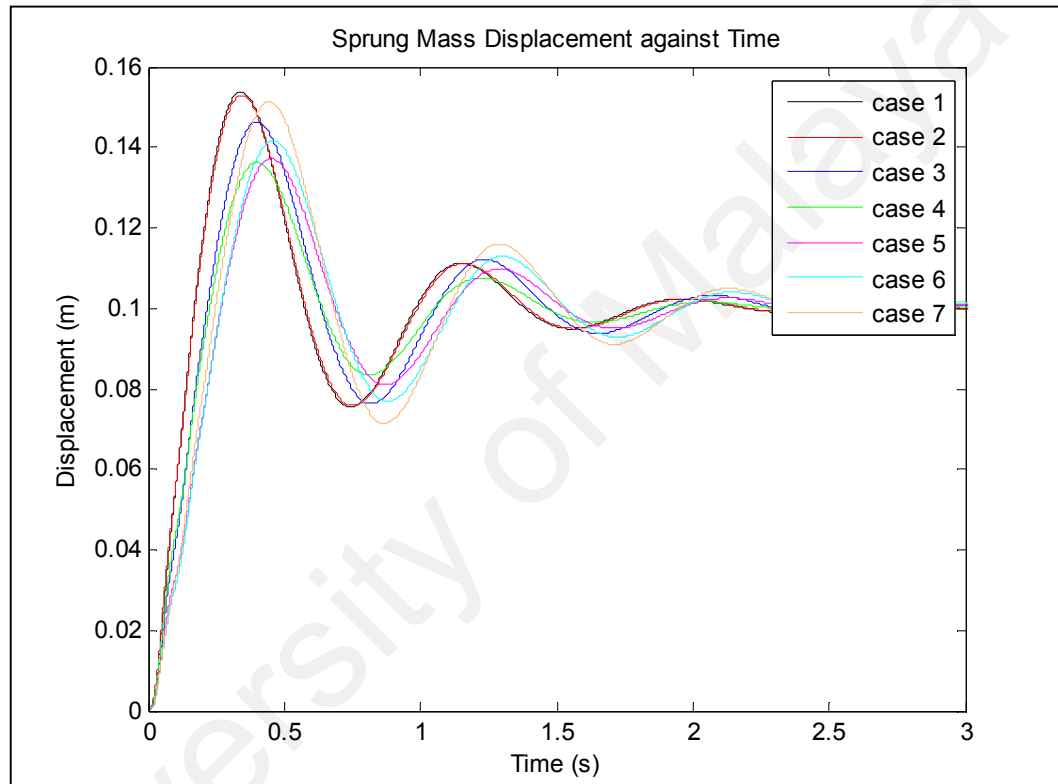
Figure 4.2: Transient responses of sprung mass due to 0.1 m step input

Several comparisons can be made between the test cases and the reference cases to evaluate the ride effectiveness of implementing the on-off switchable inerter based on force cancellation strategy. Firstly, by referring to the results of case 4 and reference case 1 (Table 4.2), there was an improvement in ride as the RMS sprung mass acceleration with random road input was decreased by 6.92 % (12.12 % for step input). The percent reduction for step input was comparable to those attained by semi-active

suspension system employing only switchable damper. As discussed previously, the increased RMS dynamic tire load became the drawback compared to reference case 1.

Another comparison can be made between case 4 and reference case 2 to evaluate the contribution of the switchable capability of an inerter to vehicle ride improvement. Results indicated that the presence of switchable inerter force gave better improvement (6.92 % and 12.12 % as stated earlier) than the slight ride enhancement brought by the presence of passive inerter force judging from the latter's mere 2.15 % (2.06 %) reduction in RMS sprung mass acceleration for the tested vehicle model.

Finally, comparison between case 5 and reference case 3 were made for the determination of the effectiveness of an on-off switchable inerter in enhancing an ordinary semi-active suspension system employing force-cancellation-based switchable damper. During simulations, reference case 3 showed a reduction in RMS sprung mass acceleration of 14.49 % (16.45 %). Meanwhile, in case 5 which employed both switchable damper and switchable inerter, the RMS sprung mass acceleration was reduced further to 16.87 % (22.47 %), marking a difference of 2.38 % (6.02 %) which approximately represented the portion of ride improvement enhanced by the switchable capability of inerter in the tested semi-active suspension. As indicated by the percentages, it was observed that greater enhancement was achieved for step input than for random road input.

4.1.3 Multi-objective performance evaluation

From the results above, an important inference regarding the proposed switchable inerter can be obtained: if only ride is considered as the sole objective in the analysis, the switchable inerter based on force cancellation strategy is capable of further lowering

the RMS sprung mass acceleration at the expense of increased RMS dynamic tire load. This, however, should not lead to the deduction that suspensions with switchable inerter are superior to those with passive inerter yet, as both sprung mass acceleration and dynamic tire load which respectively measure ride and road holding ability are equally important criteria. In fact, even for an ordinary suspension with only passive spring and damper, one can still vary the damping characteristic (in linear models, the damping coefficient) to achieve more comfortable ride by compromising the tire road holding ability. Therefore, more comprehensive information will be obtained if evaluation on the results is done by considering both performance measures together. A good way to evaluate both criteria simultaneously is to analyze the Pareto front involving the two objectives for a given suspension system, for example as done in the study by Scheibe and Smith (2009). As explained before in Section 3.2, in the context of present research which is related to vehicle suspension performance analysis, a solution is considered optimal if there is no other solution that can simultaneously improve both ride and road holding performance measures. By identifying the Pareto optimal points using the same test results, the scatter plot showing Pareto fronts for all cases (Figure 4.3) was plotted and analyzed.

Before evaluating the effectiveness of using switchable inerter, some matters are worth mentioning. Firstly, as shown in Figure 4.3, for every Pareto front (cases 2 to 7) there is a point that corresponds to minimum attainable RMS sprung mass acceleration but maximum RMS dynamic tire load. This is the solution that represents optimum inertance which maximizes ride improvement without considering the deterioration of the other objective (tire road holding ability), and is identical to the single-objective evaluation results where only ride criterion was focused. Secondly, case 1 which served as the reference case is only represented as a single point in Figure 4.3 as it did not

121

involve optimization of inertance. Judging from the figure, this is also the point of overlapping between Pareto fronts of cases 2 and 4, which represents zero passive and on-state inertances.
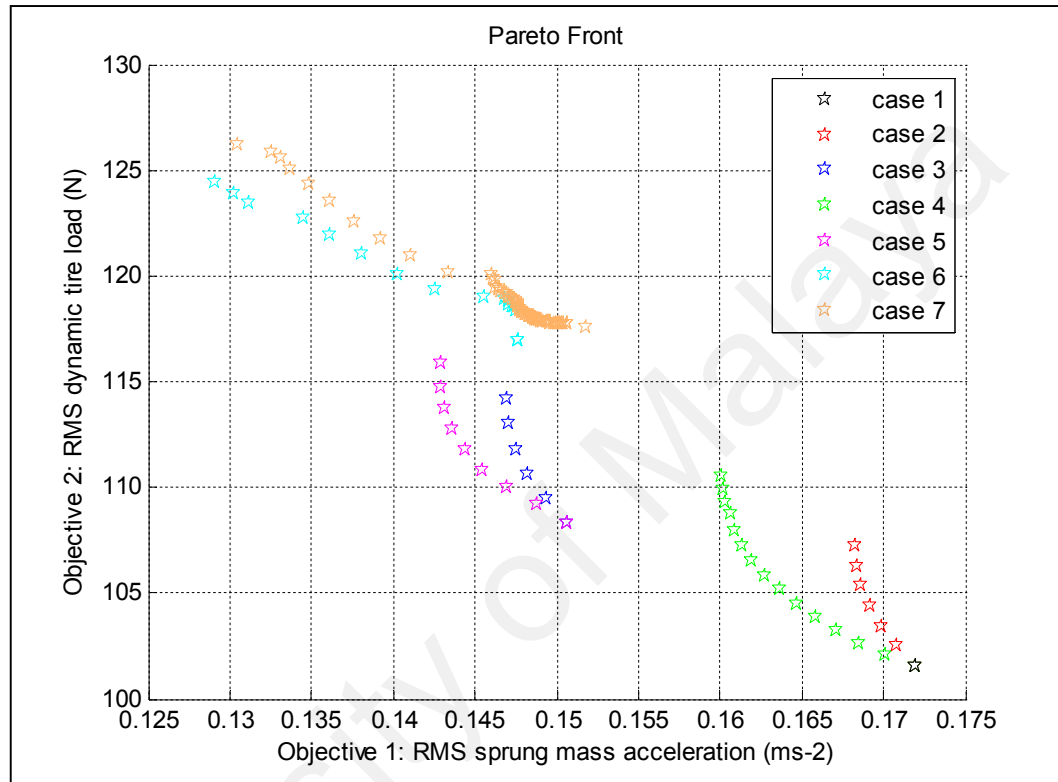
Figure 4.3: Pareto fronts with only inertance as design variable

By comparing suspension cases employing switchable inerter to corresponding cases employing passive inerter, one can observe that by allowing the inerter to be switched based on force cancellation strategy, the Pareto fronts obtained showed a shift towards lower ride objective (RMS sprung mass acceleration) and were therefore better than the Pareto fronts associated with cases employing passive inerter. To illustrate, by referring to Figure 4.3, case 4 showed an improvement over case 2, while case 5 showed an improvement over case 3. This implied that both ride and road holding ability can be further improved by the switchable capability of an otherwise passive inerter.

Meanwhile, another comparison made between case 2 and case 3 (or, correspondingly, between case 4 and case 5) revealed useful information regarding the implementation of force cancellation strategy on switchable damper. When allowed to be varied between the specific maximum and minimum damping coefficients, the Pareto front shifted (from case 2 to case 3, or from case 4 to case 5) towards the left but upwards. This implied that force cancellation was more beneficial in providing ride improvement than tire road holding improvement. However, it is important to note that this implication is valid only for the specific damping coefficients used in the analysis. From the Pareto fronts, cases 6 and 7 showed greatest reductions in RMS sprung mass acceleration, but in the evaluation of combined performance they were not the most desirable suspension cases because they gave rise to much higher RMS dynamic tire load. This can be explained by the corresponding two variants of switching algorithm which attempted to a great extent to nullify the resultant force between sprung and unsprung masses, thus causing the effect of very softly sprung suspensions with oscillatory responses. It was observed that because the two cases involved only slightly different switching algorithms, the outcomes were similar to each other.

So far, in the study related to Section 4.1, the inerter (both passive and switchable) was treated purely as an add-on element to existing vehicle suspension in the parallel arrangement. Consequently, during optimization, only the passive or on-state inertance was varied, while other suspension parameters such as the spring stiffness and damping coefficient (or maximum and minimum damping coefficients for cases with switchable damper) were fixed. While comparison between cases with switchable inerter and cases with passive inerter was possible, comparison with ordinary passive suspension, or case 1, was limited because using fixed vehicle parameters as stated in Table 3.1 resulted in only one solution or one point in Figure 4.3 as discussed

earlier. Furthermore, considering the finding in Section 3.1 that both damping rate and inertance should be optimized for greater vibration isolation in a parallel suspension layout, there is a possibility that further improvement will be attained if damping characteristic is correspondingly varied when certain inertance is used. With these in mind, optimization involving both damping coefficient and inertance as design variables was considered.

In the repeated analysis, both damping coefficient and inertance were allowed to vary within specified ranges. For inertance, the range from 0 kg to 320 kg remained the same. This range applied to cases involving passive inerter as well as switchable inerter. Meanwhile, for damping parameter values of cases with switchable damper, the minimum damping coefficient was fixed at 900 Nsm^{-1} as before, while the maximum damping coefficient was set to vary from 900 Nsm^{-1} to 6000 Nsm^{-1}. The upper limit corresponded to the situation where the damping ratio was close to one. The choice of fixing a minimum damping coefficient allowed closer emulation of the property of commercially available variable damper, so that the results obtained would be more realistic. For instance, with magnetorheological dampers, there is a fixed minimum damping level when no current is applied, and damping increases with current. To ensure consistency, the range of passive damping coefficient for case 1 was set to be identical, that is, from 900 Nsm^{-1} to 6000 Nsm^{-1}. Also, because more than one variable were considered, solving the quarter vehicle model for all combinations became increasingly time consuming and impractical. Therefore, unlike earlier analysis, the Pareto fronts were obtained with the aid of multi-objective optimization function in MATLAB$^{®}$ instead of enumerating all solutions within the design space. The plots are shown collectively as Figure 4.4.
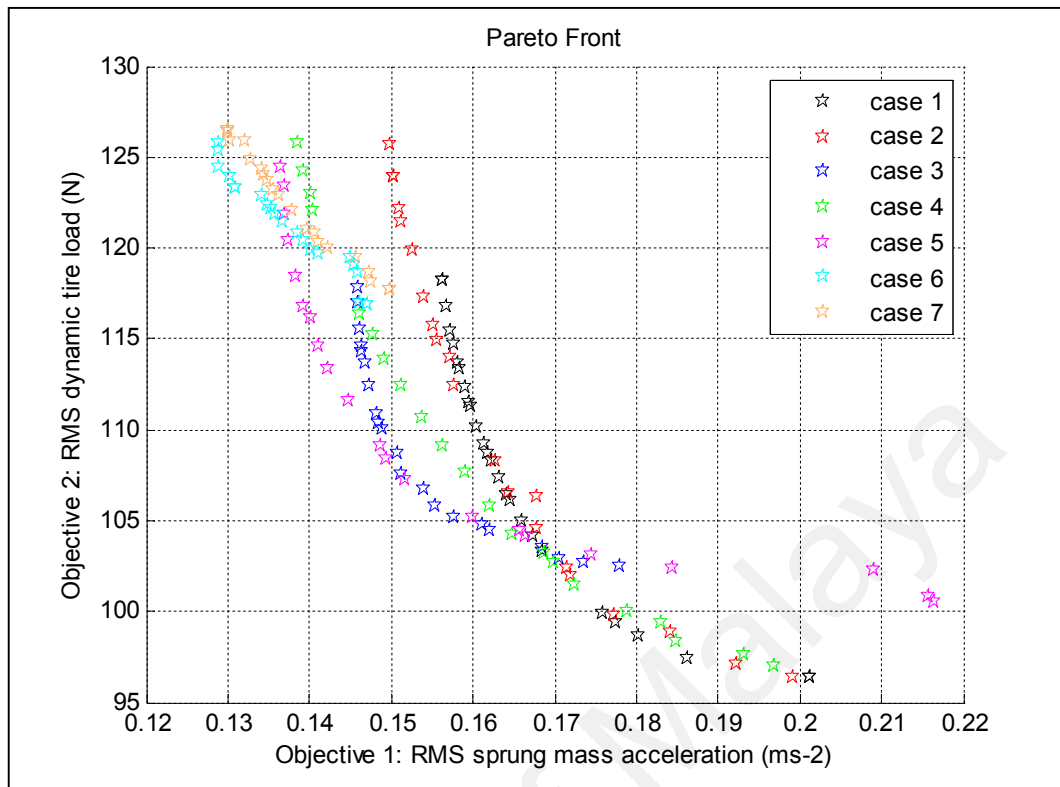
Figure 4.4: Pareto fronts with both damping coefficient and inertance as design

variables

By comparison, the repeated analysis showed the same observations: case 4 showed an improvement over case 2; so did case 5 over case 3. This indicated the advantage of switchable inerter over passive inerter. Again, the Pareto optimal points for cases 6 and 7 were close to each other. However, by allowing the passive damping coefficient (or, in some cases, maximum damping coefficient) to be varied together with inertance, several differences were observed. By comparing Figure 4.4 to Figure 4.3, the Pareto fronts (cases 2 to 5) were noticeably wider, indicating greater possibilities for optimal design solutions. This is logical as the optimization considered two design variables compared to single variable in the preceding analysis. Also, for cases 2 and 4 which employed passive damper, the Pareto fronts were better than those from Figure 4.3. Finally, when compared to the Pareto front of ordinary passive suspension (case 1),

Pareto fronts with passive and switchable inerters were generally superior, although some solutions for cases 3 and 5 were inferior to solutions obtained for ordinary passive suspension with only spring and damper. This is mainly due to the implementation of force cancellation strategy on switchable damper. For case 1 involving passive damper, the optimal solutions relevant to the right of the Pareto front are associated with high damping coefficient, since it is expected that high damping increases the RMS sprung mass acceleration (Rakheja & Sankar, 1985) but suppresses RMS dynamic tire load. The use of force cancellation strategy in switchable damper for cases 3 and 5 effects in soft suspension whenever minimum damping coefficient is set. Therefore, it tends to lower the RMS sprung mass acceleration but increase the RMS dynamic tire load. Furthermore, it was noticed in Section 4.1.2 that the presence of parallel inerter in passenger vehicle with parameters employed in this study also increased the RMS dynamic tire load. Thus, there is a general upward trend for the Pareto fronts involving cases 3 and 5 compared to case 1.

Overall, the analysis has indicated that the proposed implementation of on-off switchable inerter based on force cancellation strategy in vehicle suspensions offered greater performance improvement than suspension system with passive inerter which gave only slight improvement in the parallel layout. Thus, it can be said that this is a viable option for better adoption of inerter element in passenger vehicle suspensions.

4.2 Ride Evaluation of Suspension Employing Non-linear Inerter

It is worth to recall here that the motivation of the work in the current chapter is to respond to the non-prominent ride improvement for suspensions with original passive inerter (as observed in Chapter 3) by implementing switching algorithms to an inerter. In the preceding section, the theoretical implementation of switching algorithm based on

force cancellation strategy resulted in the inerter, and in some test cases the damper as well, to be considered as semi-active switchable element. However, in some situations, such on-off or two-state discrete switching algorithm can also describe the non-linear behavior of a suspension element which remains strictly passive. An example of non-linear suspension element is the dual or multi-rate springs. Following the matter discussed above, this section centers on the theoretical study of a different implementation of switching algorithm to inerter in vehicle suspensions to control sprung mass response. In the study, the inerter, which was termed as non-linear, was made to be switchable according to a switching algorithm or control law based on the suspension deflection (relative displacement between sprung and unsprung masses).

4.2.1 Mathematical modeling and analysis

As mentioned above, the non-linear inerter employed in the analysis was made to be switchable between on and off states depending on whether or not the relative movement between its terminals exceeded a specified free play. From the vehicle suspension's point of view, this means that the inerter element is active only when there is large suspension deflection, for instance, due to transient road input. In reality, it is reasonably possible to realize this behavior through, for example, a special rack-and-pinion mechanism with discontinuity on the rack that is used to rotate a flywheel which gives rise to inerter force (Figure 4.5). When such a rack is used, the engagement of the flywheel of an inerter can be varied: within the toothless region, the flywheel is not engaged, and the inerter is switched off; however, once the suspension deflection is beyond the mechanical play, the gears are meshed, and the flywheel shows its presence. This deliberately-created mechanical free play is highly similar to the backlash of typical gear mechanisms that results in the non-linear behavior of devices with gears. In fact, the term 'non-linear' used to describe the switching behavior of this inerter has

similarity to the studies by Wang and Su (2008a, 2008b) which considered friction, backlash and elastic effect as the non-linearities of an inerter.
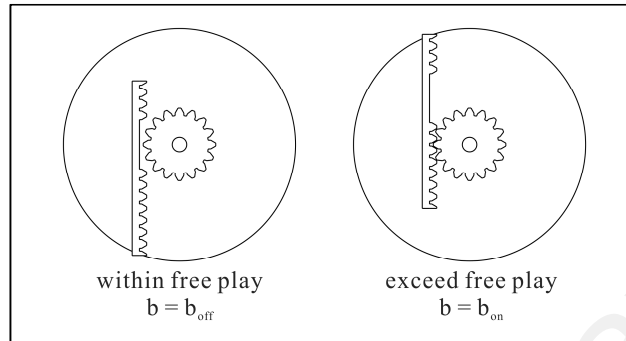
Figure 4.5: A possible realization of non-linear inerter using rack with discontinuous section

In the study, this non-linear behavior was represented mathematically as a switching algorithm as detailed by equation (4.8).

$$\text{if } |z_u - z_s| \geq a, \qquad b = b_{on},$$
$$\text{else,} \qquad b = b_{off} \tag{4.8}$$

in which z_s and z_u are the sprung and unsprung mass displacements, a is the specific free play or the limit of suspension deflection, b_{on} is the on-state inertance, and b_{off} is the off-state inertance which was set to be zero in the study. Observing from equation (4.8), it can be noted that the logical statement worked on relative displacement between sprung and unsprung masses. This type of limited-relative-displacement algorithm actually coincides with the displacement-based semi-active suspension control strategy that has been detailed in Section 2.2 along with other similarly well known strategies such as the semi-active Skyhook strategy and the force cancellation strategy. When applied to a switchable damper as in the usual case, the goal remains the same: to resist excessive

sprung mass movement. Therefore, in the application to a semi-active damper, high damping rate is set when the relative displacement is greater than a specific value, while low damping rate is set otherwise (Shen et al., 2006). However, for a non-linear inerter, the system works independently as the switch between states is inherently implemented by the device's working principle, similar to the way other non-linear elements such as a dual-rate spring work by themselves. Also, because the non-linear inerter does not draw energy for its operation, it remains a passive suspension element.

In the study, the non-linear inerter was tested comprehensively with several mathematical vehicle models, namely the two-DOF quarter vehicle model, the seven-DOF full vehicle model, and the ten-DOF handling model (although the main focus was still on the vertical dynamics). The analysis was carried out by first considering the fundamental, lumped-mass quarter vehicle model which has already been adopted in previous sections (see Section 3.1 for its schematic diagram and the equations of motion). The two-DOF quarter vehicle model was of primary importance to the study as the sprung mass attitude due to ground excitations needed to be evaluated.

As the study involved evaluation of vehicle ride from the aspect of transient vehicle body attitude, apart from assessing the vertical sprung mass acceleration obtained from the quarter vehicle model as a primary ride performance measure, it was also desirable to measure other ride-related parameters, for instance, the vehicle's roll and pitch. Basically, when the rotational responses of sprung mass due to ground inputs are needed, a seven-DOF full vehicle model is necessary. This full vehicle model is essentially an extension of the two-DOF quarter vehicle model as it incorporates the vehicle body (sprung mass) and all four wheels (unsprung masses). This contributes to the seven DOFs, which include the vertical motion of each wheel, the vehicle body's

vertical motion, roll and pitch. The free-body diagram of the full vehicle model is shown in Figure 4.6, and the equations of motion representing the DOFs are described from equations (4.9) to (4.15).
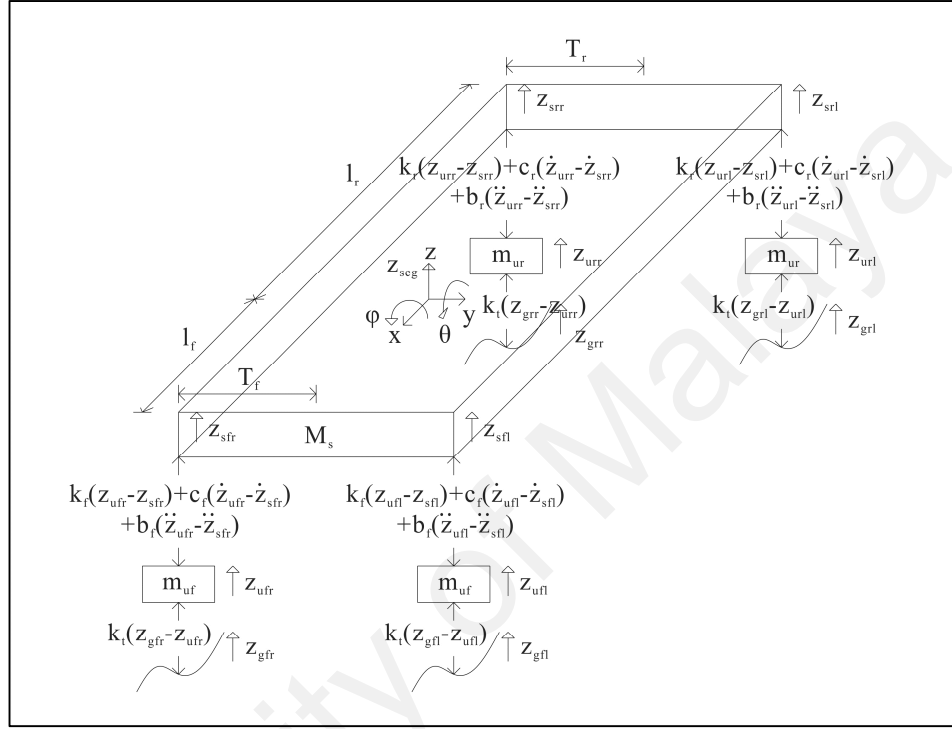
Figure 4.6: The free-body diagram of a full vehicle model employing inerter

$$M_s \ddot{z}_{scg} = k_f\big(z_{ufl} - z_{sfl}\big) + c_f\big(\dot{z}_{ufl} - \dot{z}_{sfl}\big) + b_f\big(\ddot{z}_{ufl} - \ddot{z}_{sfl}\big) + k_f\big(z_{ufr} - z_{sfr}\big)$$

$$+c_f\big(\dot{z}_{ufr} - \dot{z}_{sfr}\big) + b_f\big(\ddot{z}_{ufr} - \ddot{z}_{sfr}\big) + k_r(z_{url} - z_{srl}) + c_r(\dot{z}_{url} - \dot{z}_{srl})$$

$$+b_r(\ddot{z}_{url} - \ddot{z}_{srl}) + k_r(z_{urr} - z_{srr}) + c_r(\dot{z}_{urr} - \dot{z}_{srr}) + b_r(\ddot{z}_{urr} - \ddot{z}_{srr}) \qquad (4.9)$$

$$I_x \ddot{\varphi} = \Big(k_f\big(z_{ufl} - z_{sfl}\big) + c_f\big(\dot{z}_{ufl} - \dot{z}_{sfl}\big) + b_f\big(\ddot{z}_{ufl} - \ddot{z}_{sfl}\big)\Big)\big(T_f\big)$$

$$-\Big(k_f\big(z_{ufr} - z_{sfr}\big) + c_f\big(\dot{z}_{ufr} - \dot{z}_{sfr}\big) + b_f\big(\ddot{z}_{ufr} - \ddot{z}_{sfr}\big)\Big)\big(T_f\big)$$

$$+\big(k_r(z_{url} - z_{srl}) + c_r(\dot{z}_{url} - \dot{z}_{srl}) + b_r(\ddot{z}_{url} - \ddot{z}_{srl})\big)(T_r)$$

$$-\big(k_r(z_{urr} - z_{srr}) + c_r(\dot{z}_{urr} - \dot{z}_{srr}) + b_r(\ddot{z}_{urr} - \ddot{z}_{srr})\big)(T_r) \qquad (4.10)$$

$$I_y\ddot{\theta} = -\left(k_f(z_{ufl} - z_{sfl}) + c_f(\dot{z}_{ufl} - \dot{z}_{sfl}) + b_f(\ddot{z}_{ufl} - \ddot{z}_{sfl})\right)(l_f)$$

$$-\left(k_f(z_{ufr} - z_{sfr}) + c_f(\dot{z}_{ufr} - \dot{z}_{sfr}) + b_f(\ddot{z}_{ufr} - \ddot{z}_{sfr})\right)(l_f)$$

$$+\left(k_r(z_{url} - z_{srl}) + c_r(\dot{z}_{url} - \dot{z}_{srl}) + b_r(\ddot{z}_{url} - \ddot{z}_{srl})\right)(l_r)$$

$$+\left(k_r(z_{urr} - z_{srr}) + c_r(\dot{z}_{urr} - \dot{z}_{srr}) + b_r(\ddot{z}_{urr} - \ddot{z}_{srr})\right)(l_r) \tag{4.11}$$

$$m_{uf}\ddot{z}_{ufl} = k_t(z_{gfl} - z_{ufl}) - k_f(z_{ufl} - z_{sfl}) - c_f(\dot{z}_{ufl} - \dot{z}_{sfl}) - b_f(\ddot{z}_{ufl} - \ddot{z}_{sfl})$$

$$\tag{4.12}$$

$$m_{uf}\ddot{z}_{ufr} = k_t(z_{gfr} - z_{ufr}) - k_f(z_{ufr} - z_{sfr}) - c_f(\dot{z}_{ufr} - \dot{z}_{sfr}) - b_f(\ddot{z}_{ufr} - \ddot{z}_{sfr})$$

$$\tag{4.13}$$

$$m_{ur}\ddot{z}_{url} = k_t(z_{grl} - z_{url}) - k_r(z_{url} - z_{srl}) - c_r(\dot{z}_{url} - \dot{z}_{srl}) - b_r(\ddot{z}_{url} - \ddot{z}_{srl})$$

$$\tag{4.14}$$

$$m_{ur}\ddot{z}_{urr} = k_t(z_{grr} - z_{urr}) - k_r(z_{urr} - z_{srr}) - c_r(\dot{z}_{urr} - \dot{z}_{srr}) - b_r(\ddot{z}_{urr} - \ddot{z}_{srr})$$

$$\tag{4.15}$$

in which M_s is the total sprung mass value, I_x and I_y are the sprung mass moments of inertia about x-axis and y-axis respectively, $m_{uf,r}$ are the front and rear unsprung mass values, $z_{sfl,fr,rl,rr}$ and $z_{ufl,fr,rl,rr}$ are the sprung and unsprung mass displacements for front-left, front-right, rear-left and rear-right positions respectively, $\dot{z}_{sfl,fr,rl,rr}$ and $\dot{z}_{ufl,fr,rl,rr}$ are the corresponding velocities, $\ddot{z}_{sfl,fr,rl,rr}$ and $\ddot{z}_{ufl,fr,rl,rr}$ are the corresponding accelerations, $z_{gfl,fr,rl,rr}$ are the ground displacements, $\ddot{z}_{scg}$ is the sprung mass acceleration at the center of gravity, $\ddot{\varphi}$ and $\ddot{\theta}$ represent roll and pitch accelerations, k_t is

the tire stiffness, $k_{f,r}$, $c_{f,r}$, $b_{f,r}$ are the front and rear spring stiffnesses, damping rates and inertances respectively, $T_{f,r}$ are the front and rear half-tracks, l_f is the distance from center of gravity to front axle while l_r is the distance from center of gravity to rear axle.

In addition, a ten-DOF mathematical vehicle model was also used for further analysis of roll response. This part of analysis enabled the evaluation on the effectiveness of non-linear inerter in resisting roll due to handling maneuvers (specifically, due to steering inputs) knowing that its working principle is similar to dual-rate springs or non-linear spring setups that are capable of reducing roll during driving situations (Turrini & Ducatti, 2007). A ten-DOF vehicle model as used in the study is essentially an integration of the previously described seven-DOF model and a four-wheel, three-DOF bicycle model or handling model. The additional three DOFs are the vehicle's lateral, longitudinal and yaw motions. Specifically, the presence of lateral and longitudinal tire forces gives rise to lateral and longitudinal responses of a vehicle, while the moments due to these forces result in vehicle yaw response. This is illustrated by Figure 4.7 and equations (4.16) to (4.18):

$$M(\dot{v}_x - v_y \psi) = F_{xfl} \cos \delta_{fl} - F_{yfl} \sin \delta_{fl} + F_{xfr} \cos \delta_{fr} - F_{yfr} \sin \delta_{fr} + F_{xrl} + F_{xrr}$$

(4.16)

$$M(\dot{v}_y + v_x \psi) = F_{xfl} \sin \delta_{fl} + F_{yfl} \cos \delta_{fl} + F_{xfr} \sin \delta_{fr} + F_{yfr} \cos \delta_{fr} + F_{yrl} + F_{yrr}$$

(4.17)

$$I_z \ddot{\psi} = \left(-F_{xfl} \cos \delta_{fl} + F_{yfl} \sin \delta_{fl} + F_{xfr} \cos \delta_{fr} - F_{yfr} \sin \delta_{fr}\right)(T_f)$$

$$+\left(F_{xfl} \sin \delta_{fl} + F_{yfl} \cos \delta_{fl} + F_{xfr} \sin \delta_{fr} + F_{yfr} \cos \delta_{fr}\right)(l_f)$$

$$+(-F_{xrl} + F_{xrr})(T_r) + \left(-F_{yrl} - F_{yrr}\right)(l_r)$$

(4.18)

in which M is the total vehicle mass, I_z is the sprung mass moment of inertia about z-axis, $T_{f,r}$, $l_{f,r}$ are as defined previously, v_y and v_x are the lateral and longitudinal sprung mass velocities, $\ddot{\psi}$ is the yaw acceleration, $F_{yfl,fr,rl,rr}$ and $F_{xfl,fr,rl,rr}$ are the lateral and longitudinal tire forces for front-left, front-right, rear-left and rear-right positions respectively, $\delta_{fl,fr}$ are the front-left and front-right steer angles.
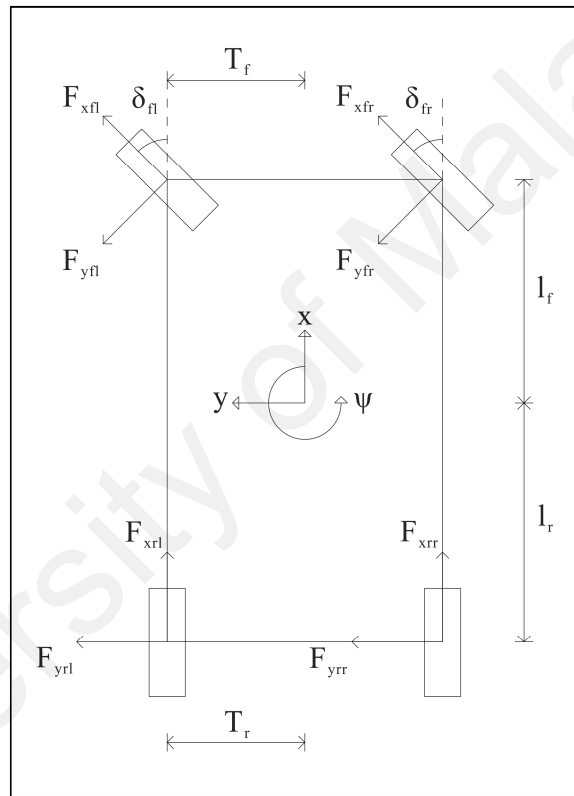
Figure 4.7: The free-body diagram of a four-wheel, three-DOF handling model

As equations (4.16) to (4.18) involve lateral and longitudinal tire forces, a mathematical representation of the tire characteristics is required. A simple approach is to use linear cornering stiffness and longitudinal stiffness that relate the tire forces to lateral slip angle and longitudinal slip ratio respectively; however, this approach does not take into consideration the factor of tire normal load. For this study, the inclusion of

133

non-linear inerter element and the load transfers during driving maneuvers affect tire normal load which, in turn, has an effect on the generation of lateral and longitudinal tire forces. Hence, in the study, a fundamental empirical tire model which included the factor of normal load was used, and the tire force representations or equations were adopted from an early study by Bakker et al. (1987) which formed the basis for latter Pacejka-type tire models. Generally, the two tire forces can be determined from equations (4.19) to (4.22):

$$F_y = D \sin(C \tan^{-1}(B\phi)) + S_v \tag{4.19}$$

$$\phi = (1 - E)(\alpha + S_h) + \frac{E}{B} \tan^{-1}\big(B(\alpha + S_h)\big) \tag{4.20}$$

$$F_x = D \sin(C \tan^{-1}(B\phi)) \tag{4.21}$$

$$\phi = (1 - E)\sigma + \frac{E}{B} \tan^{-1}(B\sigma) \tag{4.22}$$

in which F_y and F_x are the lateral and longitudinal tire forces as first defined in the previous equations, α and σ are the lateral slip angle and longitudinal slip ratio which contribute directly to the tire forces, S_h and S_v are the horizontal and vertical shifts, B, C, D, E are the stiffness factor, shape factor, peak factor and curvature factor respectively. By adopting the parameter values in the study and considering the tire normal load from the mathematical vehicle model, the tire force representations are illustrated in Figure 4.8.
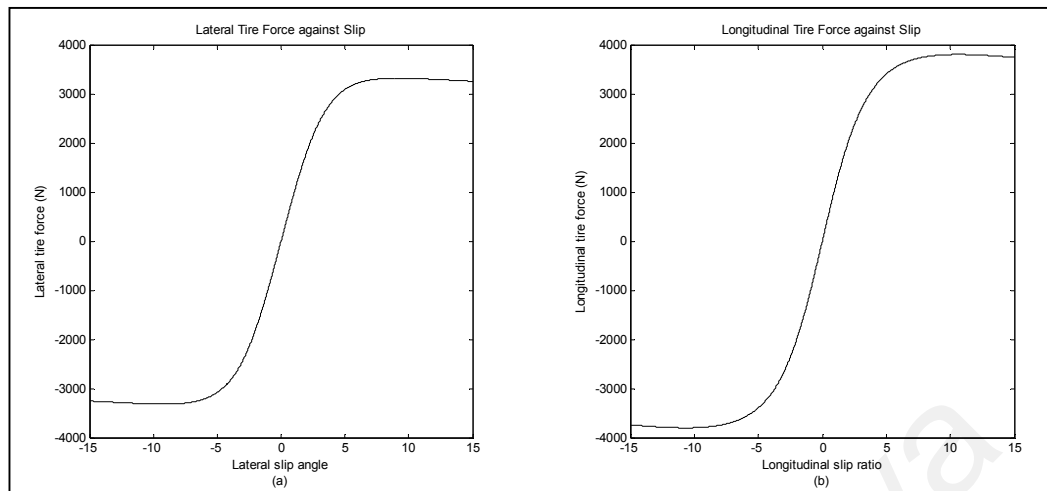
Figure 4.8: Mathematical representation of (a) lateral tire force and (b) longitudinal tire force as functions of slip

The analysis was carried out using these vehicle models by considering parameter values of a passenger vehicle adopted from Crolla and Whitehead (2003). The parameter values typical of passenger vehicle were used in the study as well as throughout the research, since the focus of this study is on ride comfort of vehicle employing non-linear inerter. Furthermore, it is the intention of this research to study the suitability of using parallel inerter in suspensions with stiffnesses commonly encountered in passenger vehicles. The parameters relevant to the full vehicle model and the front and rear quarter vehicle models are stated in Table 4.4.

Table 4.4: Relevant parameters of the passenger vehicle (Crolla & Whitehead, 2003)

Parameter	Value
Total sprung mass, M_s (kg)	1380
Sprung mass moment of inertia about x-axis, I_x (kgm^2)	380
Sprung mass moment of inertia about y-axis, I_y (kgm^2)	2444
Sprung mass moment of inertia about z-axis, I_z (kgm^2)	1500
Front quarter sprung mass, m_{sf} (kg)	372.5
Rear quarter sprung mass, m_{sr} (kg)	317.5
Front unsprung mass, m_{uf} (kg)	40.5
Rear unsprung mass, m_{ur} (kg)	45.4
Tire stiffness, k_t (Nm^{-1})	192000
Front suspension stiffness, k_f (Nm^{-1})	17000

Rear suspension stiffness, k_r (Nm^{-1})	22000
Front damping rate, c_f (Nsm^{-1})	1500
Rear damping rate, c_r (Nsm^{-1})	1500
Front half-track, T_f (m)	0.74
Rear half-track, T_r (m)	0.74
Distance from center of gravity to front axle, l_f (m)	1.25
Distance from center of gravity to rear axle, l_r (m)	1.51

The two-DOF, seven-DOF and ten-DOF models were represented and simulated in MATLAB$^{®}$/Simulink$^{®}$ to obtain vehicle responses for analysis (refer Figures A1 to A3, Appendix A for the MATLAB$^{®}$/Simulink$^{®}$ models). The sprung mass response was given primary concern in the study; therefore, in the analysis, single-objective evaluation based on ride performance measure was considered. For the two-DOF front and rear quarter vehicle models, simulations were performed for on-state inertances that ranged from 0 kg to 320 kg as in previous sections, and for each model the case with optimum inertance which resulted in minimum sprung mass acceleration was determined. Once the front and rear optimum inertances were determined, the values were then used in subsequent simulations involving seven-DOF full vehicle model and ten-DOF handling model. Note that for all cases the off-state inertance was meant to be zero as the inerter force was not present when the flywheel was not engaged during the off state.

Similar to previous sections, two types of road input were considered in the analysis, namely step and random road inputs. The step profile was given greater attention in this study, as it was expected that the non-linear inerter can control excessive sprung mass motion when subjected to large transient input. While the front and rear quarter vehicle models each had only one input from the ground, for the seven-DOF full vehicle model, an input was applied to each unsprung mass, thus there were a total of four ground inputs to the system. For the analysis involving step input, different combinations of the input were considered, including step input to the front wheels and

rear wheels to create vehicle pitch motion, and step input to the left wheels to generate vehicle roll motion. On the other hand, for random road input, all wheels were subjected to the input to emulate normal driving conditions. To ensure closeness to the reality, two different class A road profiles were generated to act as left and right tracks for the wheels. Taking 20 ms^{-1} as the vehicle's forward velocity, the inputs to the rear wheels were made to lag behind those to the front wheels for a period determined by the wheelbase of the vehicle. Finally, for the ten-DOF handling model, as the purpose of analysis is to determine vehicle roll response due to handling maneuvers only, the ground disturbances used for other models were excluded from this model, and perfectly smooth road or zero road input was considered. Meanwhile, the handling maneuvers were represented by two commonly used steering inputs, namely the step steer input and the sine steer input. The former was used to represent the event of sudden directional change, while the latter was treated as an emulation of lane change driving event.

For all simulations, the non-linear inerter was modeled to have certain values of mechanical free play, a as found in equation (4.8). For simulations involving step input, several values of free play were employed, namely 0 %, 25 %, 50 %, 75 %, and 100 % of the step height. It is worth to note here that the first represented the original passive inerter with constant inertance, while the last approximated the case which was close to having no inerter force, as the suspension deflection rarely exceeded the limit for the non-linear inerter to come to effect. Conversely, for simulations involving random road input, a reasonable, fixed limit of free play ($a = 0.01$ m) was used. Lastly, as the ten-DOF model was essentially a seven-DOF model added with a three-DOF handling model, the free play used in simulations involving the two steering inputs followed the same fixed value of 0.01 m.

4.2.2 Responses of mathematical vehicle models with non-linear inerter

Simulations using the mathematical vehicle models as described in the preceding section were meant for the evaluation of several ride-related performance measures. For the two-DOF front and rear quarter vehicle models, the resulted RMS performance parameters, namely the RMS sprung mass acceleration, RMS dynamic tire load and RMS suspension deflection were taken into consideration. Apart from the RMS parameters, as the main objective of this analysis is to assess the effectiveness of non-linear inerter in controlling sprung mass attitude, the sprung mass percent overshoot, which is one of the transient characteristics of a system, was also evaluated. For the seven-DOF full vehicle model, the rotational motions of sprung mass, namely roll and pitch, were analyzed as the two are indirectly ride-related measures. Specifically, roll displacement was determined for left-wheel step input, pitch displacement was observed for front-wheel and rear-wheel step inputs, while both were considered for ground input with random road profile. Finally, for the ten-DOF handling model, vehicle roll response due to steering maneuvers was observed to see the non-linear inerter's effectiveness in resisting sprung mass roll motion due to load disturbance. Note that for all the discussed parameters, lower values are more desirable, as they represent better control of vehicle behavior.

For tests involving two-DOF quarter vehicle models, the RMS parameters of the system and the sprung mass response due to ground inputs were obtained for assessment on the effectiveness of employing non-linear inerter. Firstly, the simulation results for the rear quarter vehicle model subjected to step input are presented in Figure 4.9.

Figure 4.9: Rear quarter vehicle response for (a) percent overshoot, (b) RMS sprung mass acceleration, (c) RMS dynamic tire load and (d) RMS suspension deflection due to step input

Observing from Figure 4.9, it is obvious that the use of limited-displacement-based non-linear inerter with various levels of mechanical free play managed to lower the sprung mass percent overshoot due to step input of 0.1 m. This reflected that the expectation of non-linear inerter being capable of controlling sprung mass behavior under large transient input was indeed true. The effect of getting decrement in sprung mass percent overshoot is very similar to that offered by tuning an ordinary passive suspension for high spring stiffness and damping rate (to obtain stiff suspension). However, unlike a stiff suspension which compromises ride performance in an effort to manage excessive sprung mass movement, the achievement of lower percent overshoot or, generally, improved transient response brought by the non-linear inerter came without deterioration in ride criterion. In fact, judging from the ride performance parameter, when suitable inertances were used, the corresponding RMS sprung mass

acceleration in Figure 4.9(b) were actually lower than that of the ordinary suspension with only passive spring and damper (which corresponded to the point of zero on-state inertance). Also, based on the same parameter, the ride performance of suspension with non-linear inerter at various free play levels was superior to the case with passive inerter (corresponding to the line of 0 % free play).

Apart from the sprung mass response, other parameters are also worth discussing. By referring to the results, it was found that the RMS suspension deflection was lower when the non-linear inerter was implemented with suitable range of inertances. This desirable effect is, again, similar to that obtained by stiffening an ordinary passive suspension, and it is an indirect indication that the sprung mass excessive movement due to ground excitation was resisted. Additionally, for the unsprung mass, it was noticed that the RMS dynamic tire load had increments compared to the ordinary passive suspension (again, the point at which on-state inertance is zero). However, with the use of non-linear inerter, for various free play levels, the RMS dynamic tire loads were lower than that resulted from using the original passive inerter (line of 0 % free play), as the inerter force for the former was occasionally not present during the off-state, thus lessening the overall tire normal load variation.

Having shown that the non-linear inerter is effective in situations involving large transient input, it is logical to turn the attention to its effect on vehicle response under normal driving conditions. Figure 4.10 shows the quarter vehicle model's response due to class A random road input.
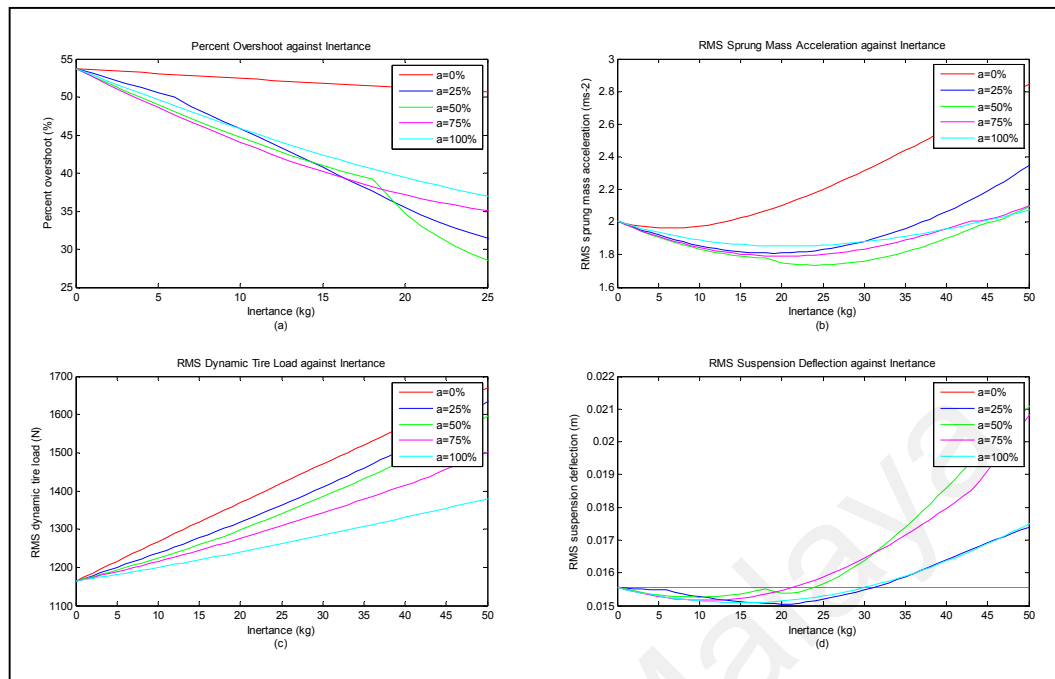
Figure 4.10: Rear quarter vehicle response for (a) RMS sprung mass acceleration, (b) RMS dynamic tire load and (c) RMS suspension deflection due to random road input

In the analysis, comparison was made between the case with passive inerter (having constant inertance) and the case for which the non-linear inerter with fixed free play of 0.01 m was employed. The results showed that the effect of non-linear inerter was not present, as the RMS parameters shown in Figure 4.10 remained the same compared with those obtained for the ordinary passive suspension. An inference can be obtained from this outcome: during regular driving on smooth road, the limit imposed on suspension deflection (the free play) was rarely hit, so the non-linear inerter had almost no effect on the vehicle response. In other words, the suspension preserved the characteristic and performance of an ordinary passive spring-damper combination. This is similar to the use of elements like dual-rate spring which maintains the original, less-stiff spring rate when the suspension rattle is small.

Meanwhile, for the analysis involving front quarter vehicle model, the results demonstrated consistency to the results for rear quarter vehicle model that has been discussed above. This can be seen from Figures 4.11 and 4.12. The results for front quarter vehicle model shared the same trend: when subjected to step input, the response involved lower sprung mass percent overshoot that was accompanied by reduction in RMS sprung mass acceleration, showing effective control of sprung mass attitude; when subjected to smooth road profile, there was again insignificant effect on the vehicle response as the suspension deflection stayed within the mechanical free play of non-linear inerter for most of the time.
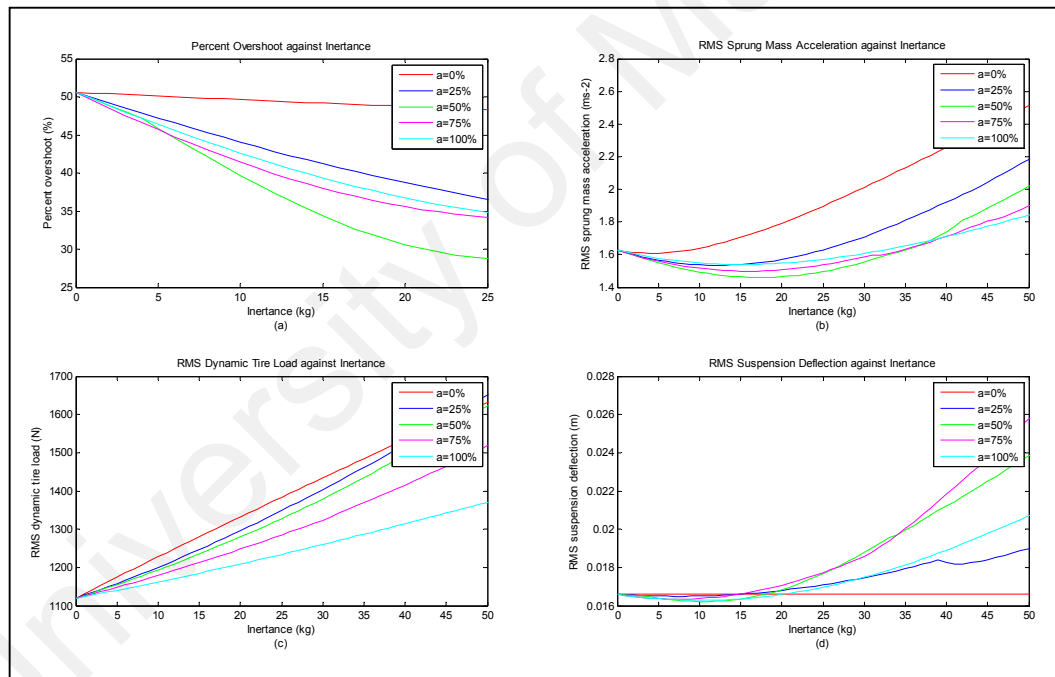
Figure 4.11: Front quarter vehicle response for (a) percent overshoot, (b) RMS sprung mass acceleration, (c) RMS dynamic tire load and (d) RMS suspension deflection due to step input
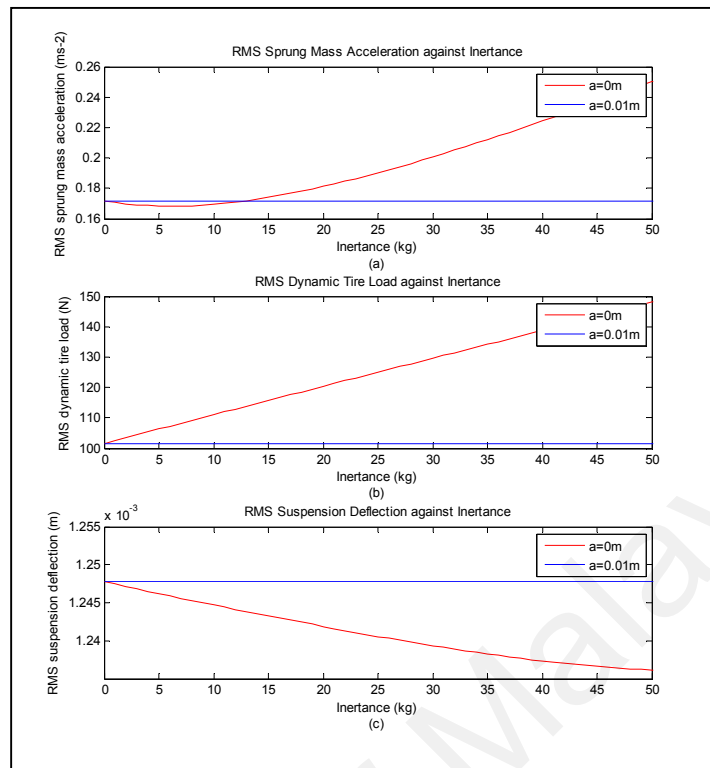
142
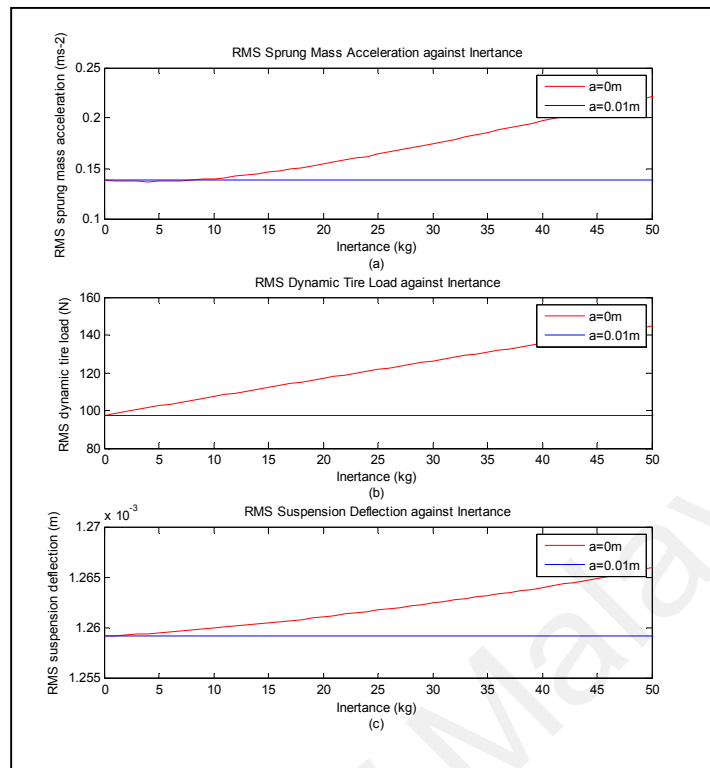
Figure 4.12: Front quarter vehicle response for (a) RMS sprung mass acceleration, (b) RMS dynamic tire load and (c) RMS suspension deflection due to random road input

Finally, in order to investigate the effect of different mechanical free play levels on the capability of non-linear inerter in controlling sprung mass response due to large transient input, the quantitative results for both front and rear models are summarized in Table 4.5, which shows the responses of quarter vehicle models employing non-linear inerter with optimum on-state inertance for each level of free play. The optimum cases were selected based on ride performance measure, that is, minimum RMS sprung mass acceleration. It is worth to recall that the case with free play of 0 % of step height corresponded to the case of original passive inerter, while the case with free play of 100 % of step height reflected a situation close to ordinary passive suspension with only spring and damper. From Table 4.5, with the optimum inertance applied to each case, of the various tested levels of free play, the level at 50 % of step height produced the lowest RMS sprung mass acceleration, showing 10.28 % (front) and 13.40 % (rear)

improvement in ride compared to the ordinary passive suspension. Similarly, ride improvement of 9.22 % (front) and 11.58 % (rear) compared to the case with original passive inerter was shown possible, indicating that the non-linear inerter can provide greater ride performance than the corresponding original passive element. The optimum on-state inertances determined from the analysis would then be used for subsequent work involving seven-DOF and ten-DOF vehicle models.

Table 4.5: Summary of front and rear quarter vehicle responses due to step input

Parameter	Without inerter	With non-linear inerter (% of step height)				
		0	25	50	75	100
Front quarter vehicle						
Optimum inertance (kg)	-	4	12	17	16	15
Percent overshoot (%)	50.6026	50.2068	42.8648	32.6352	37.4435	39.3551
RMS sprung mass acceleration (ms^{-2})	1.6276	1.6086	1.5349	1.4603	1.4986	1.5397
RMS dynamic tire load (N)	1120.0	1163.6	1218.6	1252.5	1219.4	1184.8
RMS suspension deflection (m)	0.0166	0.0166	0.0165	0.0165	0.0167	0.0164
Rear quarter vehicle						
Optimum inertance (kg)	-	6	19	24	20	21
Percent overshoot (%)	53.7161	52.9458	36.5466	29.4697	37.1581	38.8934
RMS sprung mass acceleration (ms^{-2})	2.0046	1.9633	1.8093	1.7359	1.7906	1.8523
RMS dynamic tire load (N)	1164.2	1226.4	1310.1	1332.1	1275.7	1244.5
RMS suspension deflection (m)	0.0156	0.0156	0.0151	0.0156	0.0155	0.0152

Up to this point, results from the analysis have shown that the non-linear inerter with relative-displacement-based switching algorithm is capable of controlling sprung mass vertical response. However, as far as ride comfort is concerned, a full vehicle body can respond to ground disturbances in three DOFs; apart from the vertical translational

motion, roll and pitch motions are also ride-related. When roll and pitch motions are considered, a full vehicle as used in this study is needed. In this study, simulations performed using the seven-DOF model with several ground excitations predicted responses that are illustrated in Figures 4.13 and 4.14.
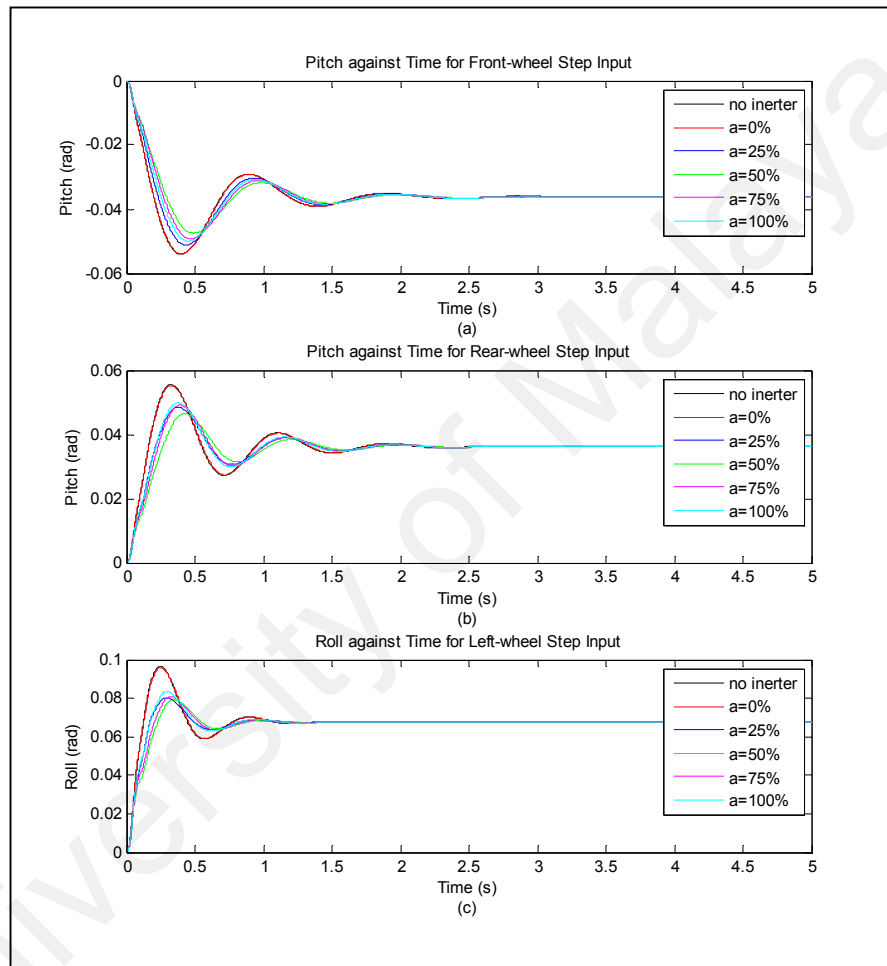
Figure 4.13: Full vehicle response for roll and pitch due to (a) front-wheel, (b) rear-wheel and (c) left-wheel step inputs

As the capability of non-linear inerter in suppressing excessive sprung mass response due to large transient input has been demonstrated earlier, it is thus reasonable to expect the suspension element to yield superior roll and pitch responses when a full vehicle is subjected to transient ground inputs. The expectation turned out to be true,

and this was supported by the results in Figure 4.13. As shown in the figure, while the case of suspension with original passive inerter (red line corresponding to 0 % free play) produced very close roll and pitch responses to the reference case without inerter (black line corresponding to no inerter), the incorporation of non-linear inerter as an added suspension element managed better pitch responses for situations involving front-wheel and rear-wheel step inputs, and provided improved roll response for the situation with left-wheel step input. The improvements came in the form of reduced peak values for both roll and pitch (which corresponded to roll and pitch overshoots). This translated to less oscillatory movement in the two rotational directions.
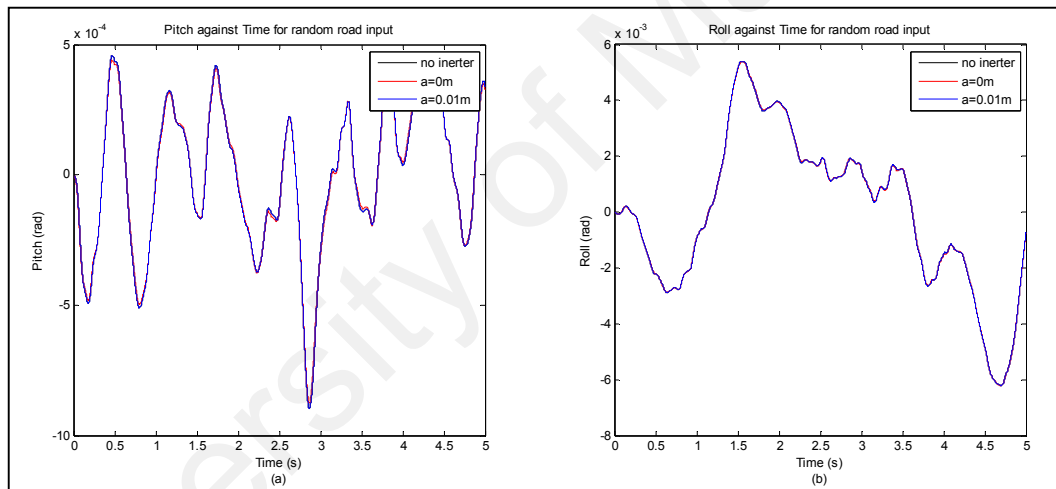
Figure 4.14: Full vehicle response for (a) pitch and (b) roll due to random road input

Meanwhile, for the simulation involving smooth random road profile, the results, as in Figure 4.14, hinted negligible effect of non-linear inerter on roll and pitch under regular driving conditions. Again, one can infer from the response that the suspension deflection rarely exceeded the specified free play during simulation, thus the suspension simply retained the characteristic brought by passive spring and damper. Overall, the results obtained from seven-DOF full vehicle model showed agreement to the results obtained from the more elementary quarter vehicle models.

146

Finally, even though the study emphasized on the ride evaluation brought by non-linear inerter and dealt with the analysis of vehicle responses due to ground inputs, the responses of vehicle due to driving maneuvers were nonetheless important. It is known that vehicle body responds not just to ground or road disturbances, but to load disturbances as well (Chen et al., 2009). In this case, vehicle roll response can also originate from steering inputs which cause load transfer. Therefore, to complement the analysis, simulation results from the ten-DOF model subjected to step and sine steering inputs were included, and they are presented in Figure 4.15. In contrary to the positive outcome in previous analyses which showed improvement in roll response when subjected to ground inputs, the vehicle roll due to both step and sine steering inputs indicated insignificant effect of non-linear inerter in resisting roll due to handling maneuvers. The useful information that can be extracted from the observation is that the non-linear inerter was effective in controlling sprung mass response due to ground disturbances, but was not effective in scenarios involving load disturbances. Non-linear inerter, therefore, had no contribution of improved vehicle response in this situation.
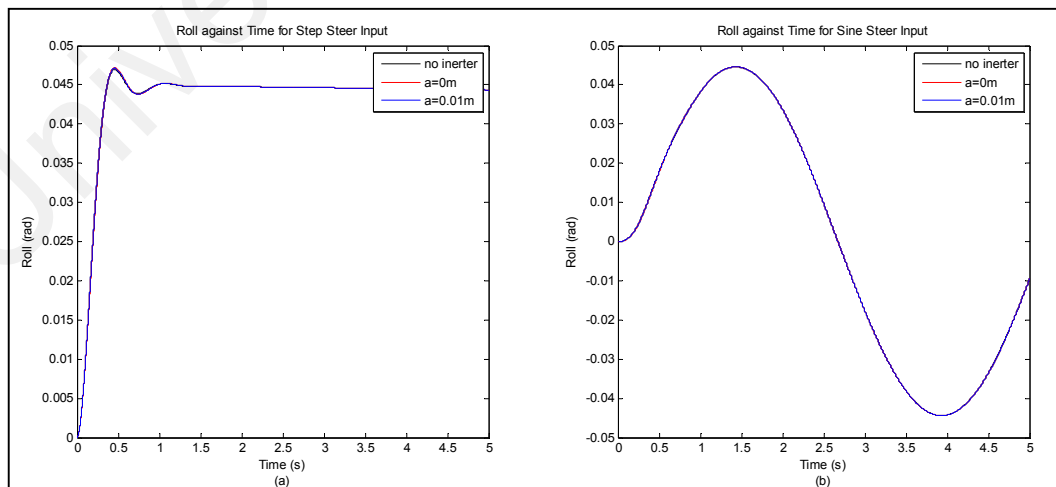
Figure 4.15: Ten-DOF vehicle model's roll response due to (a) step steering input and

(b) sine steering input

147

Thus, judging from the results of the study, the proposed non-linear inerter, when paired in parallel to passive spring and damper in a vehicle suspension, offered an effective way of controlling sprung mass behavior caused by large transient input from the ground. Combined with the finding in Section 4.1, it is reasonable to infer that the implementation of switching algorithms to a parallel inerter gives noticeable ride benefits, and thus responds to the issue of insignificant performance improvement associated with the original passive counterpart.

CHAPTER 5 INCORPORATION OF INERTER-DERIVED CONCEPT IN VEHICLE SUSPENSIONS

As a consequence of the past studies as well as the present research (Chapters 3 and 4), it is already clear that the inerter has its value in vehicle suspensions, both passive and controllable. However, being a relatively recent element compared to other fundamental suspension components like the spring and the damper, it is worth to delve deeper into the potential of further exploiting its use for greater benefit. It is known, from early studies on inerter, that this two-terminal mass element can be readily realized through various methods, such as gearing, ball-screw and hydraulic mechanisms (see Section 2.1 for detailed descriptions) which convert the rotational inertia of a flywheel to the translational effect at the two device terminals. However, regardless of the types, a less focused, yet particularly interesting feature of an inerter is that a wide range of inertances is achievable even while keeping the same flywheel mass. A look into the governing equations of the equivalent inertance reveals that this is made possible because the actual inertia property of the flywheel in an inerter is often scaled by the conversion ratio associated with the rotational-to-translational mechanism used in the device (for instance, the gear ratio of a rack-and-pinion mechanism). Following this, different inertances can be achieved by varying the relevant conversion ratio. As these mechanisms are capable of producing different effective characteristics of an inerter with the same core inertia property, it is intuitive to wonder whether this concept, which originates from the inerter device, can be borrowed and adopted in vehicle suspensions to provide an external way of varying suspension settings or not. Chapter 5 takes this matter of concept adoptability for investigation. In Section 5.1, an integration of inerter-derived concept into vehicle suspensions is presented. In the study, a gear mechanism was implemented to a typical vehicle suspension setup consisting of spring and damper

for a modified suspension layout. For methodology, the study employed a similar two-DOF mathematical model with the modified suspension layout, which was obtained by deriving the relevant equations of motion considering the addition of gear mechanism. In the study, the system was simulated with a range of gear ratios, and Pareto optimization was employed in the latter part of evaluation to determine its effect on the equivalent suspension characteristic, as well as the potential of superior suspension performance by utilizing it as an alternative way of realizing a variable suspension.

5.1 Gear Mechanism as a Method of Altering Suspension Characteristic

As mentioned in the introduction of this chapter, the present section examines the utilization of gearing system in a typical vehicle suspension setup as a means of altering, or even manipulating, the effective suspension settings. From the general knowledge on vehicle dynamics, it is clearly known that the design of any vehicle suspension should bring about good ride and road holding qualities to the vehicle, since these are the primary roles of a suspension system. However, it is also known that in reality, there is always a compromise between the two criteria whenever passive suspensions are used, which is the case for most vehicles today as passive suspension system is widely employed. A passive vehicle suspension consists of passive spring and damper which have constant properties, hence fixed suspension characteristic. Depending on the choice of suspension parameter values, the suspension can generally be characterized as being soft or hard. Basically, a soft suspension setting which uses soft spring and has low damping favors ride comfort. Consequently, it is suitable for most passenger vehicles. On the other hand, a hard suspension setting provides better handling despite compromising ride quality with the use of stiff spring and high damping, as the damping force in a passive damper tends to increase the sprung mass acceleration when it is in

the same direction as the spring force (Rakheja & Sankar, 1985). It suits the need of performance-centered vehicles. Additionally, softer suspensions tend to deflect more with the addition of load, utilizing more of the valuable suspension working space and leaving less available for dynamic fluctuations than harder suspensions do (Crolla & Whitehead, 2003). The design of vehicle suspensions, therefore, deals with the selection of suitable spring and damper properties for the vehicles.

From the review in Section 2.2, it can be seen that technological advancements have made it possible to vary suspension characteristic through controllable suspension systems, so that the design of vehicle suspensions is no longer restricted by the compromise between ride and road holding ability. A semi-active suspension system, for example, uses variable damper to attain superior ride and road holding ability to passive suspensions. Presently, variable damping, and consequently variation in suspension characteristic, is commonly realized through rheological fluids as in magnetorheological dampers (Shen et al., 2006) and electrorheological dampers (Nguyen et al., 2012). However, it can be observed that present realizations of semi-active suspension system are entirely based on changing the inherent properties of the suspension elements. For instance, the variation of damping for a magnetorheological damper is achieved by directly changing the viscosity of the rheological fluid (Bajkowski et al., 2008). This raises an interesting thought of whether the suspension characteristic can be altered by external means or mechanisms rather than through the direct variation of suspension properties, which leads to the present study.

Before exploring the dynamics of the proposed suspension layout resulted from the adoption of inerter-derived rack-and-pinion mechanism, it is worth to have a look into the underlying principle of a gearing system as well as some of its applications in

vehicle suspensions, since it is the fundamental working principle of a gear pair that eventually enables the implementation described in this section. Fundamentally, a gear can be considered as a component in mechanical system that transfers rotation from one shaft to another. It follows that the primary function of a gear is to transfer power while maintaining a definite ratio between the velocities of the shaft rotation (Hamrock et al., 2005). The transmission of power occurs due to the force exerted on gear teeth when the gears are meshed. This power transmission can be represented as equation (5.1):

$$P_2 = \eta P_1 \tag{5.1}$$

in which P_1 and P_2 are the input and output powers, η is the efficiency of power transmission. The power transmission efficiency of a gear is high and can reach 98 % (Castillo, 2002). Thus, by assuming that the loss of mechanical power is negligible and knowing that the rotational mechanical power is the product of torque and rotational velocity, the power transmission representation can be easily rewritten as equation (5.2):

$$T_1 \omega_1 = T_2 \omega_2 \tag{5.2}$$

in which T_1 and T_2 are the input and output torques while ω_1 and ω_2 are the input and output rotational velocities. The ratio of input velocity to output velocity is equal to the ratio of output gear diameter to input gear diameter which is termed the gear ratio.

From the kinematic and dynamic relations outlined in equation (5.2), a gear mechanism can therefore be viewed as a torque modifier and a rotational speed adjuster. If a force is to be altered in a system involving translational motion, then a rack, which is a gear with infinite diameter by definition (Shigley & Mischke, 2001), can be meshed

152

with gears, thus forming a rack-and-pinion mechanism which is capable of transforming rotational motion to translational motion and vice versa. Consequently, force acting on an input rack can be magnified or reduced at the output rack according to the gear ratio.

The use of gear mechanism in vehicle suspensions is rather uncommon, but not unheard of. Gearing system, specifically the rack-and-pinion mechanism, is usually employed when there is a need to achieve translational-to-rotational motion conversion in a suspension device. For instance, a previous study on regenerative suspension system (Choi et al., 2009) has demonstrated the use of a rack-and-pinion mechanism attached to an electrorheological shock absorber to convert translational motion of the piston to rotational motion of a generator which provided power source to the controllable shock absorber. More recently, such mechanism was utilized in the design of an energy-harvesting shock absorber (Z. Li et al., 2013) to achieve energy regeneration through suspension movements. Obviously, for regenerative suspension application, gear mechanism is required to enable translational-to-rotational motion conversion for the operation of rotary generator. Also, not to mention, the study on inerter in passive vehicle suspensions by Smith and Wang (2004) demonstrated the use of a rack-and-pinion type of inerter. However, the role of gear mechanism in the inerter was more than just achieving motion conversion. In a related prior study, Smith (2002) claimed that large inertances can be realized while keeping the flywheel mass small by employing sufficiently large gear ratios. Obviously, a large gear ratio scaled up the force generated by that suspension element. The same gear property is employed in the present study. In fact, a gear pair in mechanical system is often treated as an analog of transformer in electrical circuits (Bhattacharya, 2009), as a gear pair varies the torque and speed similar to the way a transformer varies the current and voltage. This complements the force-current analogy in control system study, in which mechanical

153

elements such as spring, damper and inerter (two-terminal mass) are analogous to electrical circuit elements, namely inductor, resistor and capacitor (Smith, 2002).

5.1.1 Dynamics of the proposed suspension layout

Shifting the attention back to the current proposal, in the study, the force-altering capability of a rack-and-pinion gear mechanism as found in an inerter was implemented to a passenger vehicle suspension. To gain insight into the dynamics of the resulted modified suspension setup or layout, a mathematical vehicle model was considered. Similar to most parts of the research, the study employed quarter vehicle model which has the usual vertical translational motions of the sprung and unsprung masses as its two DOFs. The suspension, consisted of a spring, a damper and the gear mechanism borrowed from an inerter, acted between the sprung and unsprung masses. This suspension layout, together with the quarter vehicle model, is shown schematically in Figure 5.1(a). For comparison purpose, Figure 5.1(b) shows the model with ordinary passive suspension consisting of only spring and damper.
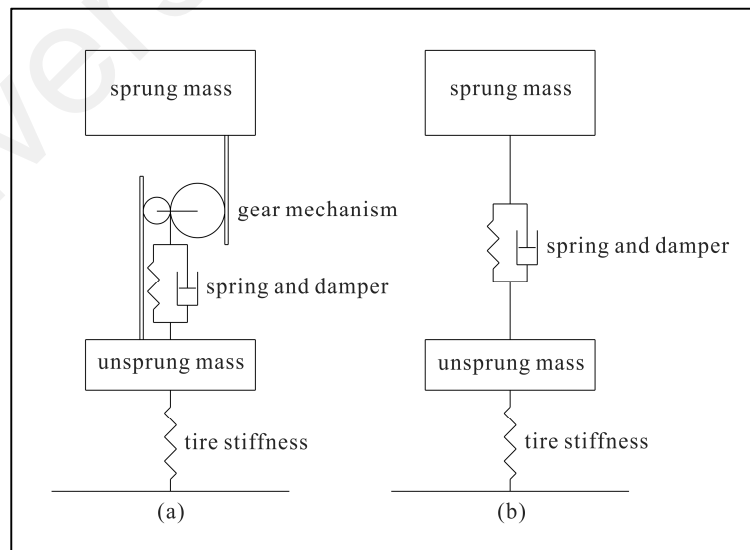
Figure 5.1: Schematic diagram of (a) quarter vehicle model with rack-and-pinion gear mechanism and (b) model with ordinary passive suspension

The inclusion of a gear mechanism between the sprung and unsprung masses resulted in the masses being related to each other kinematically following fundamental gear equation. In general, the velocities of the sprung and unsprung masses are related by a factor of gear ratio. However, it should be noted that the gear mechanism, situated on top of the spring and damper, is also vertically movable and reacts to the suspension force. Thus, specifically it is the velocities of the two masses relative to the velocity of the movable gear mechanism that are related; this is stated in equation (5.3):

$$\dot{z}_s - \dot{z}_{gr} = \frac{1}{k_{gr}}\left(\dot{z}_u - \dot{z}_{gr}\right) \tag{5.3}$$

in which $\dot{z}_s$ is the sprung mass velocity, $\dot{z}_u$ is the unsprung mass velocity, $\dot{z}_{gr}$ is the gear's linear velocity, and k_{gr} is the gear ratio used in the mechanism. Note that the integrals (displacements) and the derivatives (accelerations) share the same kinematic relation, and their equations, which are not stated here, have identical form as equation (5.3).

Theoretical analysis on this system involves the solving of equations of motion which govern the responses of the sprung mass, unsprung mass as well as the gear assembly known as the gear mass. From Figure 5.1(a), it can be observed that while the unsprung mass is acted by the suspension force, the sprung mass is supported by the output force transmitted by the rack instead of being supported by suspension force directly as in an ordinary suspension system. This enabled modification to the suspension force through the gear mechanism. By referring to the model's free-body diagram which is shown in Figure 5.2, the equations of motion for the system can be formulated as equations (5.4) to (5.6):

155

m_s

F_{out}

m_{gr}

$F_{in} \ k_s(z_u\text{-}z_{gr}) \ c_s(\dot{z}_u\text{-}\dot{z}_{gr})$

m_u
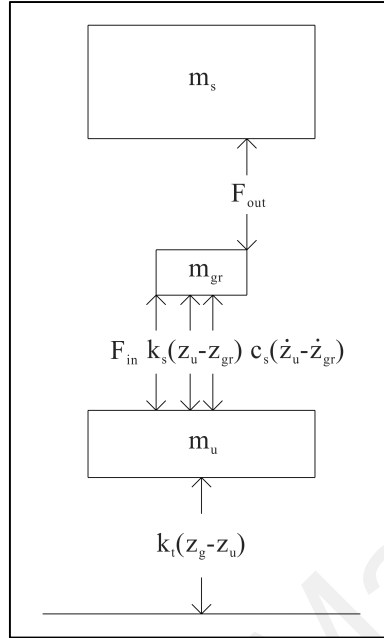
$k_t(z_g\text{-}z_u)$

Figure 5.2: Free-body diagram of the vehicle model

$$m_s \ddot{z}_s = F_{out} \tag{5.4}$$

$$m_{gr} \ddot{z}_{gr} = F_{in} + k(z_u - z_{gr}) + c(\dot{z}_u - \dot{z}_{gr}) - F_{out} \tag{5.5}$$

$$m_u \ddot{z}_u = k_t(z_g - z_u) - F_{in} - k(z_u - z_{gr}) - c(\dot{z}_u - \dot{z}_{gr}) \tag{5.6}$$

in which m_s, m_u, m_{gr} are the sprung, unsprung and gear masses, $\ddot{z}_s$, $\ddot{z}_u$, $\ddot{z}_{gr}$ are the corresponding accelerations, $\dot{z}_u$, $\dot{z}_{gr}$ are the corresponding velocities, z_u, z_{gr} are the corresponding displacements, z_g is the ground displacement, k_t, k, c are the tire stiffness, spring stiffness and damping rate respectively as before, F_{in} is the force on the input rack, and F_{out} is the force on the output rack.

A comparison between the equations for the proposed suspension layout and those for the original spring and damper combination shows how the rack-and-pinion mechanism modified the suspension dynamics. For the original passive suspension which is shown in Figure 5.1(b), the sprung mass is subjected to the suspension force which consists of the spring and damper forces, while the unsprung mass is acted by the suspension force and the tire normal force or dynamic tire load. Its equations of motion, which have been mentioned in previous chapter (equations (3.6) and (3.7)), are re-stated as equations (5.7) and (5.8) for convenience in comparison:

$$m_s \ddot{z}_s = k(z_u - z_s) + c(\dot{z}_u - \dot{z}_s) \tag{5.7}$$

$$m_u \ddot{z}_u = k_t(z_g - z_u) - k(z_u - z_s) - c(\dot{z}_u - \dot{z}_s) \tag{5.8}$$

in which the parameters are defined consistently as before. Note that the first right-hand-side term of equation (5.7) is the spring force and the second term is the damper force (this is meant for the comparison that follows). The equations of motion for the studied suspension layout have been stated as equations (5.4), (5.5) and (5.6); however, they can be rearranged into a form which enables meaningful comparison. By rearranging equation (5.5) to obtain an expression of F_{out}, considering that F_{in} is related to F_{out} by the reciprocal of k_{gr} and substituting it into equation (5.4), the sprung mass equation of motion is obtained. Similarly, by rearranging equation (5.5) to obtain F_{in}, this time considering that F_{out} is related to F_{in} by k_{gr} and substituting it into equation (5.6), the unsprung mass equation of motion is derived. Finally, by obtaining an expression of z_{gr} (and its derivatives, as they share the same form of equation) in terms of z_s and z_u (and their derivatives, respectively) through equation (5.3) and then replacing them in the new equations of motion, one obtains, in a simplified form,

equations (5.9) and (5.10) as the equations of motion for the sprung and unsprung masses.

$$m_s\ddot{z}_s = \left(\frac{k_{gr}}{k_{gr}-1}\right)^2 k(z_u - z_s) + \left(\frac{k_{gr}}{k_{gr}-1}\right)^2 c(\dot{z}_u - \dot{z}_s) - \left(\frac{k_{gr}}{k_{gr}-1}\right) m_{gr}\ddot{z}_{gr} \qquad (5.9)$$

$$m_u\ddot{z}_u = k_t(z_g - z_u) - \left(\frac{k_{gr}}{k_{gr}-1}\right)^2 k(z_u - z_s) - \left(\frac{k_{gr}}{k_{gr}-1}\right)^2 c(\dot{z}_u - \dot{z}_s) + \left(\frac{1}{k_{gr}-1}\right) m_{gr}\ddot{z}_{gr}$$

$$(5.10)$$

The working principle of the rack-and-pinion mechanism is then clear: the adoption of this mechanism following the configuration in Figure 5.1(a) scales the suspension force by a factor of $\left(\frac{k_{gr}}{k_{gr}-1}\right)^2$, in which k_{gr} is the specified gear ratio. There is also an addition (or subtraction, depending on equation) of an extra term that relates the vertical translational motion of the gear mass; however, in most cases its effect to vehicle response is expected to be small as the mass of the gear mechanism is normally small relative to the sprung and unsprung masses. This is similar to the ideal massless spring and damper assumption (which also applies to a typical inerter) that treats these suspension components as simple massless elements in dynamic analysis (Maher & Young, 2011). Thus, ignoring the last terms of equations (5.9) and (5.10), and comparing the two equations to equations (5.7) and (5.8) respectively, one can see that the gear mechanism amplifies or reduces the suspension force depending on whether the scaling factor is greater or less than one, which resembles the scaling of inertial force of an inerter. This makes it possible to emulate the effect of a hard suspension or soft suspension through the external amplification or reduction of suspension force respectively instead of changing the inherent suspension properties.

5.1.2 Effect of gear mechanism's parameters on suspension characteristic

In order to quantitatively determine the effect of this inerter-originated rack-and-pinion mechanism on the suspension response and characteristic, analysis was carried out by mathematically solving the system incorporating the proposed suspension layout. The mathematical vehicle model used in the study was once again taken from Crolla and Whitehead (2003) to maintain consistency throughout the research, and the parameter values, which can be referred in Table 3.1, are typical of a passenger vehicle.

In the study, the mathematical representation of the quarter vehicle model with modified suspension layout incorporating gear mechanism, as in equations (5.9) and (5.10), was solved using MATLAB$^{®}$/Simulink$^{®}$ for several reduction gear ratios to determine the responses of the sprung and unsprung masses (see Figure A4, Appendix A for the detailed structure of the MATLAB$^{®}$/Simulink$^{®}$ model). Then, the gear mass response was determined from equation (5.3) which shows the kinematic relationship among the sprung, unsprung and gear masses. In the initial part of the analysis, two positive gear ratios (k_{gr} = 4, 16) and two negative ratios (k_{gr} = -2, -16) were chosen, and each case was simulated. In practice, a positive gear ratio represents the situation in which the directions of movement for both the input and output racks are the same, while a negative gear ratio indicates the opposite. For each direction, small (k_{gr} = 4 or k_{gr} = -2) and large (k_{gr} = 16 or k_{gr} = -16) gear ratios were considered so that the effect of the gear ratio's magnitude on suspension response could be analyzed. In the latter part of the analysis, the effect of both gear ratio and gear mass on suspension performance was evaluated through optimization procedure. Multi-objective optimization, which considered ride and road holding criteria as design objectives while gear ratio and gear mass as design variables, was performed in MATLAB$^{®}$. For this part, the gear ratio took two ranges ($-16 \leq k_{gr} \leq -1$ and $2 \leq k_{gr} \leq 16$) for negative and positive ratios

respectively, while the gear mass took a range from 1 kg to 100 kg for a comprehensive analysis. Throughout the analysis, a step input with the same profile as used in previous chapters (step time 0 s with 0.1 m step height) was employed to obtain transient responses of the model, including some recognizable characteristics such as the sprung mass percent overshoot and settling time, in addition to the RMS suspension parameters that are important to characterize vehicle suspensions as well as for performance evaluation.

The results of mathematical simulations considering the original passive suspension (reference case) and the modified suspension with the tested gear ratios (k_{gr} = -16, -2, 4, 16) are summarized in Table 5.1 and Figure 5.3. The former states the system's transient characteristics and the relevant RMS parameters while the latter shows the responses of the sprung, unsprung and gear masses for the test cases in the form of displacements in the time domain.

Table 5.1: Responses of the quarter vehicle model due to 0.1 m step input

Parameter	Reference	k_{gr} = -16	k_{gr} = -2	k_{gr} = 4	k_{gr} = 16
RMS sprung mass acceleration (ms^{-2})	2.0046	1.8827 (-6.08 %)	1.3390 (-33.20 %)	2.6582 (+32.61 %)	2.1310 (+6.31 %)
RMS dynamic tire load (N)	1164.20	1199.50 (+3.03 %)	1568.00 (+34.68 %)	1131.20 (-2.83 %)	1137.40 (-2.30 %)
RMS suspension deflection (m)	0.0156	0.0165 (+5.77 %)	0.0234 (+50.00 %)	0.0117 (-25.00 %)	0.0146 (-6.41 %)
Sprung mass maximum overshoot (%)	53.7161	54.7774 (+1.98 %)	61.5896 (+14.66 %)	50.9203 (-5.20 %)	52.8133 (-1.68 %)
Sprung mass settling time (s)	2.0307	2.1842 (+7.56 %)	4.1158 (+102.68 %)	1.2822 (-36.86 %)	1.6146 (-20.49 %)
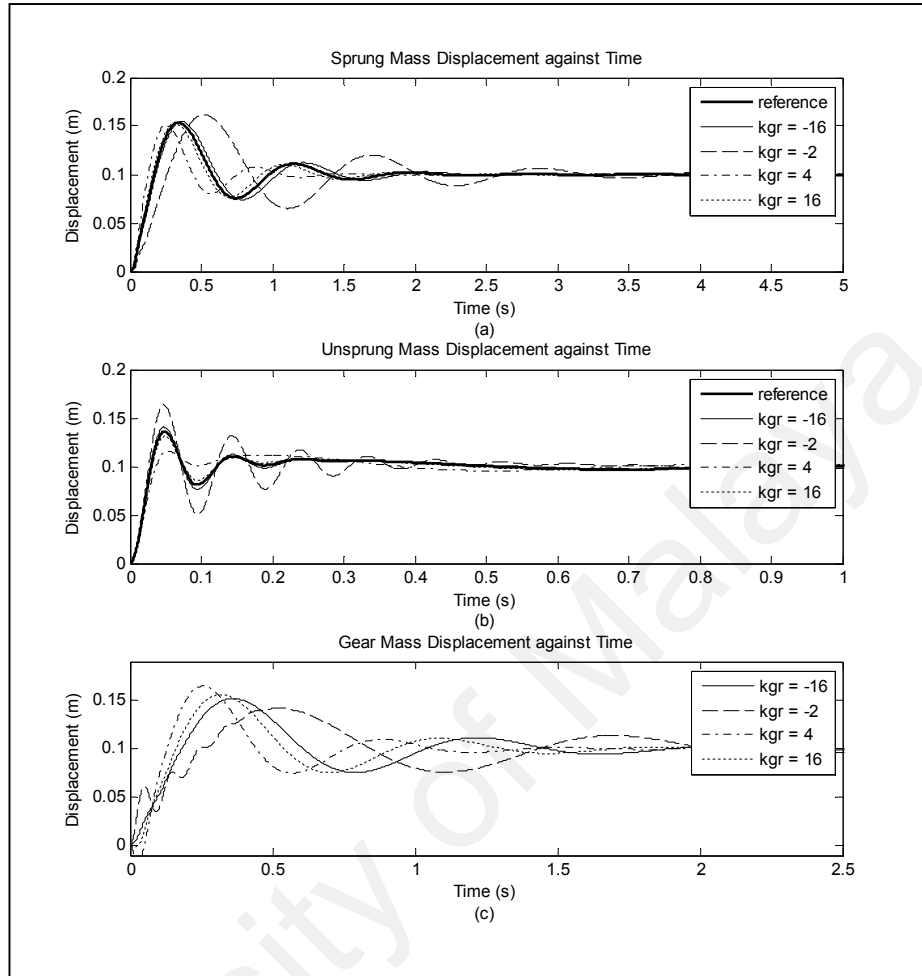
Figure 5.3: Responses of (a) sprung mass, (b) unsprung mass and (c) gear mass due to

various gear ratios

Observing from the results, response of the vehicle model varied according to the gear ratio used. For instance, when $k_{gr} = 4$, the settling time of the sprung mass was shorter than that of the original passive suspension, indicating higher damping for the quarter vehicle model as higher damping results in faster energy dissipation from the system. The RMS suspension deflection was observed to be smaller, indicating a stiffer suspension. Together with a greater value of RMS sprung mass acceleration, these gave signs of a harder suspension setting. On the other hand, the opposite response was noticed for the case with $k_{gr} = -2$: the settling time was significantly longer, the

suspension deflected more when subjected to the same input showing oscillatory ride, and the RMS sprung mass acceleration was lower. These showed soft suspension setting. Finally, when the results for large gear ratios (k_{gr} = -16, 16) were analyzed, it was noticed that the displacement responses of sprung and unsprung masses were almost the same as those from the original passive suspension (Figure 5.3). The same was true for all suspension performance parameters stated in Table 5.1, so there were only negligible changes in suspension characteristic for the two cases.

It is already known, from the theoretical derivation presented previously, that the addition of gear mechanism in the tested configuration provides a scaling effect to the suspension force by a factor of $\left(\frac{k_{gr}}{k_{gr}-1}\right)^2$, which is obviously a function of gear ratio. A plot of the proportionality factors found in equations (5.9) and (5.10) against gear ratio, as in Figure 5.4, shows the relation among these parameters. From the figure, it can be seen that when k_{gr} = 4, the scaling factor associated with the suspension force terms in the equations of motion is greater than one. On the other hand, for the case of k_{gr} = -2, the scaling factor becomes less than one. This justifies the achievement of harder and softer suspension effects as observed from the results. Note that due to the relationship being reciprocal, when the gear ratio has a large magnitude (for instance k_{gr} = -16 and k_{gr} = 16), the scaling factor approaches one, and equations (5.9) and (5.10) approach equations (5.7) and (5.8). This explains the closeness of responses for the two cases to the response for reference case.
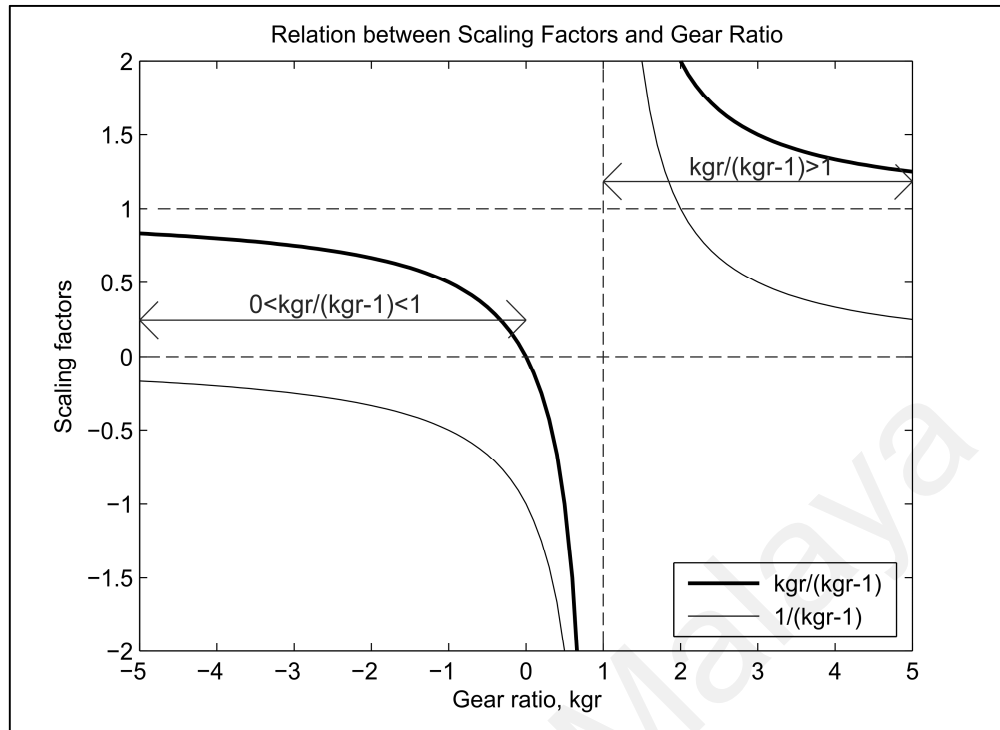
Figure 5.4: Relation between the proportionality factors and the gear ratio

Additionally, it is worth to mention the similarity between the response of sprung mass and the response of gear mass as seen from Figure 5.3. By rearranging equation (5.3) to obtain an expression for z_s (and its derivatives), the sprung mass kinematic equation is formulated as equation (5.11):

$$\dot{z}_s = \left(\frac{k_{gr}-1}{k_{gr}}\right)\dot{z}_{gr} + \left(\frac{1}{k_{gr}}\right)\dot{z}_u \qquad (5.11)$$

in which the parameters are again as defined before. Similar to equation (5.3), the sprung mass displacement and acceleration can be formulated in the same way, as they are merely the integral and derivative of the sprung mass velocity. Judging from equation (5.11), the response of sprung mass consists of two components, namely the gear mass response and the unsprung mass response. Mathematically, the former has much greater influence than the latter due to the different proportionality factors. Hence,

163

there is similarity between the sprung mass response and the gear mass response especially when k_{gr} is large in magnitude, since the proportionality factor for the gear mass response approaches one while the other approaches zero.

Up to this point, the analysis did not include the effect of gear mass, as a relatively small gear mass value (m_{gr} = 1 kg) was used in the simulations so that its effect on the suspension dynamics became negligible, and changes to suspension characteristic were solely due to the variations of gear ratio. However, if the gear mass takes a relatively significant value, then it is expected to give noticeable effect on the suspension performance measures, since the sprung and unsprung mass responses are also dependent on the last terms of equations (5.9) and (5.10) which consist of gear ratio and gear mass as parameters. It is therefore interesting to see how combinations of the two will affect the ride and road holding performances brought by the proposed suspension layout. Because ride and road holding ability are conflicting criteria, Pareto multi-objective optimization was performed in the subsequent analysis.

In the optimization procedure, both gear ratio and gear mass were the design variables, while RMS sprung mass acceleration and RMS dynamic tire load were treated as the design objectives as considered in other optimization work for the present research. For gear mass, a wide range from 1 kg to 100 kg was considered so that the effect of gear mass would be comprehensively studied, although it should be acknowledged that a large value of gear mass is only theoretically feasible but is impractical to be implemented. For gear ratio, two different ranges of $-16 \leq k_{gr} \leq -1$ and $2 \leq k_{gr} \leq 16$ were considered as they represented cases with negative and positive ratios (distinct situations requiring different physical setups of the gear mechanism). The analysis was carried out using multi-objective optimization function in MATLAB® to

obtain the solutions. For comparison purpose, optimization which considered only gear ratio as the design variable was also performed to evaluate the effect of adopting gear mass as an additional parameter of the gear mechanism. The results, which are in the form of Pareto fronts corresponding to the optimal solutions, are presented in Figure 5.5.

As expected, due to the conflicting design objectives, the optimization procedure returned Pareto fronts instead of a single optimum point. For the qualitative result comparison and evaluation in this part of the work, basically a Pareto front is superior to another if its relevant set of solutions gives lower RMS sprung mass acceleration and RMS dynamic tire load than the other set of solutions. Thus, by comparing the Pareto fronts for the case with only gear ratio as variable and the case with both gear ratio and gear mass as variables (Figure 5.5), the improvement in suspension performance brought by the inclusion of gear mass as an additional design variable can be observed. For optimization with negative ratios (Figure 5.5(a)), the two Pareto fronts were very close to each other, inferring that the gear mass had negligible effect on suspension performance within this range of ratio. However, for optimization involving positive ratios (Figure 5.5(b)), the inclusion of gear mass clearly shifted the Pareto front towards the left, benefiting RMS sprung mass acceleration which is indicative of vehicle ride. As an explanation, even though the use of gear ratio ranging from 2 to 16 provided a harder suspension setting as illustrated in Figure 5.4 and compromised ride comfort, the inclusion of gear mass compensated the deterioration of ride to a certain extent.

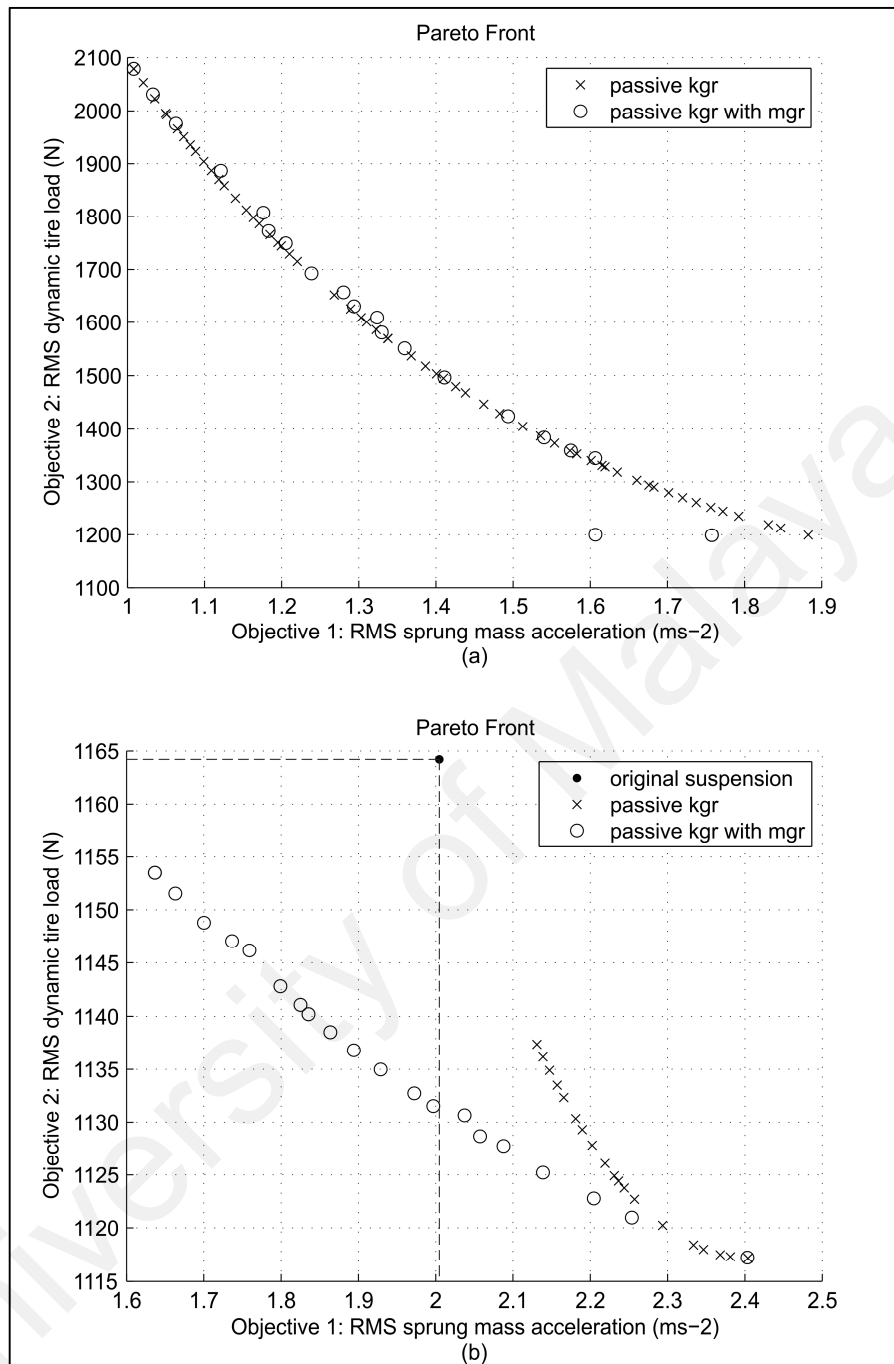Figure 5.5: Pareto fronts with and without gear mass as additional design variable for (a)

negative range of gear ratios and (b) positive range of gear ratios

In addition, an interesting finding is that certain optimal points in Figure 5.5(b) are within the region bounded by the point of original suspension performance (RMS sprung mass acceleration = 2.0046 ms^{-2} and RMS dynamic tire load = 1164.20 N as in

reference case of Table 5.1). This shows simultaneous improvement in ride and road holding ability, which means that the implementation of gear mechanism in vehicle suspension using optimized gear ratio and gear mass can overcome the compromise between ride and road holding ability associated with the corresponding passive suspension. To illustrate, taking $k_{gr} = 10$ and $m_{gr} = 64$ kg, a comparison of suspension performance measures is shown in Table 5.2.

Table 5.2: Comparison of performance between original suspension and proposed suspension with gear ratio and gear mass as parameters

Parameter	Reference	$k_{gr} = 10$, $m_{gr} = 64$ kg	Percent difference (%)
RMS sprung mass acceleration (ms^{-2})	2.0046	1.8344	-8.49
RMS dynamic tire load (N)	1164.20	1140.3	-2.05
RMS suspension deflection (m)	0.0156	0.0152	-2.56
Sprung mass maximum overshoot (%)	53.7161	53.9734	0.48
Sprung mass settling time (s)	2.0307	2.0803	2.44

5.1.3 Potential of implementing semi-active control strategy

From the derivation of equations and the result analysis in Sections 5.1.1 and 5.1.2, it is apparent that the adoption of rack-and-pinion mechanism found in a typical inerter has made the resulted suspension to be capable of scaling its characteristic through the variation of gear ratio, very much the same as the way such mechanism scales the inertia property of the flywheel of an inerter. Extending from this point, it is possible to further exploit this capability to implement semi-active control strategies to the proposed suspension, since a semi-active suspension system also depends on the characteristic switching of its suspension elements to achieve superior suspension performance. For instance, the well-known semi-active Skyhook control strategy involves the use of variable damper to obtain variation in damping rate, hence variation in a suspension's damping characteristic. The control law or switching algorithm of a

variant of this strategy, which has been described earlier in Section 2.2.2, is re-stated here as equation (5.12) for convenience:

$$\text{if } \dot{z}_s(\dot{z}_s - \dot{z}_u) > 0, \qquad c = c_{max},$$

$$\text{else,} \qquad c = c_{min} \tag{5.12}$$

in which c_{max} and c_{min} represent the maximum and minimum damping rates of a two-state switchable damper. Although not exactly identical, the switch between suspension settings can similarly be achieved in the proposed suspension layout by adopting different gear ratios. Mathematically, this can be represented by the modified switching algorithm shown in equation (5.13):

$$\text{if } \dot{z}_s(\dot{z}_s - \dot{z}_u) > 0, \qquad k_{gr} = k_{gr\_hard},$$

$$\text{else,} \qquad k_{gr} = k_{gr\_soft} \tag{5.13}$$

in which the two values of gear ratio which result in harder and softer suspension settings, k_{gr_hard} and k_{gr_soft}, respectively replace the maximum and minimum damping rates found in equation (5.12).

With the modified switching algorithm incorporated to the system, multi-objective optimization as in the preceding section was repeated to analyze possible performance benefits of implementing semi-active control strategy using the proposed method of varying suspension characteristic. For the repeated analysis, while the RMS sprung mass acceleration and RMS dynamic tire load continued to be the design objectives in the optimization, the design variables consisted of gear mass and the two different gear ratios, k_{gr_hard} and k_{gr_soft}, instead of only gear mass and single gear ratio as

168

done previously. The same variable ranges as mentioned in the preceding section were considered for the gear mass and the gear ratios; however, an additional condition of $k_{gr\_hard} < k_{gr\_soft}$ was applied in the analysis to ensure that k_{gr_hard} always brought harder suspension effect relative to that brought by k_{gr_soft}. This condition formed a linear inequality constraint in the optimization. With these settings, multi-objective optimization was carried out in MATLAB$^®$, and the results, which consisted of Pareto fronts corresponding to the optimal solutions, are presented in Figure 5.6. For comparison purpose, the optimization results from the preceding section are shown again in Figure 5.6 so that the effect of utilizing this method for realizing semi-active suspension system can be better observed.

Referring to Figure 5.6, when the Pareto front for the proposed suspension with variable gear ratio was compared against the Pareto front for the same suspension with single gear ratio, it can be seen that the implementation of semi-active control strategy lowered the RMS dynamic tire load, an improvement observable in both cases with negative gear ratios (Figure 5.6(a)) and positive gear ratios (Figure 5.6(b)). Also, similar to the observation in the preceding section, when the effect of gear mass was introduced, there was improvement in ride criterion (reduced RMS sprung mass acceleration), particularly for the case employing positive range of gear ratios. With these performance advantages, the analysis has demonstrated the benefit of implementing semi-active control strategies to the proposed suspension layout by manipulating the gear ratio to achieve desired suspension characteristics.

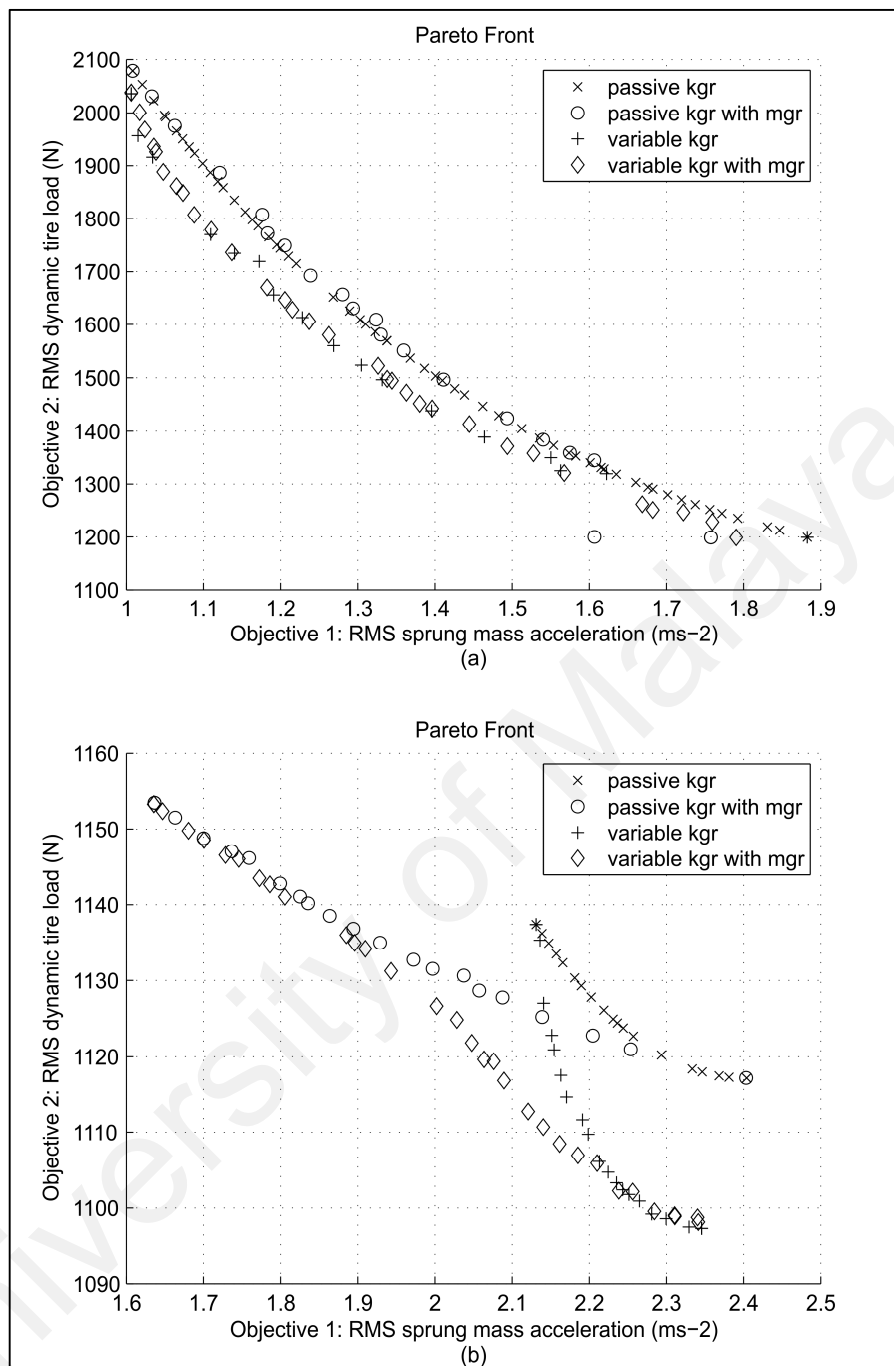Figure 5.6: Pareto fronts with constant (passive) and variable (semi-active) gear ratios

for (a) negative range of gear ratios and (b) positive range of gear ratios

Generally, this section has provided a prospect of having semi-active suspension

system with improved performance by adopting the concept found in an inerter device.

However, it is important to note that the realization of such system obviously requires

the use of variable gear ratio system, in contrast to simple gear pairing (fixed gear ratio) for a passive suspension setup. Some of the possible considerations for eventual implementation of the proposed suspension include: (i) choice of mechanism for variable gear ratio system; (ii) capability of the designed gearing system to meet the operating force requirements, particularly F_{in} and F_{out}; (iii) physical space limitation around vehicle suspension, as the additional mechanism in this configuration increases suspension height as well as occupies space; and (iv) implementation of suitable control strategy, since the employed strategy or controller should take into account the changing suspension preload besides variation in stiffness and damping rate, although a simple modified Skyhook strategy as above has also shown performance benefits. Nevertheless, the introduction of gear mechanism in a vehicle suspension still represents a viable exploitation of the concept derived from inerter.

Hence, based on the study detailed in this chapter, there exists a potential of utilizing the concept or feature which originates from a suspension element (in this case the inerter) and incorporating it in other elements (in this case the spring and damper). Even though in the study the inerter was not directly employed, the adoption of the main feature of an inerter device has demonstrated its worth as it provided a way of getting superior suspension performance. Relating back to the main direction of the current research, it is thus reasonable to claim that the inerter element, through its modifications and the adoption of derivations from its original concept, has a fairly good applicability in passenger vehicle suspensions.

CHAPTER 6 CONCLUSION

To summarize, the present research on the application of inerter element in passenger vehicle suspensions has led to several points that are worth mentioning. This chapter concludes the research by first discussing the outcomes from the various studies described in the previous chapters, followed by highlighting the contributions of knowledge from the research and, lastly, giving recommendations for future work.

6.1 Concluding Remarks

Based on the work carried out, some concluding remarks can be made. First of all, it can be said that previous studies on inerter have presented the possibility of implementation in vehicle suspensions, but have yet to demonstrate certain aspects of applicability in passenger vehicle suspensions such as the practicality of its physical implementation, the suitability in terms of performance (in certain layouts like the parallel arrangement), and its potential for further adoption or utilization. This research has demonstrated the attainment of better applicability of inerter in passenger vehicle suspensions based on these aspects. Firstly, the work in Chapter 3 presented the practical aspect of inerter's implementation. In particular, Sections 3.1 and 3.2 have shown that a parallel inerter works by cancellation with the spring force to reduce the total suspension force acting on the sprung mass which brings ride improvement, and it remains effective when paired with controllable suspension systems. Also, the versatility in its implementation can be seen from a consistent 2 % to 4 % improvement in the relevant performance measure across various tested suspension systems. Then, Section 3.3 has proven the fundamental feasibility of realizing a vehicle suspension layout with parallel inerter practically by incorporating eddy current damping to an inerter to form a combined damper-inerter setup with achievable inertances (up to 80 kg) and damping rates (up to

172

1500 Nsm^{-1}) typical of the requirement for passenger vehicle suspensions. Meanwhile, the matter of insignificant ride performance improvement for the parallel inerter was tackled in Chapter 4 by the implementation of switching algorithms to the inerter. In Section 4.1, it was shown that the implementation of semi-active switching algorithm derived from the force cancellation strategy managed to benefit ride criterion by as much as 12 %, an improvement greater than that brought by the original passive inerter (2 %) and comparable to that obtained from an ordinary semi-active suspension system using switchable damper. In Section 4.2, the use of displacement-based switching algorithm to model a non-linearity in passive inerter showed promising improvement to sprung mass response due to large transient input by lowering the overshoot from approximately 50 % to about 30 %. Finally, the work in Chapter 5 has demonstrated the potential of further exploiting the concept of inerter by adopting a feature derived from the typical inerter device and incorporating it in a vehicle suspension to form a modified suspension layout with different dynamics. Specifically, from Section 5.1, it was shown that the adoption of an inerter-originated gear mechanism to a vehicle suspension was capable as an external way of altering the effective suspension characteristic, thus providing a means of achieving variable suspensions for superior performance. Therefore, it can be concluded, from the outcomes, that greater application of inerter in passenger vehicle suspensions is achievable through modifications to its initial employment, for example by its interaction with controllable suspension systems as in the current research.

6.2 Contributions from Current Research

In general, this research has provided a greater insight into the application of inerter in passenger vehicle suspensions. The main finding of the research, as mentioned in the preceding section, is that there exists better applicability of inerter in this area through

various interactions with controllable suspension systems. In addition, the individual findings from the work, which relate back to the individual objectives of study in Section 1.1, have also extended the knowledge on inerter from past studies. These are highlighted here:

- Firstly, this research shows that the ride performance enhancement brought by a parallel inerter remains when paired with various controllable suspension systems, as an inerter in parallel arrangement affects the dynamics of the suspension by opposing the spring force and is therefore independent on the types of suspension system being used. This is an extension from previous studies as most studies only concentrated on the potential of inerter in passive suspension system, while the performance advantage in controllable suspension systems was less known.

- In terms of realization, the relevant work from current research demonstrates the feasibility of practically realizing the parallel suspension layout, through the incorporation of eddy current damping in an inerter, by proving the suitability of the achievable inertances and damping rates to be employed in passenger vehicle suspensions. This is complementary to the past studies involving the analysis and realization of inerter, since the inerter was typically considered as a separate component or device from other suspension elements and was less practical in certain implementations (such as in the parallel layout) due to the requirement of extra physical space.

- Another important finding from the current research is that it is worth to implement certain switching algorithms to an inerter for a switchable or non-linear element, as its performance improvement in the scenario of passenger vehicle suspensions is

much more prominent compared to that of a passive counterpart. This represents a leap from existing studies concerning the evaluation of suspension performance due to inerter because the inerter was always employed as a passive element with constant property, leaving the performance benefit obtainable with variable inertance largely unknown.

- Finally, this research shows that the adoption of conversion mechanism from the inerter to a typical vehicle suspension setup is viable as an external way of altering the suspension characteristic, which provides an alternative realization of a variable suspension for superior performance. Although it is already known that a wide range of inertances is achievable by scaling the effect of inertia through rotational-to-translational conversion mechanism, the approach had not been tested on other suspension elements prior to the present research. Thus, the relevant work in this research extends the knowledge on the adoptability of inerter in vehicle suspensions.

Overall, the work related to the present research has resulted in the following academic contributions in the form of journal articles and conference papers:

- Soong, M. F., Ramli, R., & Mahadi, W. N. L. (2011, Nov). *Performance analysis of inerter with controllable suspension systems*. Paper presented at the Regional Conference on Automotive Research, Kuala Lumpur, Malaysia.

- Soong, M. F., Ramli, R., & Mahadi, W. N. L. (2013). Ride evaluation of vehicle suspension employing non-linear inerter. *Applied Mechanics and Materials, 471*, 9 – 13.

- Soong, M. F., Ramli, R., & Mahadi, W. N. L. (2013). Using gear mechanism in vehicle suspension as a method of altering suspension characteristic. *Journal of Vibration and Control, 0*(0), 1 – 13.

- Soong, M. F., Ramli, R., & Mahadi, W. N. L. (2014). Vehicle suspensions with parallel inerter: Effectiveness in improving vibration isolation. *Journal of Vibroengineering, 16*(1), 256 – 265.

6.3 Recommendations for Future Research

At the present moment, the research described in this thesis has already achieved the objectives within the scope of study. Hence, the work related to the current research has laid the foundation for further exploration and development. In this section, several suggestions are pinpointed to serve as the general directions for future studies:

- In the feasibility study of combined damper-inerter device for parallel layout realization, the workflow was to assess the achievable inertances first by designing an inerter based on dimensional parameters, followed by evaluating the range of achievable damping rates by electromagnetic-related parametric variation. Although this methodology is generally valid, it should be noted that the dimensional parameters also have an effect on eddy current damping. Thus, a possible extension to the present work is to design, or optimize, both inerter and damper concurrently for simultaneous achievements of the desirable inertance and damping rate.

- An objective of this research is to determine the possibility of further performance advantage from the inerter element, and the outcome of related study in the research has demonstrated the worth of implementing switching algorithms to an inerter for a

176

switchable element. A logical move from this point is to develop the physical realization of a switchable or variable inerter. The design and development of variable-inertia devices is a distinct but relevant area of research and can be considered as a direction of future work.

- It is apparent that studies in the current research have put much emphasis on evaluating the ride performance of inerter in vehicle suspensions. This is because the focus of this research is on applying the inerter in passenger vehicles, and ride performance typically receives greater attention for passenger vehicles compared to handling performance. However, this by no means justifies that the latter is not important. As a suggestion, further analyses of vehicle responses due to standard handling maneuvers can be carried out to complement present work.

- So far, the vehicle responses and performance parameters were computed using fundamental mathematical vehicle models. The reason is that this research deals with ways of employing the inerter in vehicle suspensions, and the evaluation on these ideas favors the use of simple yet reliable representations of a vehicle for clearer result analysis. However, as the research has already yielded fundamentally promising outcomes, future work can take the direction of applying these implementations of inerter to more detailed vehicle models, for example realistic multi-body model with greater number of DOFs or mathematical model with finer representations, to obtain realistic responses for quantitative analysis.

It is hoped that this research, together with the recommendations highlighted above, will eventually lead to a widespread adoption of the inerter element in passenger vehicle suspensions for greater suspension performance.

REFERENCES

Bagheri, A., Mahmoodabadi, M. J., Rostami, H., & Kheybari, S. (2011). Pareto optimization of a two-degree of freedom passive linear suspension using a new multi-objective genetic algorithm. *International Journal of Engineering Transactions A: Basics, 24*(3), 291 – 299.

Bajkowski, J., Nachman, J., Shillor, M., & Sofonea, M. (2008). A model for a magnetorheological damper. *Mathematical and Computer Modelling, 48*(1 – 2), 56 – 68.

Bakker, E., Nyborg, L., & Pacejka, H. B. (1987). Tyre modelling for use in vehicle dynamics studies. *SAE Technical Paper, 870421*, 1 – 15.

Ben, L. Z., Hasbullah, F., & Faris, F. W. (2014). A comparative ride performance of passive, semi-active and active suspension systems for off-road vehicles using half car model. *International Journal of Heavy Vehicle Systems, 21*(1), 26 – 41.

Bhattacharya, S. K. (2009). *Control systems engineering* (2nd ed.). Delhi: Dorling Kindersley.

Cao, D., Song, X., & Ahmadian, M. (2011). Editors' perspectives: Road vehicle suspension design, dynamics, and control. *Vehicle System Dynamics, 49*(1 – 2), 3 – 28.

Castillo, J. M. D. (2002). The analytical expression of the efficiency of planetary gear trains. *Mechanism and Machine Theory, 37*(2), 197 – 214.

Chen, M. Z. Q., Hu, Y., Huang, L., & Chen, G. (2014). Influence of inerter on natural frequencies of vibration systems. *Journal of Sound and Vibration, 333*(7), 1874 – 1887.

Chen, M. Z. Q., Papageorgiou, C., Scheibe, F., Wang, F. C., & Smith, M. C. (2009). The missing mechanical circuit element. *IEEE Circuits and Systems Magazine, 9*(1), 10 – 26.

Choi, S. B., Choi, Y. T., Chang, E. G., Han, S. J., & Kim, C. S. (1998). Control characteristics of a continuously variable ER damper. *Mechatronics, 8*(2), 143 – 161.

Choi, S. B., Seong, M. S., & Kim, K. S. (2009). Vibration control of an electrorheological fluid-based suspension system with an energy regenerative mechanism. *Proceedings of the Institution of Mechanical Engineers, Part D: Journal of Automobile Engineering, 223*(4), 459 – 469.

Crews, J. H., Mattson, M. G., & Buckner, G. D. (2011). Multi-objective control optimization for semi-active vehicle suspensions. *Journal of Sound and Vibration, 330*(23), 5502 – 5516.

Crolla, D. A., & Whitehead, J. P. (2003). *Vehicle dynamics, control and suspensions*. Leeds: University of Leeds.

Dong, X., Yu, M., Liao, C., & Chen, W. (2010). Comparative research on semi-active control strategies for magneto-rheological suspension. *Nonlinear Dynamics, 59*(3), 433 – 453.

Ebrahimi, B. (2009). Development of hybrid electromagnetic dampers for vehicle suspension systems (Doctoral dissertation). Retrieved from https://uwspace.uwaterloo.ca/bitstream/handle/10012/4375/Babak_Ebrahimi_Ph D_Thesis.pdf?sequence=1

Ebrahimi, B., Bolandhemmat, H., Khamesee, M. B., & Golnaraghi, F. (2011). A hybrid electromagnetic shock absorber for active vehicle suspension systems. *Vehicle System Dynamics, 49*(1 – 2), 311 – 332.

Ebrahimi, B., Khamesee, M. B., & Golnaraghi, F. (2009). Eddy current damper feasibility in automobile suspension: Modeling, simulation and testing. *Smart Materials and Structures, 18*(1) 015017, 1 – 12.

Ebrahimi, B., Khamesee, M. B., & Golnaraghi, M. F. (2008). Design and modeling of a magnetic shock absorber based on eddy current damping effect. *Journal of Sound and Vibration, 315*(4 – 5), 875 – 889.

ElMadany, M. M., & Abduljabbar, Z. S. (1999). Linear quadratic gaussian control of a quarter-car suspension. *Vehicle System Dynamics, 32*(6), 479 – 497.

Evangelou, S., Limebeer, D. J. N., Sharp, R. S., & Smith, M. C. (2004). Steering
compensation for high-performance motorcycles. *Proceedings of the 43rd IEEE
Conference on Decision and Control, Atlantis, Paradise Island, Bahamas*, 749 –
754.

Evangelou, S., Limebeer, D. J. N., Sharp, R. S., & Smith, M. C. (2006). Control of
motorcycle steering instabilities. *IEEE Control Systems Magazine, 26*(5), 78 –
88.

Evangelou, S., Limebeer, D. J. N., Sharp, R. S., & Smith, M. C. (2007). Mechanical
steering compensator for high-performance motorcycles. *Journal of Applied
Mechanics – Transactions of the ASME, 74*(2), 332 – 346.

Faris, W. F., BenLahcene, Z., & Ihsan, S. I. (2010). Assessment of different semi-active
control strategies on the performance of off-road vehicle suspension systems.
International Journal of Vehicle Systems Modelling and Testing, 5(2/3), 254 –
271.

Gay, S. E. (2005). *Contactless magnetic brake for automotive applications* (Doctoral
dissertation). Retrieved from
http://repository.tamu.edu/bitstream/handle/1969.1/ETD-TAMU-1005/GAY-
DISSERTATION.pdf

Georgiou, G., Verros, G., & Natsiavas, S. (2007). Multi-objective optimization of
quarter-car models with a passive or semi-active suspension system. *Vehicle
System Dynamics, 45*(1), 77 – 92.

Gillespie, T. D. (1992). *Fundamentals of vehicle dynamics*. Warrendale: Society of Automotive Engineers.

Goncalves, F. D. (2001). *Dynamic analysis of semi-active control techniques for vehicle applications* (Master's thesis). Retrieved from http://scholar.lib.vt.edu/theses/available/etd-08142001-105010/unrestricted/Final_Thesis.pdf

Goncalves, F. D., & Ahmadian, M. (2003). A hybrid control policy for semi-active vehicle suspensions. *Shock and Vibration, 10*(1), 59 – 69.

Gopal, M. (2002). *Control systems: Principles and design*. Boston: McGraw-Hill.

Gubitosa, M., Anthonis, J., Albarello, N., & Desmet, W. (2009). A system engineering approach for the design optimization of a hydraulic active suspension. *Proceedings of the 2009 Vehicle Power and Propulsion Conference, Dearborn, Michigan, USA*, 1122 – 1130.

Guglielmino, E., Sireteanu, T., Stammers, C. W., Ghita, G., & Giuclea, M. (2008). *Semi-active suspension control: Improved vehicle ride and road friendliness*. London: Springer.

Gysen, B. L. J., van der Sande, T. P. J., Paulides, J. J. H., & Lomonova, E. A. (2011). Efficiency of a regenerative direct-drive electromagnetic active suspension. *IEEE Transactions on Vehicular Technology, 60*(4), 1384 – 1393.

Hamrock, B. J., Schmid, S. R., & Jacobson, B. O. (2005). *Fundamentals of machine elements* (2nd ed.). Boston: McGraw Hill.

Hu, Y., Li, C., & Chen, M. Z. Q. (2012). Optimal control for semi-active suspension with inerter. *Proceedings of the 31st Chinese Control Conference, Hefei, China*, 2301 – 2306.

International Organization for Standardization. (1995). *Mechanical vibration -- road surface profiles -- reporting of measured data* (ISO 8608:1995). Geneva: International Organization for Standardization.

Johnsson, A., Berbyuk, V., & Enelund, M. (2012). Pareto optimisation of railway bogie suspension damping to enhance safety and comfort. *Vehicle System Dynamics, 50*(9), 1379 – 1407.

Karnopp, D. (1989). Permanent magnet linear motors used as variable mechanical dampers for vehicle suspensions. *Vehicle System Dynamics, 18*(4), 187 – 200.

Karnopp, D., Crosby, M. J., & Harwood, R. A. (1974). Vibration control using semi-active force generators. *Journal of Engineering for Industry, 96*(2), 619 – 626.

Konak, A., Coit, D. W., & Smith, A. E. (2006). Multi-objective optimization using genetic algorithms: A tutorial. *Reliability Engineering and System Safety, 91*(9), 992 – 1007.

Kuznetsov, A., Mammadov, M., Sultan, I., & Hajilarov, E. (2011). Optimization of improved suspension system with inerter device of the quarter-car model in vibration analysis. *Archive of Applied Mechanics, 81*(10), 1427 – 1437.

Lazar, I. F., Neild, S. A., & Wagg, D. J. (2014). Using an inerter-based device for structural vibration suppression. *Earthquake Engineering & Structural Dynamics, 43*(8), 1129 – 1147.

Levesley, M. C., Ramli, R., Stembridge, N., & Crolla, D. A. (2007). Multi-body co-simulation of semi-active suspension systems. *Proceedings of the Institution of Mechanical Engineers, Part K: Journal of Multi-body Dynamics, 221*(1), 99 – 115.

Li, C., & Liang, M. (2012). Characterization and modeling of a novel electro-hydraulic variable two-terminal mass device. *Smart Materials and Structures, 21*(2) 025004, 1 – 12.

Li, C., Liang, M., Wang, Y., & Dong, Y. (2012a). Vibration suppression using two-terminal flywheel. Part I: Modeling and characterization. *Journal of Vibration and Control, 18*(8), 1096 – 1105.

Li, C., Liang, M., Wang, Y., & Dong, Y. (2012b). Vibration suppression using two-terminal flywheel. Part II: Application to vehicle passive suspension. *Journal of Vibration and Control, 18*(9), 1353 – 1365.

Li, H., Liu, H., Gao, H., & Shi, P. (2012). Reliable fuzzy control for active suspension systems with actuator delay and fault. *IEEE Transactions on Fuzzy Systems, 20*(2), 342 – 357.

Li, H., Yu, J., Hilton, C., & Liu, H. (2013). Adaptive sliding-mode control for nonlinear active suspension vehicle systems using T-S fuzzy approach. *IEEE Transactions on Industrial Electronics, 60*(8), 3328 – 3338.

Li, Z., Zuo, L., Luhrs, G., Lin, L., & Qin, Y. (2013). Electromagnetic energy-harvesting shock absorbers: Design, modeling, and road tests. *IEEE Transactions on Vehicular Technology, 62*(3), 1065 – 1074.

Liu, Y., Waters, T. P., & Brennan, M. J. (2005). A comparison of semi-active damping control strategies for vibration isolation of harmonic disturbances. *Journal of Sound and Vibration, 280*(1 – 2), 21 – 39.

Long, Z., Li, C., Huang, B., & Wen, W. (2009). Simulation research on braking torque of eddy current retarder. *Proceedings of the First International Workshop on Education Technology and Computer Science*, 521 – 525.

Maciejewski, I., Kiczkowiak, T., & Krzyzynski, T. (2011). Application of the pareto-optimal approach for selecting dynamic characteristics of seat suspension systems. *Vehicle System Dynamics, 49*(12), 1929 – 1950.

Maher, D., & Young, P. (2011). An insight into linear quarter car model accuracy. *Vehicle System Dynamics, 49*(3), 463 – 480.

Maiorana, J., Minaker, B. P., Zhang, D., & Malik, M. A. (2005). Cosimulation of active suspension. *SAE Technical Paper, 2005 – 01 – 0984*, 1 – 9.

Mirzaei, S. (2007). A flexible electromagnetic damper. *Proceedings of the 2007 IEEE International Electric Machines and Drives Conference, Antalya, Turkey*, 959 – 962.

Mirzaei, S., Saghaiannejad, S. M., Tahani, V., & Moallem, M. (2001). Electromagnetic shock absorber. *Proceedings of the 2001 IEEE International Electric Machines and Drives Conference*, 760 – 764.

Montgomery, H. (2004). Current flow patterns in a faraday disc. *European Journal of Physics, 25*(2), 171 – 183.

Mouleeswaran, S. (2012). Design and development of PID controller-based active suspension system for automobiles. In M. Vagia (Ed.), *PID controller design approaches – Theory, tuning and application to frontier areas* (pp. 71 – 98). Rijeka: InTech.

Ngatchou, P., Zarei, A., & El-Sharkawi, M. A. (2005). Pareto multi objective optimization. *Proceedings of the 13th International Conference on Intelligent Systems Application to Power Systems, Arlington, VA*, 84 – 91.

Nguyen, Q. H., Choi, S. B., & Park, Y. G. (2012). An analytical approach to optimally design of electrorheological fluid damper for vehicle suspension system. *Meccanica, 47*(7), 1633 – 1647.

Nie, J., Zhang, X., & Chen, L. (2010). Suspension employing inerter and optimization based on vibration isolation theory on electrical-mechanical analogies. *Proceedings of the 2010 International Conference on Optoelectronics and Image Processing, Haikou, China*, 481 – 484.

Nise, N. S. (2008). *Control systems engineering* (5th ed.). Singapore: John Wiley & Sons.

Papageorgiou, C., Houghton, N. E., & Smith, M. C. (2009). Experimental testing and analysis of inerter devices. *Journal of Dynamic Systems, Measurement, and Control – Transactions of the ASME, 131*(1) 011001, 1 – 11.

Papageorgiou, C., & Smith, M. C. (2005). Laboratory experiment testing of inerters. *Proceedings of the 44th IEEE Conference on Decision and Control, Seville, Spain*, 3351 – 3356.

Paré, C. A. (1998). *Experimental evaluation of semiactive magneto-rheological suspensions for passenger vehicles* (Master's thesis). Retrieved from http://scholar.lib.vt.edu/theses/public/etd-51598-19251/materials/etd.pdf

Rakheja, S., & Sankar, S. (1985). Vibration and shock isolation performance of a semi-active on-off damper. *Journal of Vibration, Acoustics, Stress, and Reliability in Design, 107*(4), 398 – 403.

Rao, S. S. (2009). *Engineering optimization: Theory and practice* (4th ed.). Hoboken, NJ: John Wiley & Sons.

Savaresi, S. M., Silani, E., Bittanti, S., & Porciani, N. (2003). On performance evaluation methods and control strategies for semi-active suspension systems. *Proceedings of the 42nd IEEE Conference on Decision and Control, Maui, Hawaii, USA*, 2264 – 2269.

Scheibe, F., & Smith, M. C. (2009). Analytical solutions for optimal ride comfort and tyre grip for passive vehicle suspensions. *Vehicle System Dynamics, 47*(10), 1229 – 1252.

Sharma, K., Crolla, D. A., & Wilson, D. A. (1992, Sept). *Derivation of a control law for a 3 state switchable damper suspension system for improving road vehicle ride characteristics*. Paper presented at the International Symposium on Theory of Machines and Mechanisms, Nagoya, Japan.

Shen, Y., Golnaraghi, M. F., & Heppler, G. R. (2006). Semi-active vibration control schemes for suspension systems using magnetorheological dampers. *Journal of Vibration and Control, 12*(1), 3 – 24.

Shigley, J. E., & Mischke, C. R. (2001). *Mechanical engineering design* (6th ed.). Boston: McGraw Hill.

Smith, M. C. (2002). Synthesis of mechanical networks: The inerter. *IEEE Transactions on Automatic Control, 47*(10), 1648 – 1662.

Smith, M. C. (2008). Force-controlling mechanical device. *United States Patent, US 7316303 B2*.

Smith, M. C., & Wang, F. C. (2004). Performance benefits in passive vehicle suspensions employing inerters. *Vehicle System Dynamics, 42*(4), 235 – 257.

Sodano, H. A., Bae, J. S., Inman, D. J., & Belvin, W. K. (2005a). Concept and model of eddy current damper for vibration suppression of a beam. *Journal of Sound and Vibration, 288*(4 – 5), 1177 – 1196.

Sodano, H. A., Bae, J. S., Inman, D. J., & Belvin, W. K. (2006). Improved concept and model of eddy current damper. *Journal of Vibration and Acoustics – Transactions of the ASME, 128*(3), 294 – 302.

Sodano, H. A., & Inman, D. J. (2007). Non-contact vibration control system employing an active eddy current damper. *Journal of Sound and Vibration, 305*(4 – 5), 596 – 613.

Sodano, H. A., & Inman, D. J. (2008). Modeling of a new active eddy current vibration control system. *Journal of Dynamic Systems, Measurement, and Control – Transactions of the ASME, 130*(2) 021009, 1 – 11.

Sodano, H. A., Inman, D. J., & Belvin, W. K. (2005b). New semi-active damping concept using eddy currents. *Proceedings of the SPIE 5760*, 293 – 304.

Swift, S. J., Smith, M. C., Glover, A. R., Papageorgiou, C., Gartner, B., & Houghton, N. E. (2013). Design and modelling of a fluid inerter. *International Journal of Control, 86*(11), 2035 – 2051.

Taskin, Y., Yagiz, N., & Yuksek, I. (2013). Lumped parameter identification of a quarter car test rig. *Journal of Physics: Conference Series, 410* 012089, 1 – 4.

Thompson, A. G. (1976). An active suspension with optimal linear state feedback. *Vehicle System Dynamics, 5*(4), 187 – 203.

Thompson, A. G. (1984). Optimal and suboptimal active suspensions for road vehicles. *Vehicle System Dynamics, 13*(2), 61 – 72.

Tsai, M. C., & Huang, C. C. (2011). Development of a variable-inertia device with a magnetic planetary gearbox. *IEEE/ASME Transactions on Mechatronics, 16*(6), 1120 – 1128.

Turrini, J., & Ducatti, C. (2007). Shock absorbers with internal rebound spring for roll angle control. *SAE Technical Paper, 2007-01-2545*.

Van Sickel, J. H., Venkatesh, P., & Lee, K. Y. (2008). Analysis of the pareto front of a multi-objective optimization problem for a fossil fuel power plant. *Proceedings of the 2008 IEEE Power and Energy Society General Meeting – Conversion and Delivery of Electrical Energy in the 21st Century*, Pittsburgh, PA, 1 – 8.

Verros, G., Natsiavas, S., & Papadimitriou, C. (2005). Design optimization of quarter-car models with passive and semi-active suspensions under random road excitation. *Journal of Vibration and Control, 11*(5), 581 – 606.

Wang, F. C., & Chan, H. A. (2008). Mechatronic suspension design and its applications to vehicle suspension control. *Proceedings of the 47th IEEE Conference on Decision and Control, Cancun, Mexico*, 3769 – 3774.

Wang, F. C., & Chan, H. A. (2011). Vehicle suspensions with a mechatronic network strut. *Vehicle System Dynamics, 49*(5), 811 – 830.

Wang, F. C., Chen, C. W., Liao, M. K., & Hong, M. F. (2007). Performance analyses of building suspension control with inerters. *Proceedings of the 46th IEEE Conference on Decision and Control, New Orleans, LA, USA*, 3786 – 3791.

Wang, F. C., Hong, M. F., & Chen, C. W. (2010). Building suspensions with inerters. *Proceedings of the Institution of Mechanical Engineers, Part C: Journal of Mechanical Engineering Science, 224*(8), 1605 – 1616.

Wang, F. C., Hong, M. F., & Lin, T. C. (2011). Designing and testing a hydraulic inerter. *Proceedings of the Institution of Mechanical Engineers, Part C: Journal of Mechanical Engineering Science, 225*(1), 66 – 72.

Wang, F. C., & Liao, M. K. (2010). The lateral stability of train suspension systems employing inerters. *Vehicle System Dynamics, 48*(5), 619 – 643.

Wang, F. C., Liao, M. K., Liao, B. H., Su, W. J., & Chan, H. A. (2009). The performance improvements of train suspension systems with mechanical networks employing inerters. *Vehicle System Dynamics, 47*(7), 805–830.

Wang, F. C., & Su, W. J. (2008a). Impact of inerter nonlinearities on vehicle suspension control. *Vehicle System Dynamics, 46*(7), 575 – 595.

Wang, F. C., & Su, W. J. (2008b). Inerter nonlinearities and the impact on suspension control. *Proceedings of the 2008 American Control Conference, Seattle, Washington, USA*, 3245 – 3250.

Wang, F. C., Yu, C. H., Chang, M. L., & Hsu, M. (2006). The performance improvements of train suspension systems with inerters. *Proceedings of the 45th IEEE Conference on Decision and Control, San Diego, CA, USA*, 1472 – 1477.

Wang, R., Meng, X., Shi, D., Zhang, X., Chen, Y., & Chen, L. (2014). Design and test of vehicle suspension system with inerters. *Proceedings of the Institution of Mechanical Engineers, Part C: Journal of Mechanical Engineering Science, 228*(15), 2684 – 2689.

Wilson, D. A., Sharp, R. S., & Hassan, S. A. (1986). The application of linear optimal control theory to the design of active automotive suspensions. *Vehicle System Dynamics, 15*(2), 105 – 118.

Yao, G. Z., Yap, F. F., Chen, G., Li, W. H., & Yeo, S. H. (2002). MR damper and its application for semi-active control of vehicle suspension system. *Mechatronics, 12*(7), 963 – 973.

Yeh, E. C., & Tsao, Y. J. (1992). Fuzzy control for active suspension design. *Proceedings of the Intelligent Vehicles '92 Symposium*, 92 – 97.

Ying, Z. D., Xu, X. F., & Zhu, J. A. (2010). Analysis of simulation design of the disc eddy current braking device. *Proceedings of the 2010 International Conference on Computer, Mechatronics, Control and Electronic Engineering, Chang Chun, China*, 309 – 311.

Zhang, X., Ahmadian, M., & Guo, K. (2010). A comparison of a semi-active inerter and a semi-active suspension. *SAE Technical Paper, 2010 – 01 – 1903*.

Zhang, X., Ahmadian, M., & Guo, K. (2012). On the benefits of semi-active suspensions with inerters. *Shock and Vibration, 19*(3), 257 – 272.

Zuo, L., Scully, B., Shestani, J., & Zhou, Y. (2010). Design and characterization of an electromagnetic energy harvester for vehicle suspensions. *Smart Materials and Structures, 19*(4) 045003, 1 – 10.

APPENDICES

Appendix A Structures of the Relevant MATLAB®/Simulink® Models

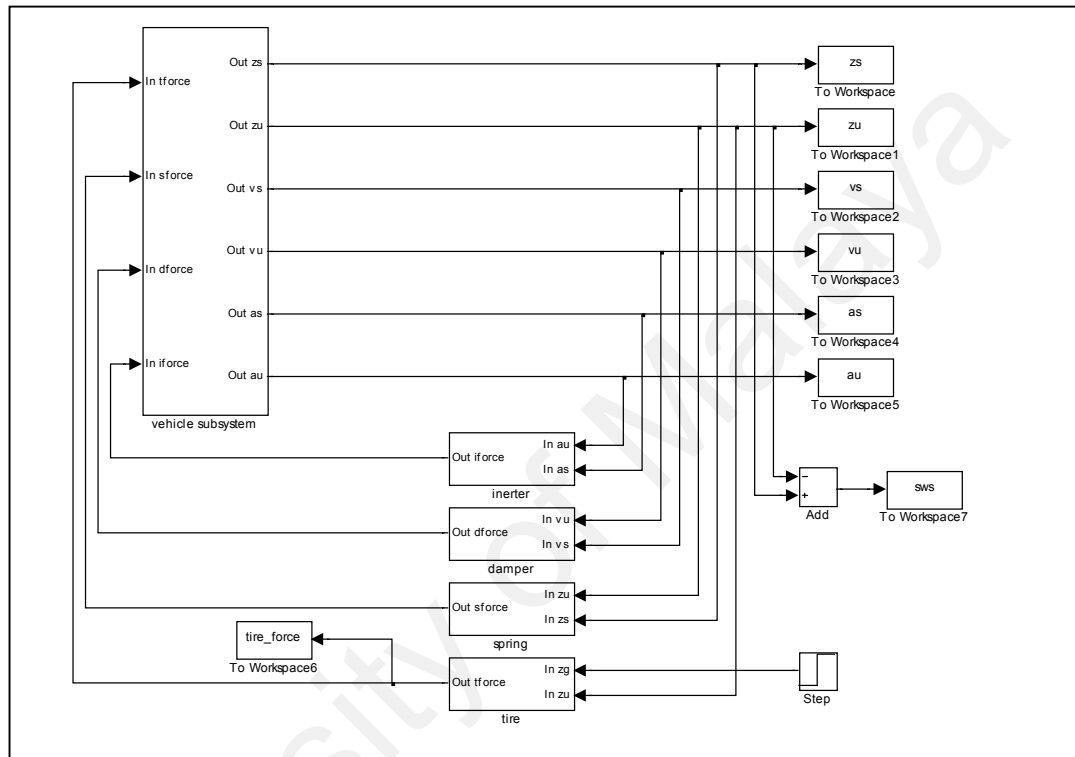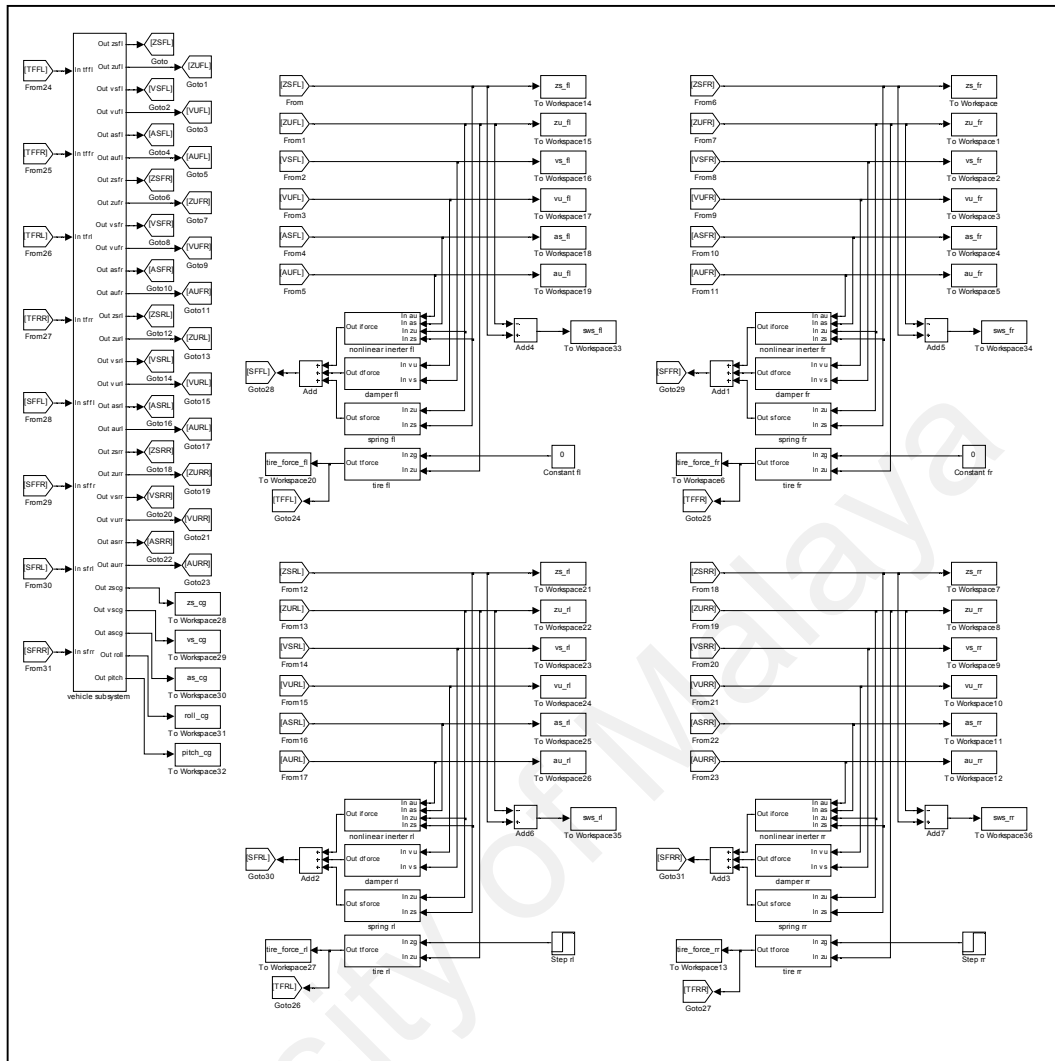Figure A1: Detailed structure of the MATLAB®/Simulink® block diagram for quarter

vehicle model

Figure A2: Detailed structure of the MATLAB®/Simulink® block diagram for seven-

DOF full vehicle model

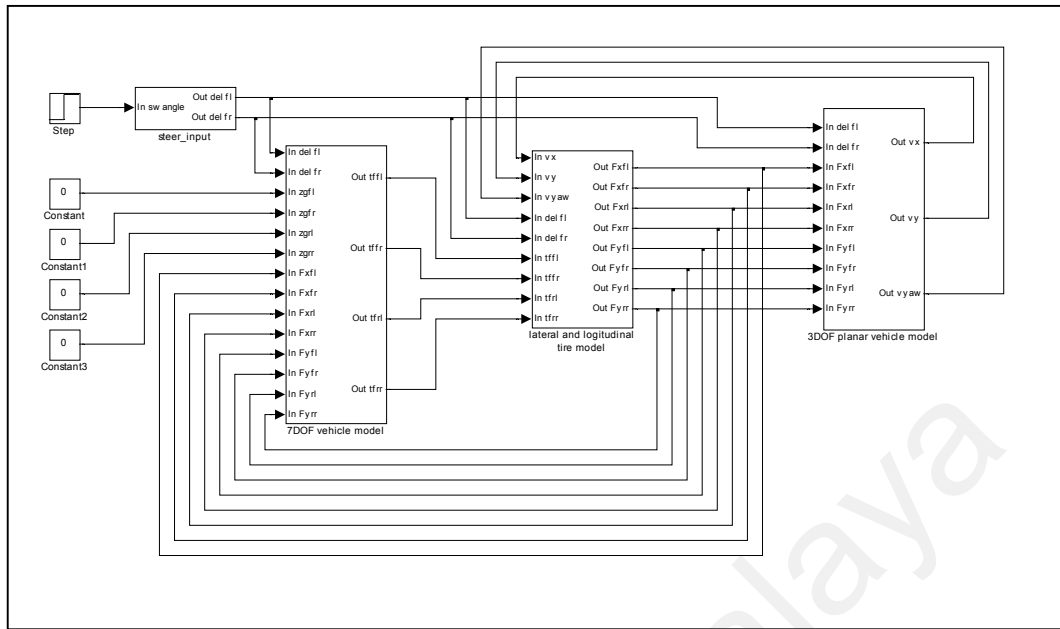Figure A3: Detailed structure of the MATLAB®/Simulink® block diagram for ten-DOF

handling model
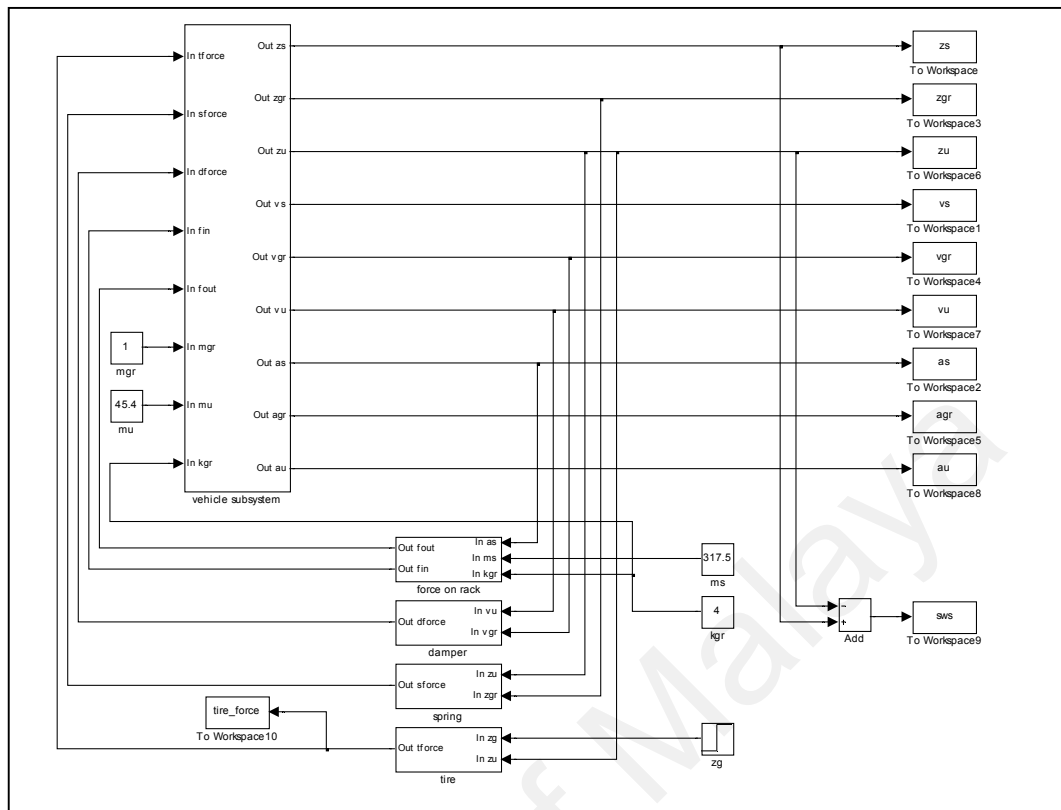
Figure A4: Detailed structure of the MATLAB$^{®}$/Simulink$^{®}$ quarter vehicle model

incorporating the proposed suspension layout with gear mechanism

Appendix B Estimation of Stiffness and Damping Rate for Scaled Quarter Vehicle Model
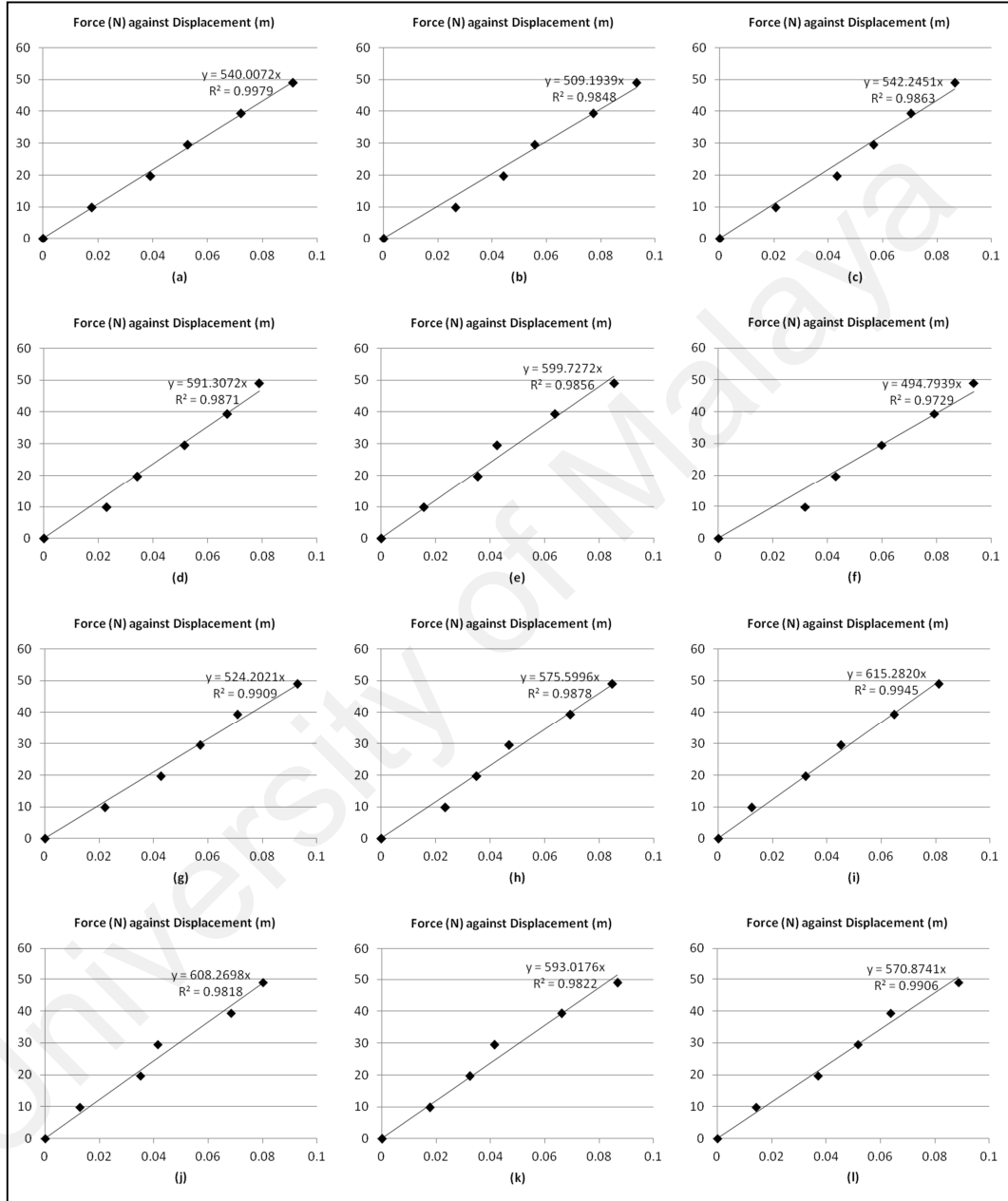

Figure B1: Estimation of suspension stiffness with static load test from (a) result set 1 to (l) result set 12
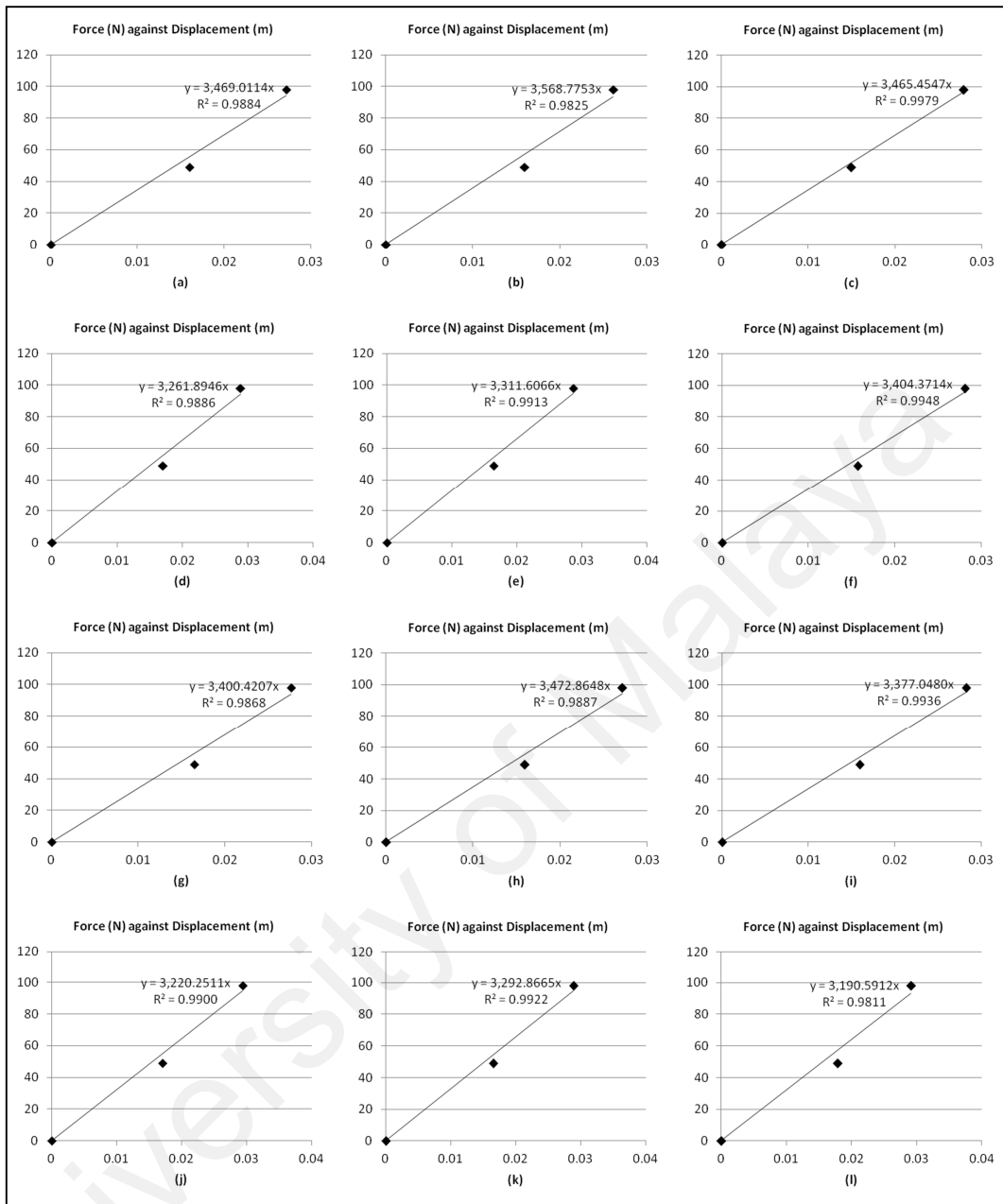
Figure B2: Estimation of tire stiffness with static load test from (a) result set 1 to (l) result set 12
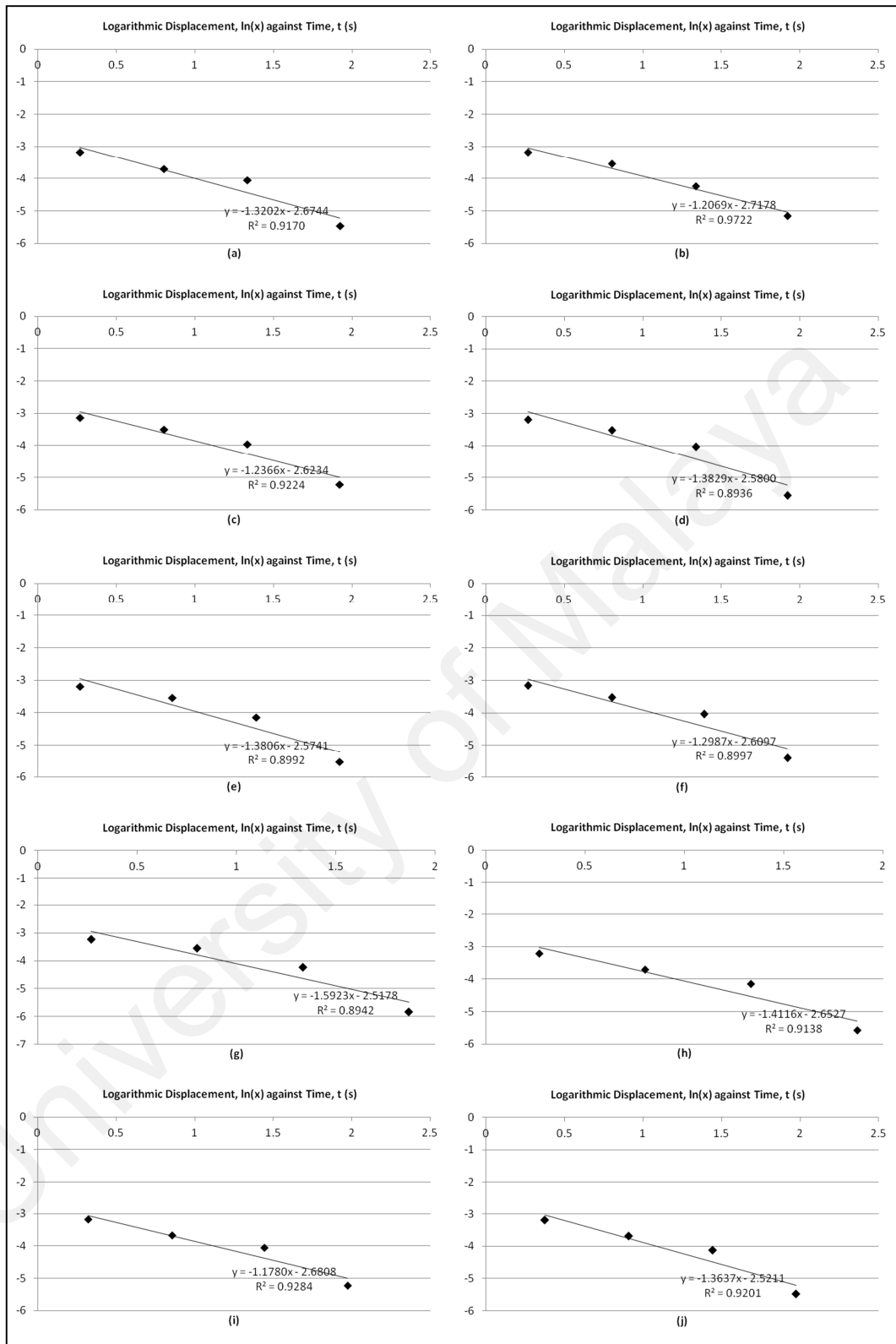
Figure B3: Estimation of suspension damping rate with dynamic load test from (a)

result set 1 to (j) result set 10

Appendix C Pareto Optimal Solutions for Passive Inerter Analysis

Table C1: Pareto optimal solutions for passive vehicle suspension due to step and

random road inputs

Objective 1: RMS sprung mass acceleration (ms^{-2})	Objective 2: RMS dynamic tire load (N)	Variable 1: Damping rate (Nsm^{-1})
Step input		
1.9088	1331.9	956
1.9088	1331.9	956
1.9090	1321.4	978
1.9103	1304.8	1013
1.9112	1298.7	1027
1.9159	1276.4	1081
1.9178	1269.9	1097
1.9336	1234.0	1202
1.9471	1214.2	1270
1.9655	1194.0	1351
1.9780	1183.0	1401
1.9921	1172.4	1455
1.9996	1167.4	1482
2.0251	1152.9	1571
2.0406	1145.6	1623
2.0644	1136.2	1699
2.1024	1124.5	1817
2.1193	1120.4	1869
2.1477	1114.7	1954
2.3073	1102.3	2416
2.3073	1102.3	2416
Random road input		
0.1544	130.0	705
0.1544	130.0	705
0.1544	129.5	711
0.1544	128.1	730
0.1545	126.7	750
0.1546	125.3	772
0.1547	124.7	781
0.1554	120.8	849
0.1561	118.4	895
0.1566	117.2	922
0.1574	115.2	966
0.1588	112.7	1032
0.1596	111.5	1065
0.1601	110.8	1086
0.1611	109.6	1127
0.1710	102.0	1470
0.1726	101.2	1523
0.1756	100.0	1618
0.1841	97.8	1877
0.2011	96.4	2398
0.2011	96.4	2398

Table C2: Pareto optimal solutions for passive vehicle suspension with parallel inerter

due to step and random road inputs

Objective 1: RMS sprung mass acceleration (ms^{-2})	Objective 2: RMS dynamic tire load (N)	Variable 1: Damping rate (Nsm^{-1})	Variable 2: Inertance (kg)
Step input			
1.8374	1463.2	886	6.3
1.8374	1463.2	886	6.3
1.8377	1447.7	910	6.2
1.8412	1408.6	965	5.8
1.8463	1384.0	983	4.7
1.8515	1364.0	1012	4.3
1.8758	1306.6	1095	2.8
1.8839	1286.5	1163	3.2
1.9128	1260.9	1144	0.6
1.9221	1243.0	1349	4.3
1.9642	1201.0	1466	2.9
1.9771	1187.4	1480	1.9
2.0097	1173.2	1604	2.5
2.0330	1166.4	1684	3.0
2.0505	1147.2	1692	1.1
2.0862	1139.3	1815	1.6
2.0970	1126.6	1804	0.1
2.1496	1117.7	1973	0.5
2.1781	1115.3	2063	0.8
2.2245	1108.7	2190	0.5
2.2362	1104.4	2212	0.0
Random road input			
0.1462	136.7	740	6.1
0.1462	136.7	740	6.1
0.1470	132.8	761	4.6
0.1490	127.1	827	3.5
0.1506	123.3	940	5.3
0.1513	121.4	948	4.1
0.1518	121.2	914	2.7
0.1551	116.1	998	1.7
0.1557	114.8	1080	3.1
0.1569	113.5	1130	3.5
0.1591	112.4	1222	4.9
0.1602	110.5	1244	3.8
0.1604	110.2	1245	3.6
0.1618	108.4	1248	2.0
0.1639	106.8	1309	1.8
0.1661	105.6	1397	2.4
0.1695	103.5	1487	1.9
0.1733	103.0	1630	3.4
0.1787	100.3	1764	2.0
0.1810	99.4	1823	1.5
0.2036	96.5	2476	0.0

Table C3: Pareto optimal solutions for passive vehicle suspension with serial inerter due

to step and random road inputs

Objective 1: RMS sprung mass acceleration (ms^{-2})	Objective 2: RMS dynamic tire load (N)	Variable 1: Damping rate (Nsm^{-1})	Variable 2: Inertance (kg)
Step input			
1.8433	1309.4	1025	319.3
1.8433	1309.4	1025	319.3
1.8434	1305.0	1035	327.7
1.8469	1285.6	1075	392.7
1.8513	1261.7	1140	394.5
1.8534	1249.6	1187	335.3
1.8622	1239.2	1204	453.9
1.8708	1216.7	1297	378.9
1.8792	1206.9	1356	323.2
1.8885	1195.4	1390	384.2
1.9264	1168.0	1514	509.3
1.9378	1159.6	1586	439.4
1.9482	1154.7	1609	487.8
1.9641	1151.9	1715	333.6
1.9785	1143.3	1675	625.1
2.0111	1132.2	1775	675.3
2.0310	1126.3	1851	645.8
2.0575	1124.1	2017	418.7
2.0742	1117.4	1995	641.2
2.1105	1112.7	2116	626.0
2.1738	1107.2	2277	754.7
2.2089	1106.4	2384	761.3
2.2183	1106.1	2407	781.1
Random road input			
0.1462	124.3	812	174.2
0.1462	124.3	812	174.2
0.1462	122.1	854	176.6
0.1465	121.1	868	197.5
0.1466	119.1	914	184.2
0.1468	118.4	930	183.7
0.1472	117.0	963	188.8
0.1488	113.4	1052	218.9
0.1497	111.5	1117	206.6
0.1514	110.6	1124	290.0
0.1520	108.6	1233	204.3
0.1524	108.4	1220	239.6
0.1563	105.3	1379	244.1
0.1602	103.9	1390	448.7
0.1611	102.7	1536	275.4
0.1638	101.6	1570	360.1
0.1679	100.2	1694	395.9
0.1739	98.9	1901	387.3
0.1810	97.6	1994	749.7
0.1892	97.4	2345	497.8
0.1923	96.9	2354	757.9

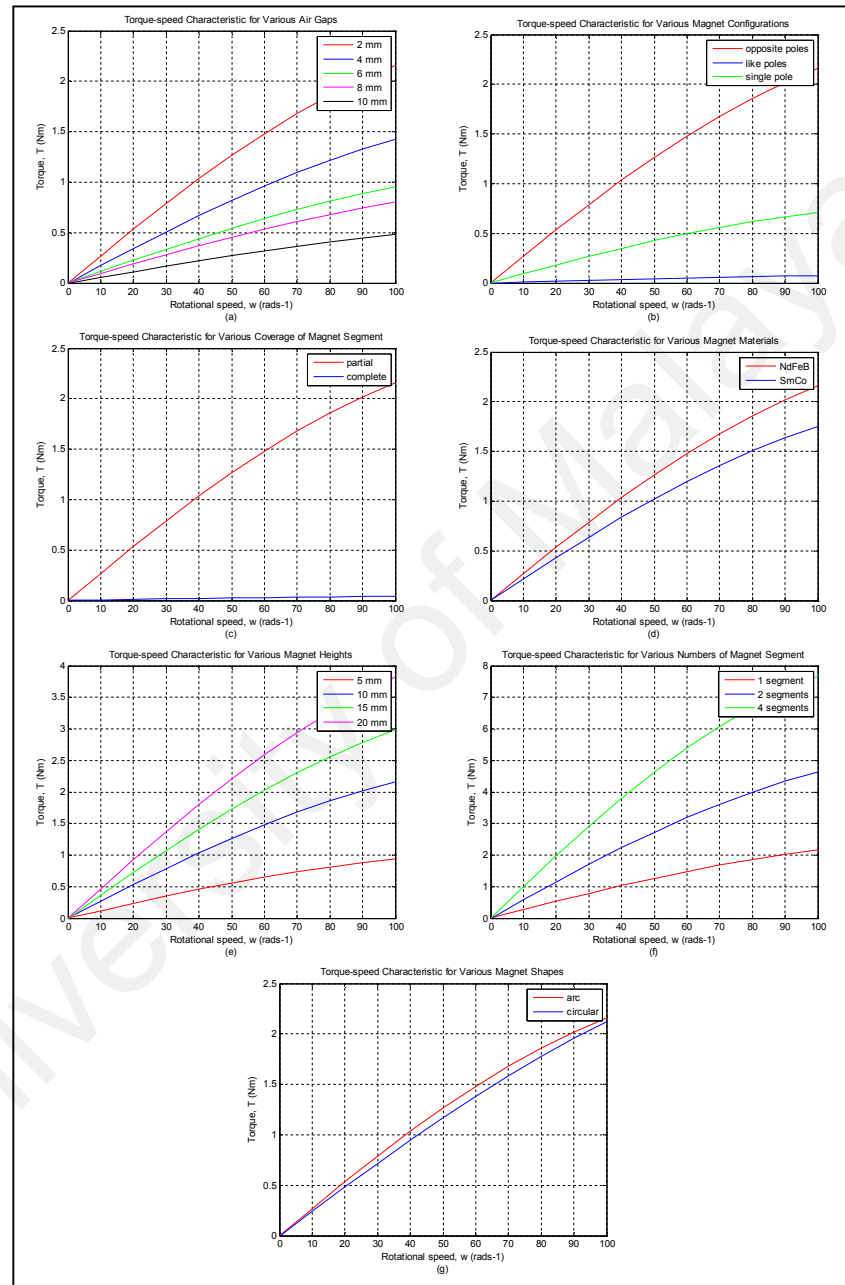# Appendix D Rotational Damping Characteristics for Variations of Eddy Current Damper

Figure D1: Rotational damping characteristics for the ball-screw design due to parametric variations in (a) air gap, (b) magnet configuration, (c) coverage of magnet segment, (d) magnet material, (e) height of magnet, (f) number of magnet segment and (g) magnet shape
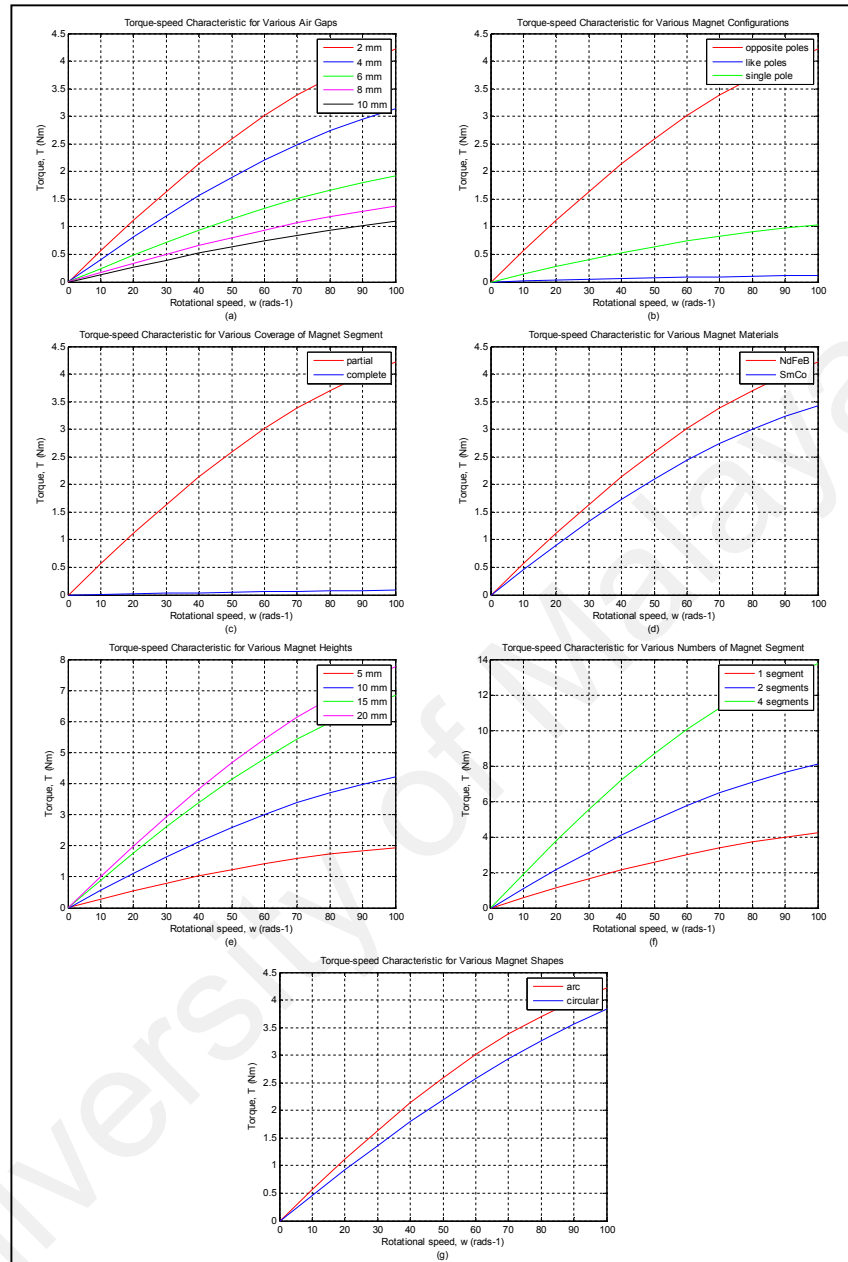
Figure D2: Rotational damping characteristics for the rack-and-pinion design due to parametric variations in (a) air gap, (b) magnet configuration, (c) coverage of magnet segment, (d) magnet material, (e) height of magnet, (f) number of magnet segment and (g) magnet shape